

Ich versichere hiermit an Eides Statt, dass ich die vorliegende Masterarbeit selbstständig und ohne unzulässige fremde Hilfe erbracht habe. Ich habe keine anderen als die angegebenen Quellen und Hilfsmittel benutzt. Für den Fall, dass die Arbeit zusätzlich auf einem Datenträger eingereicht wird, erkläre ich, dass die schriftliche und die elektronische Form vollständig übereinstimmen. Die Arbeit hat in gleicher oder ähnlicher Form noch keiner Prüfungsbehörde vorgelegen.

Aachen, den 29.09.2023

Contents

1	Neutrinos and the Large Scale Structure	2
1.1	Massive Neutrinos	2
1.2	Massless Neutrinos	5
2	The Nonlinear Power Spectrum	7
2.1	The Halo Model	7
2.2	The <code>HMCODE</code> Implementation	13
3	The Photometric Probe	17
3.1	The Formalism of Cosmic Sheer Observations	18
3.2	Extracting the Covariance from Theory	22
3.3	The Effect of Massive Neutrinos	24
4	The Spectroscopic Probe	28
4.1	Extracting the Power Spectrum from Observation	29
4.2	Extracting the Power Spectrum from Theory	33
4.3	The Effect of Massive Neutrinos	35
5	Methodology	38
5.1	The Markov Chain Monte Carlo Method	39
5.2	The Fisher Information Method	41
6	Validation of the Forecasting Pipeline	46
6.1	The Einstein-Bolzmann Solvers	48
6.2	Comparison of the different Fisher Information Methods	51
6.3	The validity of the Fisher approximation	54
6.4	Bias from Modeling	56
7	Results	63

Chapter 1

Neutrinos and the Large Scale Structure

In this chapter, we will briefly discuss the effects that neutrinos have on the matter power spectrum. For a more in-depth discussion of all the effects that neutrinos have on our universe, we refer to the main source of this chapter [[Lesgourgues et al., 2013](#)]. In the first section, we will give a phenomenological overview of the effect of massive neutrinos on the large-scale structure(LSS). Then we will remark on the effect that additional massless neutrinos have on the matter power spectrum. These discussions will also be representative of other simple dark matter models. Simply put any relativistic, collisionless, thermalized particle acts like a neutrino on the large-scale structure of the universe.

1.1 Massive Neutrinos

When discussing the effect of the massive neutrinos on the power spectrum the main effect can be very roughly described with three main phenomenological statements:

- Massive neutrinos stop clustering on scales larger than their free streaming scale that is related to their velocity.
- Massive neutrinos lead to an overall steplike suppression of the power spectrum by an amount proportional to their mass.
- Massive neutrinos change the redshift of matter-to-radiation equality essentially shifting the peak of the matter power spectrum.

The first effect leads to a suppression of the power spectrum for scales smaller than some scale k_* . This can be understood from the following reasoning. The free-streaming scale represents a scale under which collisionless particles can not be confined, if we define it analogously to the Jeans wavenumber we find a free-streaming wavenumber

$$k_{\text{fs}} = \sqrt{\frac{3}{2}} \frac{a H}{c_\nu}. \quad (1.1)$$

For relativistic neutrinos, c_ν is one while for nonrelativistic neutrinos we can find the thermal velocity by dividing the mean momentum by the neutrino mass. This leads to

$$c_\nu = \approx \frac{8.78 \cdot 10^{-3}}{a} \frac{0.06 \text{ eV}}{m_\nu}$$

$$k_{\text{fs}} \approx 4.66 \cdot 10^{-3} \frac{m_\nu}{0.06 \text{ eV}} a^2 \frac{H}{H_0} h \text{ Mpc}^{-1}. \quad (1.2)$$

During matter domination for the relativistic case, the free streaming wavenumber falls with η^{-1} and for the nonrelativistic case the wavenumber grows with η . This means that at the transition from relativistic to nonrelativistic we find the largest scale at which neutrinos stopped clustering. We denote this scale with k_{\min} (we will call it the minimum clustering scale), and it is precisely where the steplike suppression of the neutrinos starts. Given that the transition to the nonrelativistic regime happens during matter domination, k_{\min} can be approximated by

$$k_{\min} \approx 7.96 \cdot 10^{-3} \sqrt{\frac{\Omega_m}{0.3}} \sqrt{\frac{m_\nu}{0.06 \text{ eV}}} h \text{ Mpc}^{-1}. \quad (1.3)$$

To describe the second effect we first need to dissect our matter perturbation into baryons, CDM and massive neutrinos. We can write

$$\delta_m = f_c \delta_c + f_b \delta_b + f_\nu \delta_\nu. \quad (1.4)$$

The factors f_X are the fractional contribution of the species X to the total energy density of the universe. The equations of motion drive the neutrino perturbations to an equilibrium similar to the cold constituents. However, due to the high velocity of the neutrinos, there is non-negligible pressure and anisotropic stress. This leads to

- (a) a small-scale suppression of the neutrino perturbation that is approximately given by

$$\delta_\nu \propto \left(\frac{k_{\text{fs}}}{k} \right)^2 \delta_c$$

on scales smaller than the free streaming scale.

- (b) a scale-dependent growth rate that is reduced compared to the cold matter constituents until the equilibrium has been reached.

For the following discussion, we will only look at what will happen to the matter perturbations for scales much larger than the minimum clustering scale. Because of the two reasons stated above, on these scales, we use that at late times typical $|\delta_\nu| \ll \delta_c$. We can now expand equation 1.4 to find

$$\langle \delta_m(k) \delta_m^*(k') \rangle \approx (f_c + f_b)^2 \left\langle \frac{(f_c \delta_c(k) + f_b \delta_b(k))(f_c \delta_c^*(k') + f_b \delta_b^*(k'))}{(f_c + f_b)^2} \right\rangle$$

$$:= (f_c + f_b)^2 \langle \delta_{cb}(k) \delta_{cb}^*(k') \rangle \quad (1.5)$$

$$\iff P_{mm}(k) \approx (1 - f_\nu)^2 P_{cb}(k), \quad (1.6)$$

where we have defined the perturbation of the CDM+baryon field δ_{cb} and its respective power spectrum. After the baryon drag epoch, i.e. after baryons decouple from the radiation field, the equations of motion for this new density contrast are simplified to

$$\delta''_{cb} + \frac{a'}{a} \delta'_{cb} - 4 a^2 \pi G \langle \rho_c + \rho_b \rangle \delta_{cb} = 0, \quad (1.7)$$

where the prime denotes derivatives with respect to conformal time.

The third term is starting to look like the Friedmann–Lemaître equation minus the effect of massive neutrinos. If we add them we can write

$$\delta''_{cb} + \frac{a'}{a} \delta'_{cb} - \frac{3}{2} (1 - f_\nu) (a')^2 \delta_{cb} = 0. \quad (1.8)$$

If we assume that we are deep into matter domination such that the bulk of neutrinos are already non-relativistic. The neutrino density thus scales with a^{-3} . At this time the background evolution matches the neutrinoless case, and we can write that $a \propto \eta^2$. If we insert the conformal time into the equality we can solve the differential equation to find

$$\delta''_{cb} + \frac{2}{\eta} \delta'_{cb} - \frac{6}{\eta^2} (1 - f_\nu) \delta_{cb} = 0. \quad (1.9)$$

$$\implies \delta_{cb} \propto \eta^{\alpha \pm} \quad \text{with} \quad \alpha_{\pm} = -\frac{1}{2} \pm \frac{1}{2} \sqrt{25 - 24f_\nu} \quad (1.10)$$

This gives us one growing mode and a decaying mode. The result we find is different from the result of the neutrinoless universe where for the growing mode we find $\delta \propto a$. When we also use that neutrinos contribute very little to the total energy density, i.e. $f_\nu \ll 1$, we can find an approximate solution

$$\delta_{cb} = A_- a^{-\frac{3}{2} + \frac{3}{5} f_\nu} + A_+ a^{1 - \frac{3}{5} f_\nu}. \quad (1.11)$$

If we neglect the decaying mode, inserting the result for δ_{cb} into the Poisson equation we also find

$$k^2 \Psi = -\frac{3}{2} (1 - f_\nu) (a')^2 \delta_{cb} \propto a^{-\frac{3}{5} f_\nu}. \quad (1.12)$$

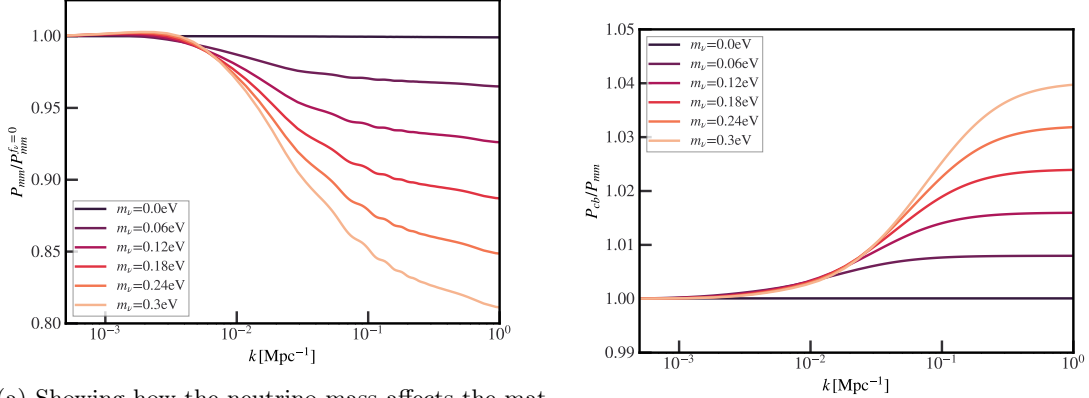
We can conclude that due to the massive neutrinos, we see that not only does the density contrast of clustering matter grow slower, but also that the metric perturbations slowly decay. From numerical calculations, we can find a rough estimate of the suppression on scales much smaller than the minimal clustering scale. For $f_\nu \ll 1$ the overall suppression of the power spectrum can be estimated with

$$\frac{P_{cb}}{P_{cb}^{f_\nu=0}} \approx 1 - 6 f_\nu, \quad (1.13)$$

or for the total matter power spectrum $P_{mm}/P_{mm}^{f_\nu=0} \approx 1 - 8 f_\nu$. We illustrate the suppression of the power spectrum and the difference between the CDM+baryon spectrum and the total matter power spectrum in figure 1.1. In the figure we have fixed the total nonrelativistic matter density to match the low redshift expansion history between the different models this means reducing the cold dark matter density. These changes also lead to further suppression of the power spectrum on the smallest scales, essentially tilting the plateau further.

The last effect of massive neutrinos is the shifting of the redshift of equality. When fixing the

Figure 1.1: The effect of changing N_{eff} when fixing different quantities as explained in the Text. The Ratios were multiplied with a factor to better differentiate between them.



(a) Showing how the neutrino mass affects the matter power spectrum. For the comparison we fixed $\{h, \Omega_b, \Omega_m\}$

(b) Amplification of the CDM+baryon power spectrum for different neutrino masses

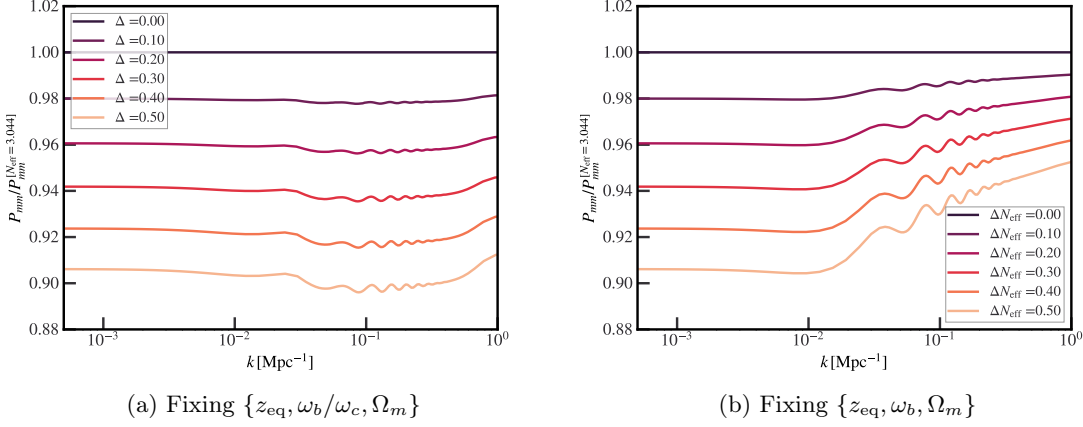
density parameters of radiation, total matter, and baryons additional neutrinos shift the redshift of equality by a factor of $(1 - f_\nu)$. This is due to the neutrinos being ultra-relativistic at the time of equality and thus not contributing to the matter density. The shift of the redshift of equality leads to a shift in the peak of the matter power spectrum as it is given from the wavenumber that crossed the Hubble horizon precisely at equality. The slight wiggles in the ratio come from a change in the expansion history at earlier times shifting the scale of the BAO. We note that when we combine our *Euclid* probes with *Planck*, the CMB experiments strongly constrain the angular scale θ_s , the redshift of equality z_{eq} , and the physical density parameter of baryons, ω_b . It can be shown that when fixing these quantities a change in the neutrino mass only leads to a more scale-independent suppression and a slight shift in the phase of the BAOs.

1.2 Massless Neutrinos

The effect of additional massless neutrinos on the matter power spectrum can be separated into background effects and perturbation effects. For the latter we can already guess that these will be small. The main contribution of massless neutrinos to the matter power spectrum must happen during radiation domination as they become negligible during matter domination. During radiation domination on scales smaller than the Hubble horizon, it can be shown that the massless neutrinos have very little effect on the evolution of cold perturbations. This is because the massless neutrino perturbations crossing the Hubble horizon show an oscillatory behaviour. When decomposing the equations of motion for the perturbations into fast oscillating modes and slowly growing modes, we see that cold matter is primarily determined by slow modes. As a consequence, we can treat the massless neutrino perturbations as free streaming one matter domination starts.

The background effects of additional massive neutrinos have to be analysed a bit more carefully. Depending on what quantities are fixed other quantities need to change as well. Firstly we start

Figure 1.2: The effect of changing N_{eff} when fixing different quantities as explained in the Text. The Ratios were multiplied with a factor to better differentiate between them.



with the parametrization of additional massless relics, for this, we use the parameter N_{eff} . We write, that the density of total radiation is given as

$$\rho_r = \rho_\gamma \left[1 + \frac{7}{8} \left(\frac{4}{11} \right)^{4/3} N_{\text{eff}} \right] \quad (1.14)$$

This means, that when fixing the density parameters of matter a change of N_{eff} coincides with a change of the redshift of equality, shifting the peak of the power spectrum. In order to fix the redshift of equality we need to scale ω_m as ω_γ is very tightly constrained by Firas.

The overall amplitude of the matter power spectrum is related to the amplitude of scalar perturbations A_s as well as the total matter density parameter Ω_m . The latter is proportional to the physical density of total matter by $\omega_m = \Omega_m h^2$. If we also want to fix the amplitude of the matter power spectrum without changing A_s we have to scale h accordingly.

Next, if we want to subtract that effect then we need to rescale the matter density. Depending on if we switch ω_b or ω_c this changes the ratio of ω_b/ω_c . This ratio is crucial in the large-scale amplitude of the power spectrum as well as the amplitude of the BAOs. To cancel this effect we need to equally scale the CDM and baryon density. What would be left in this set of fixed variables is a change in ω_b , that changes the phase of the BAOs. We have no longer the freedom to fix this effect.

We could have also decided to fix ω_b this would need us to change the ratio of cold dark matter to baryons and suppress the large-scale plateau. We illustrate the effects of changing N_{eff} for both cases in figure 1.2.

Chapter 2

The Nonlinear Power Spectrum

With the Euclid mission, we will be able to probe deeply the non-linear regime of the matter power spectrum. The non-linear power spectrum can not be calculated using just perturbation theory, so to predict the dynamics we would resort back to N-body simulations. As running such simulations are computationally expensive we have different codes to obtain the nonlinear power spectrum. In this work, we use two different codes called `HALOFIT` [Mead et al., 2021] and `HMCODE` [Takahashi et al., 2020]. Both codes agree with each other on the level of 6% but at the level of the *Euclid* mission's precision, this is already too much. We will show later on how the choice of the non-linear code will bias our parameter inference. Since `HMCODE` is better at matching N-body simulations of cosmologies with DE and massive Neutrinos than `HALOFIT`, we will use it for the forecast for the massive neutrinos while we will use `HALOFIT` for the forecast of modified gravity as the fitting formula was done with the power spectrum of `HALOFIT` as a pseudo.

Both codes are based on the halo model to predict the non-linear power spectrum. In the first section we will go over the basics of the halo model.

The codes differ in that `HALOFIT` is a direct functional fit of the power spectrum from the halo model. `HMCODE` on the other hand is a semi-analytical model where the individual ingredients of the halo model are fitted. They are then combined in the context of a modified halo model to better match N-body simulations. In the second section, we will then go over the implementation of `HMCODE` we used and explain where the critical modelling of massive neutrinos is important.

2.1 The Halo Model

The halo model describes how the non-linear power spectrum is calculated using a sum of two terms

$$P_{mm}(k, z) = P^{1h}(k, z) + P^{2h}(k, z). \quad (2.1)$$

The first "one halo term", $P^{1h}(k, z)$, dominates at smaller scales and is calculated solely from the intrinsic properties of halos. The second term is called the "two-halo term", $P^{2h}(k, z)$, it dominates at larger scales and describes the spacial correlation between two halos. To get to this point we will need to discuss how to extract a power spectrum from a density map.

We start by stating that all the derivation is done at one point in time, but it is the time dependence

can be added afterwards. The main assumption of the halo model is that the total matter field, ρ , can be written as a sum over different halos, i.e. all the matter is inside halos. The second assumption is that the density profile of halos, ρ_H , is only a function of their mass, M_i and the relative position to their centre, \mathbf{x}_i . These assumptions lead to

$$\rho(\mathbf{x}) = \sum_i \rho(\mathbf{x} - \mathbf{x}_i, M_i) = \int \sum_i \delta(M' - M_i) \delta^{(3)}(\mathbf{x}' - \mathbf{x}_i) \rho_H(\mathbf{x} - \mathbf{x}', M') d^3\mathbf{x}' dM' \quad (2.2)$$

In the last step, we have artificially added a sum over Dirac-delta distributions to pull out the dependence on the particular realization of the universe out of the halo density profile. The sum in the integral itself can be understood as a random realization of an underlying probability density, $\langle dn/dM \rangle$, i.e., the number density per mass interval $M, M + dM$. This can be understood in the following way. Imagine that the universe is separated into small volume bins, δV_i , and mass bins, δM_j , such that in each bin there is only the centre of one halo with its mass in that particular mass bin. This would define a random variable S^{ij} such that

$$S^{ij} = \begin{cases} 1 & \text{when a halo is in the corresponding bins } ij \\ 0 & \text{otherwise} \end{cases}$$

The expectation value of this variable is given by the probability of finding a galaxy in this bin. One could either integrate the underlying probability or take the ensemble average of particular realizations. This leads to

$$\langle S^{ij} \rangle = \int_{\delta M_j} \int_{\delta V_i} \left\langle \frac{dn}{dM} \right\rangle (M) d^3\mathbf{x} dM \quad (2.3)$$

$$\stackrel{!}{=} \left\langle \int_{\delta M_j} \int_{\delta V_i} \sum_k \delta(M - M_k) \delta^{(3)}(\mathbf{x} - \mathbf{x}_k) d^3\mathbf{x} dM \right\rangle \quad (2.4)$$

$$\iff \left\langle \frac{dn}{dM} \right\rangle (M) = \left\langle \sum_i \delta(M - M_i) \delta^{(3)}(\mathbf{x} - \mathbf{x}_i) \right\rangle. \quad (2.5)$$

This can be used to find a normalization condition for the probability density by evaluating the expectation value of the density field

$$1 \stackrel{!}{=} \frac{1}{\langle \rho \rangle} \left\langle \int \sum_i \delta(M' - M_i) \delta^{(3)}(\mathbf{x}' - \mathbf{x}_i) \rho_H(\mathbf{x} - \mathbf{x}', M') d^3\mathbf{x}' dM' \right\rangle \quad (2.6)$$

$$\begin{aligned} &= \frac{1}{\langle \rho \rangle} \int \left\langle \sum_i \delta(M' - M_i) \delta^{(3)}(\mathbf{x}' - \mathbf{x}_i) \right\rangle \rho_H(\mathbf{x} - \mathbf{x}', M') d^3\mathbf{x}' dM' \\ &= \frac{1}{\langle \rho \rangle} \int \left\langle \frac{dn}{dM} \right\rangle (M') \rho_H(\mathbf{x} - \mathbf{x}', M') d^3\mathbf{x}' dM' \\ &= \int \frac{M'}{\langle \rho \rangle} \left\langle \frac{dn}{dM} \right\rangle (M') dM'. \end{aligned} \quad (2.7)$$

In the first line, we have used that the halo profile of a single halo with mass M' and location \mathbf{x}' is independent of a particular realization of the universe and such can be factored out of the ensemble average. In the next step, we can use this to find an expression for the density contrast,

$$\delta(\mathbf{x}) = \frac{\rho(\mathbf{x}) - \langle \rho \rangle}{\langle \rho \rangle} = \frac{1}{\langle \rho \rangle} \int \left[\sum_i \delta(M' - M_i) \delta^{(3)}(\mathbf{x}' - \mathbf{x}_i) - \left\langle \frac{dn}{dM} \right\rangle (M') \right] \rho_H(\mathbf{x} - \mathbf{x}', M') d^3 \mathbf{x}' dM' \quad (2.8)$$

$$:= \int \left\langle \frac{dn}{dM} \right\rangle (M') \delta_H(\mathbf{x}', M') \frac{\rho_H(\mathbf{x} - \mathbf{x}', M')}{\langle \rho \rangle} d^3 \mathbf{x}' dM'. \quad (2.9)$$

We have defined a new halo distribution contrast, δ_H , that compares the realization of halo masses and centres to their underlying uniform distribution. The next step is to calculate the two-point correlation function, $\xi(\mathbf{x}_1, \mathbf{x}_2) = \langle \delta(\mathbf{x}_1) \delta(\mathbf{x}_2) \rangle$. For this we will need to evaluate the same term, but with the halo distribution contrast. We write it as

$$\langle \delta_H(\mathbf{x}_1, M_1) \delta_H(\mathbf{x}_2, M_2) \rangle = \left[\left\langle \frac{dn}{dM} \right\rangle_1 \left\langle \frac{dn}{dM} \right\rangle_2 \right]^{-1} \left\langle \left(\sum_i \delta^{(4)}(\tilde{\mathbf{x}}_1 - \tilde{\mathbf{x}}_i) - \left\langle \frac{dn}{dM} \right\rangle_1 \right) \times \left(\sum_j \delta^{(4)}(\tilde{\mathbf{x}}_2 - \tilde{\mathbf{x}}_j) - \left\langle \frac{dn}{dM} \right\rangle_2 \right) \right\rangle \quad (2.10)$$

$$= \left[\left\langle \frac{dn}{dM} \right\rangle_1 \left\langle \frac{dn}{dM} \right\rangle_2 \right]^{-1} \left[\left\langle \sum_i \delta^{(4)}(\tilde{\mathbf{x}}_1 - \tilde{\mathbf{x}}_i) \sum_j \delta^{(4)}(\tilde{\mathbf{x}}_2 - \tilde{\mathbf{x}}_j) \right\rangle + \left\langle \frac{dn}{dM} \right\rangle_1 \left\langle \frac{dn}{dM} \right\rangle_2 \right]. \quad (2.11)$$

We have used the shorthand notations $\delta^{(4)}(\tilde{\mathbf{x}} - \tilde{\mathbf{x}}_i) = \delta^{(3)}(\mathbf{x} - \mathbf{x}_i) \delta(M - M_i)$ for the four dimensional Dirac delta and $\langle dn/dM \rangle_i = \langle dn/dM \rangle(M_i)$ for the halo mass function.

In the next step we will separate the integrals that show up in the calculation of the two-point correlation function into bins like before, this allows us to find the random variables S^{ij} again. For notation's sake, we will slice up the integration space into four-dimensional volumes with one index. We will then find integrals like

$$\mathcal{I}_g = \iint g(\tilde{\mathbf{x}}_1, \tilde{\mathbf{x}}_2) \left\langle \sum_i \delta^{(4)}(\tilde{\mathbf{x}}_1 - \tilde{\mathbf{x}}_i) \sum_j \delta^{(4)}(\tilde{\mathbf{x}}_2 - \tilde{\mathbf{x}}_j) \right\rangle d^4 \tilde{\mathbf{x}}_1 d^4 \tilde{\mathbf{x}}_2 \quad (2.12)$$

$$= \sum_{\mu} \sum_{\nu} g(\tilde{\mathbf{x}}_{\mu}, \tilde{\mathbf{x}}_{\nu}) \langle S^{\mu} S^{\nu} \rangle, \quad (2.13)$$

with an arbitrary function g . In the easy case the indices μ and ν are the same, and we find

$$\langle S^{\mu} S^{\mu} \rangle = \langle S^{\mu} \rangle = \int_{\delta V_{\mu}^{(4)}} \left\langle \frac{dn}{dM} \right\rangle_1 d^4 \tilde{\mathbf{x}}_1. \quad (2.14)$$

For the term with two different indices, we need to use the two-point correlation function of halo seed densities of equation 2.10. This leads to

$$\langle S^\mu S^\nu \rangle = \int_{\delta V_\mu^{(4)}} \int_{\delta V_\nu^{(4)}} \langle \delta_H(\tilde{\mathbf{x}}_1) \delta_H(\tilde{\mathbf{x}}_2) - 1 \rangle \left\langle \frac{dn}{dM} \right\rangle_1 \left\langle \frac{dn}{dM} \right\rangle_2 d^4 \tilde{\mathbf{x}}_1 d^4 \tilde{\mathbf{x}}_2 \quad (2.15)$$

$$:= \int_{\delta V_\mu^{(4)}} \int_{\delta V_\nu^{(4)}} (\xi_H(\tilde{\mathbf{x}}_1, \tilde{\mathbf{x}}_2) - 1) \left\langle \frac{dn}{dM} \right\rangle_1 \left\langle \frac{dn}{dM} \right\rangle_2 d^4 \tilde{\mathbf{x}}_1 d^4 \tilde{\mathbf{x}}_2. \quad (2.16)$$

With this, we can find the value of \mathcal{I}_g and relate it to the original integral by joining the bins together. We find

$$\mathcal{I}_g = \sum_{\mu \nu} g(\tilde{\mathbf{x}}_\mu, \tilde{\mathbf{x}}_\nu) \langle S^\mu S^\nu \rangle \quad (2.17)$$

$$\begin{aligned} &= \sum_{\mu \neq \nu} \int_{\delta_\mu^{(4)}} \int_{\delta_\nu^{(4)}} g(\tilde{\mathbf{x}}_\mu, \tilde{\mathbf{x}}_\nu) (\xi_H(\tilde{\mathbf{x}}_1, \tilde{\mathbf{x}}_2) - 1) \left\langle \frac{dn}{dM} \right\rangle_1 \left\langle \frac{dn}{dM} \right\rangle_2 d^4 \tilde{\mathbf{x}}_1 d^4 \tilde{\mathbf{x}}_2 \\ &\quad + \sum_\mu \int_{\delta_\mu^{(4)}} g(\tilde{\mathbf{x}}_\mu, \tilde{\mathbf{x}}_\mu) \left\langle \frac{dn}{dM} \right\rangle_1 d^4 \tilde{\mathbf{x}}_1 \end{aligned} \quad (2.18)$$

$$\begin{aligned} &= \sum_{\mu \neq \nu} \int_{\delta_\mu^{(4)}} \int_{\delta_\nu^{(4)}} g(\tilde{\mathbf{x}}_1, \tilde{\mathbf{x}}_2) (\xi_H(\tilde{\mathbf{x}}_1, \tilde{\mathbf{x}}_2) - 1) \left\langle \frac{dn}{dM} \right\rangle_1 \left\langle \frac{dn}{dM} \right\rangle_2 d^4 \tilde{\mathbf{x}}_1 d^4 \tilde{\mathbf{x}}_2 \\ &\quad + \sum_\mu \int_{\delta_\mu^{(4)}} g(\tilde{\mathbf{x}}_1, \tilde{\mathbf{x}}_1) \left\langle \frac{dn}{dM} \right\rangle_1 d^4 \tilde{\mathbf{x}}_1 \end{aligned} \quad (2.19)$$

$$\begin{aligned} &= \iint g(\tilde{\mathbf{x}}_1, \tilde{\mathbf{x}}_2) (\xi_H(\tilde{\mathbf{x}}_1, \tilde{\mathbf{x}}_2) - 1) \left\langle \frac{dn}{dM} \right\rangle_1 \left\langle \frac{dn}{dM} \right\rangle_2 d^4 \tilde{\mathbf{x}}_1 d^4 \tilde{\mathbf{x}}_2 \\ &\quad + \iint g(\tilde{\mathbf{x}}_1, \tilde{\mathbf{x}}_2) \left\langle \frac{dn}{dM} \right\rangle_1 \delta^{(4)}(\tilde{\mathbf{x}}_1 - \tilde{\mathbf{x}}_2) d^4 \tilde{\mathbf{x}}_1 d^4 \tilde{\mathbf{x}}_2 \end{aligned} \quad (2.20)$$

$$= \iint g(\tilde{\mathbf{x}}_1, \tilde{\mathbf{x}}_2) \left\langle \frac{dn}{dM} \right\rangle_1 \left[\left\langle \frac{dn}{dM} \right\rangle_2 (\xi_H(\tilde{\mathbf{x}}_1, \tilde{\mathbf{x}}_2) - 1) + \delta^{(4)}(\tilde{\mathbf{x}}_1 - \tilde{\mathbf{x}}_2) \right] d^4 \tilde{\mathbf{x}}_1 d^4 \tilde{\mathbf{x}}_2 \quad (2.21)$$

In the fourth line we use that the function g is varying slowly in one bin and thus can be approximated as the value at the bin center. We then combine the microcells in line six and artificially add an integration over $\tilde{\mathbf{x}}_2$ to find the final result. When comparing equations 2.12 and 2.21 we find an expression for the halo seed density two-point correlation function,

$$\left\langle \sum_i \delta^{(4)}(\tilde{\mathbf{x}}_1 - \tilde{\mathbf{x}}_i) \sum_j \delta^{(4)}(\tilde{\mathbf{x}}_2 - \tilde{\mathbf{x}}_j) \right\rangle = \left\langle \frac{dn}{dM} \right\rangle_1 \left[\left\langle \frac{dn}{dM} \right\rangle_2 (\xi_H(\tilde{\mathbf{x}}_1, \tilde{\mathbf{x}}_2) - 1) + \delta^{(4)}(\tilde{\mathbf{x}}_1 - \tilde{\mathbf{x}}_2) \right] \quad (2.22)$$

$$\langle \delta_H(\mathbf{x}_1, M_1) \delta_H(\mathbf{x}_2, M_2) \rangle = \xi_H(\mathbf{x}_1, \mathbf{x}_2, M_1, M_2) + \left[\left\langle \frac{dn}{dM} \right\rangle(M_1) \right]^{-1} \delta^{(3)}(\mathbf{x}_1 - \mathbf{x}_2) \delta(M_1 - M_2). \quad (2.23)$$

With this, we can find the two-point correlation function to be

$$\begin{aligned}\xi(\mathbf{x}_1, \mathbf{x}_2) &= \iint \left\langle \frac{dn}{dM} \right\rangle_1 \left\langle \frac{dn}{dM} \right\rangle_2 \langle \delta_H(\tilde{\mathbf{x}}'_1) \delta_H(\tilde{\mathbf{x}}'_2) \rangle \frac{\rho_H(\mathbf{x}_1 - \mathbf{x}'_1, M'_1)}{\langle \rho \rangle} \frac{\rho_H(\mathbf{x}_2 - \mathbf{x}'_2, M'_2)}{\langle \rho \rangle} d^4 \tilde{\mathbf{x}}'_1 d^4 \tilde{\mathbf{x}}'_2 \\ &= \iint \xi_H(\mathbf{x}'_1, \mathbf{x}'_2, M'_1, M'_2) \left\langle \frac{dn}{dM} \right\rangle_1 \left\langle \frac{dn}{dM} \right\rangle_2 \frac{\rho_H(\mathbf{x}_1 - \mathbf{x}'_1, M'_1)}{\langle \rho \rangle} \frac{\rho_H(\mathbf{x}_2 - \mathbf{x}'_2, M'_2)}{\langle \rho \rangle} d^4 \tilde{\mathbf{x}}'_1 d^4 \tilde{\mathbf{x}}'_2 \\ &\quad + \int \left\langle \frac{dn}{dM} \right\rangle_1 \frac{\rho_H(\mathbf{x}_1 - \mathbf{x}'_1, M'_1)}{\langle \rho \rangle} \frac{\rho_H(\mathbf{x}_2 - \mathbf{x}'_1, M'_1)}{\langle \rho \rangle} d^4 \tilde{\mathbf{x}}'_1.\end{aligned}\tag{2.24}$$

In the next step, we note that the halo over densities, δ_H , are biased tracers of the matter over densities, δ_m . We assume that the bias is a function of the mass of the halo but not its location due to the isotropy of space, and is linear. With this we can find

$$\xi_H(\mathbf{x}_1, \mathbf{x}_2, M_1, M_2) = b(M_1) b(M_2) \xi_m(\mathbf{x}_1, \mathbf{x}_2).$$

Our initial assumptions that all the matter should be in halos argues that the bias function should be a function close to unity and thus the integral

$$\int b(M) \left\langle \frac{dn}{dM} \right\rangle \frac{\rho_H(\mathbf{x}, M)}{\langle \rho \rangle} d^3 \mathbf{x} dM \approx 1.\tag{2.25}$$

To find the power spectrum we start with the Fourier transformation of the density contrast

$$\delta(\mathbf{k}) = \frac{1}{(2\pi)^3} \int \left\langle \frac{dn}{dM} \right\rangle (M') \delta_H(\mathbf{x}', M') \frac{\rho_H(\mathbf{x} - \mathbf{x}', M')}{\langle \rho \rangle} \exp[-i\mathbf{k} \cdot \mathbf{x}] d^3 \mathbf{x}' dM' d^3 \mathbf{x}\tag{2.26}$$

$$= \int \left\langle \frac{dn}{dM} \right\rangle (M') \delta_H(\mathbf{x}', M') \frac{\rho_H(\mathbf{k}, M')}{\langle \rho \rangle} \exp[-i\mathbf{k} \cdot \mathbf{x}'] d^3 \mathbf{x}' dM'\tag{2.27}$$

In the next step, we need to calculate the expectation value of the density contrast. We will then

insert the two-point correlation of halo density contrast from equation 2.23 to find

$$\begin{aligned} \langle \delta(\mathbf{k}_1) \delta^*(\mathbf{k}_2) \rangle &= \int \xi(\mathbf{x}_1 - \mathbf{x}_2) b(M_1) b(M_2) \left\langle \frac{dn}{dM} \right\rangle_1 \left\langle \frac{dn}{dM} \right\rangle_2 \frac{\rho_H(\mathbf{k}_1, M_1)}{\langle \rho \rangle} e^{-i\mathbf{k}_1 \cdot \mathbf{x}_1} \\ &\quad \times \frac{\rho_H(\mathbf{k}_2, M_2)}{\langle \rho \rangle} e^{i\mathbf{k}_2 \cdot \mathbf{x}_2} d^3 \mathbf{x}_1 d^3 \mathbf{x}_2 dM_1 dM_2 \\ &\quad + \int \left\langle \frac{dn}{dM} \right\rangle_1 \frac{\rho_H(\mathbf{k}_1, M_1)}{\langle \rho \rangle} \frac{\rho_H(\mathbf{k}_2, M_1)}{\langle \rho \rangle} e^{-i\mathbf{x}_1 \cdot [\mathbf{k}_1 - \mathbf{k}_2]} d^3 \mathbf{x}_1 dM_1 \end{aligned} \quad (2.28)$$

$$\begin{aligned} &= \int P_{mm}(\mathbf{k}') b(M_1) \left\langle \frac{dn}{dM} \right\rangle_1 \frac{\rho_H(\mathbf{k}_1, M_1)}{\langle \rho \rangle} e^{-i\mathbf{x}_1 \cdot [\mathbf{k}_1 - \mathbf{k}']} \\ &\quad \times b(M_2) \left\langle \frac{dn}{dM} \right\rangle_2 \frac{\rho_H(\mathbf{k}_2, M_2)}{\langle \rho \rangle} e^{i\mathbf{x}_2 \cdot [\mathbf{k}_2 - \mathbf{k}']} d^3 \mathbf{x}_1 d^3 \mathbf{x}_2 dM_1 dM_2 d^3 \mathbf{k}' \\ &\quad + (2\pi)^3 \int \left\langle \frac{dn}{dM} \right\rangle_1 \left[\frac{\rho_H(\mathbf{k}_1, M_1)}{\langle \rho \rangle} \right]^2 \delta(\mathbf{k}_1 - \mathbf{k}_2) dM_1 \end{aligned} \quad (2.29)$$

$$\begin{aligned} &= (2\pi)^6 \int P_{mm}(\mathbf{k}_1) b(M_1) \left\langle \frac{dn}{dM} \right\rangle_1 \frac{\rho_H(\mathbf{k}_1, M_1)}{\langle \rho \rangle} \delta(\mathbf{k}_1 - \mathbf{k}_2) \\ &\quad \times b(M_2) \left\langle \frac{dn}{dM} \right\rangle_2 \frac{\rho_H(\mathbf{k}_2, M_2)}{\langle \rho \rangle} dM_1 dM_2 \\ &\quad + (2\pi)^3 \int \left\langle \frac{dn}{dM} \right\rangle_1 \left[\frac{\rho_H(\mathbf{k}_1, M_1)}{\langle \rho \rangle} \right]^2 \delta(\mathbf{k}_1 - \mathbf{k}_2) dM_1. \end{aligned} \quad (2.30)$$

In the first step, we have inserted that the two-point correlation function of matter is the Fourier back transformed matter power density. Then we have factored out plane waves such that after integration over real space we are left with Dirac delta distributions, we then use them to simplify the integrals in the last step. After We factor out the remaining Dirac deltas we find the expression of the power spectrum as the sum of the one-halo and two-halo terms. The first Term is the two-halo term and is given by

$$P^{2h}(k) := P_{mm}(k) \left[(2\pi)^3 \int b(M) \left\langle \frac{dn}{dM} \right\rangle(M) \frac{\rho(\mathbf{k}, M)}{\langle \rho \rangle} dM \right]^2. \quad (2.31)$$

Its interpretation is that it is the correlation of two separate halos. The integral itself can be understood as a mean over the galaxy shapes with a small bias stemming from the fact, that very massive halos cluster much more strongly than normal matter. It is also proportional to the matter power spectrum because these halos are formed from seeds of initial matter perturbations. We infer from this that their spatial correlation is given by the matter power spectrum.

The second term is the one-halo term. It is given by

$$P^{1h}(k) := (2\pi)^3 \int \left\langle \frac{dn}{dM} \right\rangle(M) \left[\frac{\rho(\mathbf{k}, M)}{\langle \rho \rangle} \right]^2 dM. \quad (2.32)$$

In the context of galaxy clustering the interpretation of this term would be as shot noise. In this context, it is a bit more subtle as it now correlates the matter in one halo with itself. This gives it its functional dependence of ρ^2 . The integral itself can again be understood as a mean over the halo distribution such that this term becomes the mean self-correlation.

2.2 The HMCODE Implementation

Both components need firstly the Fourier transformation of the halo density profile

$$\rho_H(k, z, M) = \int e^{i\mathbf{k} \cdot \mathbf{r}} \rho_H(r, z, M) d^3 r = \int_0^{r_{\lim}} 4\pi r^2 \frac{\sin(kr)}{kr} \rho(r, z, M) dr. \quad (2.33)$$

The cutoff radius, r_{\lim} , is defined via the mass of the Halo. It is calculated by requiring that the mass enclosed by a sphere of that radius is given by

$$M = \frac{4\pi}{3} r_{\lim}^3 \Delta_H(z) \bar{\rho}, \quad (2.34)$$

where Δ_H is a density contrast, describing how much higher the halo density is than the underlying matter density of the universe $\bar{\rho}$. It was calculated in Einstein-de Sitter cosmologies that the Halo after virialization has an overdensity of ≈ 178 . To account for cosmologies with Ω_m different from one and massive neutrinos we use a fitting formula from Mead [Mead, 2016]. It is fitted to use only parameters that govern the formation of structure like the (integrated) growthrate and Ω_m . To handle massive neutrinos an additional correction factor as a function of f_ν is added to the fitting formula. To keep the fitting parameters for cosmologies with massive neutrinos and dark energy the same, the growthrates and mass fraction that enter the fitting formula are calculated in an equivalent cosmology where the massive neutrinos and the dark energy are converted to CDM and Λ respectively.

The halo density profile ρ is taken as a modified FNW [Navarro et al., 1997] profile

$$\rho(r, z, M) \propto \frac{1}{\frac{r}{r_s \nu^\eta} \left(1 + \frac{r}{r_s \nu^\eta} \right)}, \quad (2.35)$$

where the parameter ν^η is a parameter further bloating the halo shape was added. The proportionality factor in front is used to fix the mass of the halo. The parameter ν is the peak-height variable defined via

$$\nu = \frac{\delta_c(z)}{\sigma_M^{cb}(z)}. \quad (2.36)$$

The mass M defines a radius R_σ over which we calculate the variance of the smoothed field. The relation is setting the scale to the radius of a sphere of background matter density with mass M . This leads to a definition similar to r_{\lim}

$$M = \frac{4\pi}{3} R_\sigma^3 \bar{\rho}.$$

The variable δ_c is the critical overdensity that matter distributions must reach to collapse into a halo. It was computed in Einstein-de Sitter to be close to 1.686. To more accurately model spherical collapse δ_c is taken as a fitting function from [Nakamura and Suto, 1997], and modified to account for the presence of massive neutrinos through a correction factor. Similar to Δ_H the fitting formula only is a function of the (integrated) growthrate and Ω_m calculated in an equivalent cosmology in the presence of massive neutrinos and dark energy.

The parameter ν essentially quantifies how likely it is for given matter overdensities to collapse. That is why we use the variance of the CDM+baryon field to calculate it, as we know that neutrinos are not slow enough to cluster on scales of halos. It is often encountered in the context of

peak-background split formalism and spherical collapse models like the ones from Press-Schächter [Press and Schechter, 1974]. The parameter η is a free parameter in the HMCODE model and is fitted to be $\eta(z) = \mathcal{A}_\eta \times [\sigma_8^{cb}(z)]^{\alpha_\eta}$. The functional form is chosen like this because it should be a function of a parameter that describes the collapse of the halo and not just cosmological parameters.

Finally, The halo shape radius, r_s , parametrizes the radial profile of the halo density, and it is related to the boundary of the halo, r_{\lim} , via the halo concentration, c ,

$$r_{\lim} = c r_s.$$

This parameter affects the innermost structure of the halo thus affecting the matter power spectrum on the smallest scales. We take its functional form to be

$$c(M, z) = \mathcal{B} \left[\frac{1 + z_f(M, z)}{1 + z} \right] \frac{D(z_c)}{D^{\text{eqq}}(z_c)} \frac{D(z)}{D^{\text{eqq}}(z)} \quad (2.37)$$

The factor \mathcal{B} is a free constant that was fitted to the N-body simulations. The term z_f that appears in the equation is the redshift at which the halo is formed. We consider a halo of mass M to be formed when its innermost part crosses the critical density. If we then assume normal growth we find the implicit equation

$$\frac{D(z_f)}{D(z)} \sigma_{\gamma M}^{cb}(z) = \delta_c(z), \quad (2.38)$$

with the free parameter γ chosen to be 1%, defining what innermost part actually means. The formula is equivalent to asking when a smaller halo of mass γM would have formed. The redshift of formation z_f often ends up being very high, indicating, that the properties of halos are set very early in their evolution. Still in some cases z_f could end up being earlier than the redshift z . In these cases, we set $z_f = z$. The next two factors account for the effect of dark energy further modifying the dynamics of collapse. The first is an empirical correction factor that was obtained from fits of the NFW profile to N-body simulations by [Dolag et al., 2004]. The redshift of collapse z_c would be calculated similarly as z_f , but we can use that the ratio becomes constant at high redshifts and just use a high redshift of $z_c = 10$. For high redshifts z , this factor would need to vanish, as then the effect of dark energy is negligible. The second fraction was added for this purpose in HMCODE. The next ingredient to calculate the one-halo term and the two-halo term is the halo mass function, $\frac{dn}{dM}$. As we know from equation 2.7 it has to be normalized. That is why it is more convenient to use the normalized halo mass function $F(\nu, z)$. We take it as

$$F(\nu, z) d\nu = \frac{M}{\bar{\rho}} \frac{dn}{dM} dM = A \left[1 + \frac{1}{(q \nu^2)^p} \right] e^{-q \nu^2 / 2} d\nu. \quad (2.39)$$

It is a modified version of the Press Schechter function with free parameters q and p . The parameter A is calculated from the normalization. We use the standard values for these

$$p = 0.3, \quad q = 0.707, \quad A = 0.21616.$$

The final ingredient that we would need to calculate the two-halo term would be the halo mass bias. To calculate it one would need to follow the peak-background split formalism, where we assume that all matter perturbations that cross the critical overdensity collapse into halos. The bias itself asks, how much stronger more massive halos cluster and can thus be calculated from the derivative of the halo mass function with respect to the peak-height variable. In reality, we do not need the

bias to calculate the two-halo term. Like stated before the bias is a function close to unity and thus the integral that goes into the two-halo term is approximately 1, as seen in equation 2.25.

To better match simulations the final formula for the two-halo term is modified in two regards. Firstly the power spectrum in the two-halo term is replaced by a power spectrum where the wiggles of the BAO have been smoothed out to an extent. This is a well-understood effect of gravitational evolution. The exact formulation of the "de-wiggling" is a topic of current debate, but a simple approach is followed in `HMCODE`.

We start with the linear power spectrum obtained by our Boltzmann solver, P_{mm}^{lin} . We then divide it with the Eisenstein-Hu no-wiggle power spectrum approximation. We then smooth the ratio by coevolving it with a broad Gaussian filter. After multiplying again with the approximation we find the smoothed power spectrum, P_{smt} . The "de-wiggled" power spectrum is given then as a weighted sum

$$P_{\text{dw}} = e^{-g(k,z)} P_{mm}^{\text{lin}}(k, z) + (1 - e^{-g(k,z)}) P_{\text{smt}}(k, z) \quad (2.40)$$

$$g(k, z) = k^2 \frac{1}{6\pi^2} \int_0^\infty P_{mm}^{\text{lin}}(k, z) dk := k^2 \sigma_v^2(z). \quad (2.41)$$

The second modification of the two-halo spectrum is that by default it does not contain an early dip of the power spectrum that occurs in the one-loop correction in the effective field theory approach of the LSS. Its physical interpretation is that the growth of voids, in reality, is slower than predicted in linear perturbation theory and leads to an overestimate of the power spectrum on very large scales. This effect is modelled by a multiplication of the de-wiggled power spectrum with a function fitted to dampen the power spectrum by a factor $(1 - f_D)$ past a scale k_D .

The final two-halo power spectrum in `HMCODE` is given by

$$P^{2h}(k, z) = P_{\text{dw}}(k, z) \left[1 - f_D(z) \frac{k^{n_D}(z)}{k_D^{n_D}(z) + k^{n_D}} \right]. \quad (2.42)$$

The functions $k_D(z)$ and $f_D(z)$ have the same functional form as the shape parameter, $\eta(z)$, that appears in the FNW profile. We again use the variance of the CDM+baryon field in the functional form to fit as massive neutrinos should not affect the universal collapse dynamics. The parameter n_D is also a free parameter and is fitted to the N-body simulations.

The one halo term has also two modifications done to it compared to the one obtained from the halo model. Firstly in equation 2.8 we assume that halos make up the matter density contrast of the universe. Since only cold matter clusters in halos, we need to correct this and multiply the halo density profile with a factor $(1 - f_\nu)$.

The second modification we need to do is a suppression of the one halo term on large scales. It turns out that the one halo term in the standard halo model becomes constant on the largest scales, but because of energy conservation, a virialized halo should lead to a power spectrum growing with k^4 . To account for this we multiply the one halo power spectrum such that our final formula is given by

$$P^{1h}(k, z) = (1 - f_\nu)^2 (2\pi)^3 \int_0^\infty \left\langle \frac{dn}{dM} \right\rangle(M) \left[\frac{\rho(k, M)}{\langle \rho \rangle} \right]^2 dM \frac{k^4}{k_*(z)^4 + k^4}. \quad (2.43)$$

The transition wave number, k_* , is fitted to a functional form like the transition wave number of the two-halo term k_D .

A final problem of the halo model is, that it is not well suited to describe the correlation in the transition region from the one-halo term to the two-halo term. This is due to neglecting that very close halos or overlapping subhalos correlate with each other. Neglecting these effects leads to an up to 20% underestimate of the power spectrum. To better model the transition we have added a smoothing parameter $\alpha(z)$. As this parameter affects the spectral index of the power spectrum, its functional form is not a function of the variance of the CDM+baryon field but of the effective spectral index of its power spectrum, n_{eff} . To calculate it we can use the definition of the variance in real space to find

$$3 + n_{\text{eff}}(z) = - \frac{d \log \sigma_{cb}(R, z)}{d \log R}(R_c, z), \quad (2.44)$$

where R_c is defined as the radius where the standard derivation of the CDM+baryon field crosses the critical overdensity $\delta_c(z)$. The final fitting formula for α is then

$$\alpha(z) = \mathcal{A}_\alpha [\mathcal{C}_\alpha]^{n_{\text{eff}}(z)}. \quad (2.45)$$

With the transition smoothing we define our nonlinear power spectrum as

$$P_{mm}^{\text{nl}}(k, z) = \left[(P^{1h}(k, z))^{\alpha(z)} + (P^{2h}(k, z))^{\alpha(z)} \right]^{1/\alpha(z)}. \quad (2.46)$$

Chapter 3

The Photometric Probe

The second instrument of the *Euclid* mission we will cover is the photometric instrument. It is supposed to measure the galaxy shape of one billion galaxies and use redshift information from ground-based observatories to conduct a weak shearing and a galaxy clustering survey. In order to quickly measure the redshift of one billion galaxies the collaboration uses a photometric method to measure the redshift. A photometric redshift is obtained by measuring the apparent brightness magnitude in different colour bands. These color brightnesses are compared to each other leading to a redshift estimate.

The observable in this case is not the power spectrum like for the spectroscopic probe but some two-dimensional overdensity field Θ that can either correspond to the lensing map or the galaxy map. We obtain from these maps the moments a_{lm} via decomposition into spherical harmonics. Using their orthogonality relation we find

$$a_{\ell,m} = \int_{S_2} \Theta(\Omega) Y_{\ell m}^*(\Omega) d^2\Omega. \quad (3.1)$$

We can then build a vector by calculating these moments for each z bin. The final likelihood is modelled as a Gaussian where the observed spherical moments are modelled to have a zero mean and covariance C_ℓ^{th} , that can be extracted from theory. Because of the isotropy of space, the covariance matrix can not depend on the azimuth quantum number m . The covariance matrix correlates the multipoles for the same ℓ and m to the ones from different z bins. The formula for the likelihood is thus given by

$$\mathcal{L} \propto \prod_{\ell m} \left[\frac{1}{\sqrt{\det C_\ell}} \exp \left(-f_{\text{sky}} \frac{1}{2} \vec{a}_{\ell m} \cdot (C_\ell^{\text{th}})^{-1} \vec{a}_{\ell m}^* \right) \right]. \quad (3.2)$$

This expression can be further simplified by calculating an estimator of the covariance of the moments. To find the real covariance one would need to mean over different realizations of the universe but by using that the covariance is independent of m we can find

$$(C_\ell^{\text{obs}})_{ij} \approx (\hat{C}_\ell^{\text{obs}})_{ij} = \frac{1}{2\ell+1} \sum_{m=-\ell}^{\ell} (a_{\ell m})_i (a_{\ell m})_j^*. \quad (3.3)$$

After factoring out a factor $\sqrt{\det \hat{C}_\ell^{\text{obs}}}$ from the likelihood normalization we can write it using only products of $\hat{C}_\ell^{\text{obs}}$ and C_ℓ^{th} . For that, we also need to pull the product into the exponential and use the summation over m to find the estimator again. After pulling the product over ℓ into the exponential we are left with

$$\chi^2 = f^{\text{sky}} \sum_{\ell=\ell_{\min}}^{\ell_{\max}} (2\ell+1) \left[\log \left(\frac{\det \hat{C}_\ell^{\text{obs}}}{\det C_\ell^{\text{th}}} \right) + \text{Tr} \left[(C_\ell^{\text{th}})^{-1} \hat{C}_\ell^{\text{obs}} \right] - N_{\text{bin}} \right], \quad (3.4)$$

where N_{bin} is the number of redshift bins.

The structure of this chapter is the following: We will first briefly explain the basics of shearing and the shearing formalism. We will then go over how we obtain the covariance matrix from theory. Finally, we will more carefully adjust the recipe to correctly model the effect of massive neutrinos.

3.1 The Formalism of Cosmic Sheer Observations

Cosmic shearing is a very rich and deep topic where the slight deformations of galaxy shapes are traced back to the gravitational potential on the line of sight. As these potential are related to the matter perturbations $\bar{\rho}\delta$ via the Poisson equation,

$$\begin{aligned} \Delta(\Psi + \Phi) &= 8\pi G a^2 \bar{\rho} \delta \\ &= 3 H_0^2 \frac{\Omega_m}{a} \delta, \end{aligned}$$

it can be used to probe the underlying large-scale structure of the universe. The deformations are a transformation that maps angular separations in observed space $\boldsymbol{\Omega}$ to angular separations in unlensed space $\boldsymbol{\beta}$. We can then define the linear transformation A as

$$A = \frac{\partial \boldsymbol{\beta}}{\partial \boldsymbol{\Omega}} = \begin{pmatrix} 1 - \kappa - \gamma_1 & -\gamma_2 \\ -\gamma_2 & 1 - \kappa + \gamma_1 \end{pmatrix}. \quad (3.5)$$

The parameter κ is called the convergence and describes the overall change in the size of the observed shape while the parameters γ_1 and γ_2 describe the sheer or the overall rotation of the shape. Since in the context of cosmic shearing, the true sizes of galaxies are inaccessible by shape measurement alone, the real observable is the complex, reduced sheer

$$g := \frac{\gamma}{1 - \kappa}, \quad \text{with } \gamma = \gamma_1 + i\gamma_2. \quad (3.6)$$

The reduced sheer can be related to the observed ellipticity ϵ of galaxies. We define the complex ellipticity of a galaxy we can define elliptic regions of constant intensity with minor to major axis ratio b/a , and rotation angle ϕ $\epsilon = (a-b)/(a+b) \times \exp(2i\phi)$. This leads to the observed ellipticity being given by

$$\epsilon = \frac{\epsilon^2 + g}{1 + g^* \epsilon^s}, \quad (3.7)$$

where ϵ^s denotes the intrinsic ellipticity due to the random rotation of the disc-like galaxies. Typical values of the intrinsic ellipticity are in the order of $\mathcal{O}(0.1)$ with zero mean, while the reduced sheer

is typically of order $\mathcal{O}(0.01)$. By averaging over many galaxies and using that g is much smaller than ϵ^s we can find the estimator of g

$$\langle \epsilon \rangle = \left\langle \frac{\epsilon^2 + g}{1 + g^* \epsilon^s} \right\rangle \approx \langle \epsilon^s + g \rangle = g. \quad (3.8)$$

The next step is to relate the lensing parameters to each other and the metric perturbations to extract from that the overdensity field Θ . We can use that photons travel on null geodesics to find that the travel time t as

$$t = \int (1 - (\Phi + \Psi)) dr,$$

where the integration is carried out on the light path of the photon. By using that photons always take a path that minimises the travel time under slight variation we find that the deflection angle $d\alpha$ is given by

$$d\alpha = -\nabla_{\perp}(\Phi + \Psi) dr, \quad (3.9)$$

where we have denoted the derivative of the potentials perpendicular to the path with ∇_{\perp} in real coordinates. This translates into a change of comoving separation and thus a change of observation angle

$$dx = (\eta - \eta') d\alpha = -(\eta - \eta') \nabla_{\perp}(\Phi + \Psi) d\eta' \quad (3.10)$$

$$x = \eta \Omega - \int_0^\eta (\eta - \eta') [\nabla_{\perp}(\Phi + \Psi)(x(\eta'), \eta') - \nabla_{\perp}(\Phi + \Psi)(0, \eta')] d\eta', \quad (3.11)$$

where we have defined that the observed photons originated at a comoving distance η and the gravitational potential is placed at the comoving distances η' . The difficulty of this integration is, that the comoving separation of the two photon paths x appears again in the integral itself. Since the effect of the lens is assumed to be very weak, we can do a Born approximation where the zeroth order solution x^0 is inserted into the integral. This solution is the unlensed path $x^0 = \eta \Omega$. With this the matrix elements of the transformation A can be calculated to

$$A_{ij} = \delta_{ij} - \int_0^\eta \frac{(\eta - \eta') \eta'}{\eta} \frac{\partial^2}{\partial x_i \partial x_j} (\Phi + \Psi)(\eta' \Omega, \eta') d\eta'. \quad (3.12)$$

The first derivative for x_i is the component of ∇_{\perp} while the derivative for x_j appears with the factor η' due to the chain rule. Using the inverse of this chain rule, both derivatives can be pulled out of the integral to finally find the lensing potential ψ from the lensing parameters κ and γ can be calculated

$$A_{ij} := \delta_{ij} - \frac{\partial^2}{\partial \Omega_i \partial \Omega_j} \psi, \quad (3.13)$$

$$\psi := \int_0^\eta \frac{(\eta - \eta')}{\eta \eta'} (\Phi + \Psi)(\eta' \Omega, \eta') d\eta'. \quad (3.14)$$

The parameters are now calculated as

$$\begin{aligned}\kappa &= \frac{1}{2} \left[\frac{\partial^2}{\partial \Omega_1^2} + \frac{\partial^2}{\partial \Omega_2^2} \right] \psi \\ \gamma_1 &= \frac{1}{2} \left[\frac{\partial^2}{\partial \Omega_1^2} - \frac{\partial^2}{\partial \Omega_2^2} \right] \psi \\ \gamma_2 &= \frac{\partial^2}{\partial \Omega_1 \partial \Omega_2} \psi.\end{aligned}\tag{3.15}$$

The equation for the convergence parameter κ can be transformed into the Poisson equation by adding a term $\partial^2/\partial\eta^2$. The integral over the second derivative has negligible impact as the photons tend to travel on paths where the positive and negative contributions cancel out. We find

$$\begin{aligned}\kappa(\eta \boldsymbol{\Omega}, \eta) &= \frac{1}{2} \int_0^\eta \frac{(\eta - \eta')\eta'}{\eta} \underbrace{\left[\frac{\partial^2}{\partial x_1^2} + \frac{\partial^2}{\partial x_2^2} + \frac{\partial^2}{\partial \eta^2} \right]}_{=\Delta} (\Phi + \Psi)(\eta' \boldsymbol{\Omega}, \eta') d\eta' \\ &= \frac{3 H_0^2 \Omega_m}{2} \int_0^\eta \frac{(\eta - \eta')\eta'}{\eta} \frac{1}{a(\eta')} \delta(\eta' \boldsymbol{\Omega}, \eta') d\eta'.\end{aligned}\tag{3.16}$$

This equation describes how the convergence can be used as a density contrast field to calculate the spherical multipole moments. Since we still need to average over multiple galaxies in a redshift bin i , we need to convolve the convergence with the galaxy distribution n_i and find

$$\Theta_i^L(\boldsymbol{\Omega}) = \int_{\eta_{\min}}^{\eta_{\max}} n_i(\eta) \kappa(\eta \boldsymbol{\Omega}, \eta) d\eta\tag{3.17}$$

$$\begin{aligned}&= \frac{3 H_0^2 \Omega_m}{2} \int_{\eta_{\min}}^{\eta_{\max}} \int_0^\eta n_i(\eta) \frac{(\eta - \eta')\eta'}{\eta} \frac{1}{a(\eta')} \delta(\eta' \boldsymbol{\Omega}, \eta') d\eta' d\eta \\ &= \frac{3 H_0^2 \Omega_m}{2} \int_{\eta_{\min}}^{\eta_{\max}} \int_\eta^{\eta_{\max}} n_i(\eta') \frac{(\eta' - \eta)\eta}{\eta'} \frac{1}{a(\eta)} \delta(\eta \boldsymbol{\Omega}, \eta) d\eta' d\eta \\ &= \int_{z_{\min}}^{z_{\max}} \frac{1}{H(z)} \frac{3 H_0^2 \Omega_m}{2} (1+z) \eta(z) \int_z^{z_{\max}} \hat{n}_i(z') \frac{\eta(z') - \eta(z)}{\eta(z')} dz' \delta(\eta(z) \boldsymbol{\Omega}, \eta(z)) dz \\ &:= \int_{z_{\min}}^{z_{\max}} \frac{1}{H(z)} W_i^L(z) \delta(\eta(z) \boldsymbol{\Omega}, \eta(z)) dz.\end{aligned}\tag{3.18}$$

In the last step, we have defined the lensing window function W^L . Since galaxies have a gravitational effect on each other, the galaxy shapes get correlated additionally to the effect of lensing. This effect of intrinsic alignment (IA) is difficult to model such that we will treat it as a nuisance effect. In our forecast, we add to our lensing window function an additional window function W^{IA} . The exact modelling of the lensing window function is discussed after an Intermezzo about Galaxy clustering as the derivation is done similarly. We will assume that the IA density contrast is a biased tracer of the matter density contrast like for Galaxy Clustering.

We will now briefly go over the phenomenology of IA. Firstly due to IA close galaxies will have no random orientation anymore. Thus, in equation 3.8 the mean of ϵ^s does not equal zero. In reality,

when we do our averaging we would need to give close galaxies a smaller weight to lessen this effect. Another speciality about the IA is that its sign is the opposite of the lensing. It becomes apparent if one again imagines two spherical galaxy configurations, one that is in the foreground and where the galaxies are aligned due to their tidal forces. The background galaxies appear such that their shapes are aligned tangentially around the foreground galaxies. The foreground galaxy has a perpendicular alignment as the galaxies have their shapes pointing towards each other. The lensing signal is reduced overall.

Last but not least, IA is special in that its distortion of galaxy shapes does not come with a convergence κ like for shearing. One could use that to lessen the effect of the IA by checking if the convergence is enough to explain the ellipticity of the galaxies or directly using the convergence as the observable. The difficulty would be, that the convergence is inaccessible by galaxy shape measurements alone. There are some proposed methods to measure the convergence by measuring the magnification, as lensed galaxies appear brighter due to the Liouville theorem. This is not further discussed here, but it is the subject of current research.

Intermezzo: Galaxy Clustering in Angular Space

Since we can also do galaxy clustering with the photometric probe, we will do a brief revision of it's observable but this time in angular space. The idea is similar to the spectroscopic probe. We assume that the galaxy field is a biased tracer of the underlying matter field. Assuming a linear bias, we can relate the density contrast of the galaxies to the density contrast of matter

$$\delta_g(\eta \boldsymbol{\Omega}, \eta) = b(\eta) \delta(\eta \boldsymbol{\Omega}, \eta).$$

Like in the case of weak lensing, we need to average over a redshift bin i with a galaxy distribution $n_i(\chi)$. We can then expand with $H(z)$ to find a similar expression of the observable using a window function

$$\Theta_i^G(\boldsymbol{\Omega}) = \int_{\eta_{\min}}^{\eta_{\max}} n_i(\eta) \delta_g(\eta \boldsymbol{\Omega}, \eta) d\eta \quad (3.19)$$

$$\begin{aligned} &= \int_{\eta_{\min}}^{\eta_{\max}} n_i(\eta) b(\eta) \delta(\eta \boldsymbol{\Omega}, \eta) d\eta \\ &= \int_{z_{\min}}^{z_{\max}} \frac{1}{H(z)} H(z) \hat{n}_i(z) b(z) \delta(\eta \boldsymbol{\Omega}, z) dz \\ &:= \int_{z_{\min}}^{z_{\max}} \frac{1}{H(z)} W_i^G(z) \delta(\eta(z) \boldsymbol{\Omega}, \eta(z)) dz. \end{aligned} \quad (3.20)$$

This does not account for the observational effects like RSD that were discussed in the chapter about the spectroscopic probe. The modelling and implementation of these are left for future work. Nevertheless, a brief overview of this can be found in [Collaboration et al., 2023].

Continuing our modelling of IA, we use an observationally motivated model that the IA density contrast is given by

$$\delta_{\text{IA}}(\eta \boldsymbol{\Omega}, \eta) = \mathcal{A}_{\text{IA}} \mathcal{C}_{\text{IA}} \Omega_m \frac{\mathcal{F}_{\text{IA}}(\eta)}{D(\eta)} \delta(\eta \boldsymbol{\Omega}, \eta). \quad (3.21)$$

The factor \mathcal{A}_{IA} is the bias amplitude that we are going to vary in our analysis, while \mathcal{C}_{IA} is a fixed normalization. The factor $D(\eta)$ is the linear growth factor. The factor \mathcal{F}_{IA} is an extension to the standard IA model and is given by a function

$$\mathcal{F}_{\text{IA}}(z) = a(\eta)^{-\eta_{\text{IA}}} \left[\frac{\langle L \rangle(\eta)}{L_*(\eta)} \right]^{\beta_{\text{IA}}}. \quad (3.22)$$

The functions $\langle L \rangle$ and L_* denote the time-dependent mean luminosity and characteristic luminosity of galaxies respectively. The parameter β_{IA} is fixed while we vary η_{IA} around its fiducial value. We can now follow the derivation from galaxy clustering to find our window function for IA

$$W_i^{\text{IA}} = \mathcal{A}_{\text{IA}} \mathcal{C}_{\text{IA}} \Omega_m \frac{\mathcal{F}_{\text{IA}}(z)}{D(z)} H(z) \hat{n}_i(z). \quad (3.23)$$

To deal with IA we will now use this window function to modify our old lensing window function

$$W^{\text{L}}(z) \rightarrow W^{\text{L}}(z) - W^{\text{IA}}(z), \quad (3.24)$$

where we use the minus sign as the effect of IA reduces the normal shearing signal.

3.2 Extracting the Covariance from Theory

We can now do the derivation of the covariance either using the observable of lensing or clustering. In reality, there is even more information than just the two observable on their own. Since the galaxies trace the matter distribution on which the lensing occurs, there is additional information in the cross-correlation of lensing and galaxy clustering. We can calculate the correlation by taking the mean of the spherical moments of different observable. Since we deliberately chose our definitions with the window functions to be the same between both probes all elements of the covariance matrix can be calculated the same. We define $(C_\ell^{\text{XY}})_{ij} = \langle (a_{\ell m}^{\text{X}})_i (a_{\ell m}^{\text{Y}})_j \rangle$, where X and Y could either be G or L. Inserting our definitions of the observables in comoving coordinates, we find

$$(C_\ell^{\text{XY}})_{ij} = \int_{\eta_{\min}}^{\eta_{\max}} \int_{\eta_{\min}}^{\eta_{\max}} \int_{S_2} \int_{S_2} W_i^{\text{X}}(\eta) W_j^{\text{Y}}(\eta') Y_{\ell m}(\Omega) Y_{\ell m}^*(\Omega') \langle \delta(\eta \Omega) \delta(\eta' \Omega') \rangle d^2\Omega d^2\Omega' d\eta d\eta'. \quad (3.25)$$

The mean over the density contrast δ will lead to an unequal time power spectrum P . If we use the orthogonality of the spherical harmonics, we find

$$(C_\ell^{\text{XY}})_{ij} = \int_{\eta_{\min}}^{\eta_{\max}} \int_{\eta_{\min}}^{\eta_{\max}} \int_0^{k_{\max}} \frac{2k^2}{\pi} W_i^{\text{X}}(\eta) W_j^{\text{Y}}(\eta') j_\ell(\eta k) j_\ell(\eta' k) P(k, \eta, \eta') dk d\eta d\eta',$$

where the $j_\ell(x)$ are the spherical Bessel functions. We can now use that these functions are strongly centred around $x = \ell + 1/2$ and replace them with Dirac distributions. This is the so-called Limber approximation and it gives

$$j_\ell(k \eta) \approx \sqrt{\frac{\pi}{2\ell+1}} \delta \left(k \eta - (\ell + \frac{1}{2}) \right). \quad (3.26)$$

Inserting this into the definition from C_ℓ gives the full formula for the covariance

$$\begin{aligned} (C_\ell^{\text{XY}})_{ij} &= \int_{\eta_{\min}}^{\eta_{\max}} \frac{1}{\eta^2} W_i^X(\eta) W_j^Y(\eta) P_{mm} \left[k = \frac{\ell + \frac{1}{2}}{\eta}, \eta \right] d\eta \\ &= \int_{z_{\min}}^{z_{\max}} \frac{W_i^X(z) W_j^Y(z)}{\eta^2(z) H(z)} P_{mm} \left[k = \frac{\ell + \frac{1}{2}}{\eta(z)}, z \right] dz. \end{aligned} \quad (3.27)$$

To obtain the galaxy distribution per redshift bin in redshift space $\hat{n}_i(z)$ we start with the overall distribution of galaxies $\hat{n}(z)$. We model it as a polynomial with an exponential cut-off

$$\hat{n}(z) = \left(\frac{z}{z_0} \right)^2 \exp \left[- \left(\frac{z}{z_0} \right)^{1.5} \right]. \quad (3.28)$$

When there is no photometric redshift error, we could just multiply the distribution with some uniform window-picking function. The redshift error can make it that the galaxies are counted in the wrong bin which leads to a bleeding of the bins into each other. To describe this we convolve the galaxy distribution with a sum of two Gaussians

$$\begin{aligned} p(z, z') &= \frac{1 - f_{\text{out}}}{\sqrt{2\pi} \sigma_b (1+z)} \exp \left[\frac{1}{2} \left(\frac{z - c_b z' - z_b}{\sigma_b (1+z)} \right)^2 \right] \\ &\quad + \frac{f_{\text{out}}}{\sqrt{2\pi} \sigma_0 (1+z)} \exp \left[\frac{1}{2} \left(\frac{z - c_0 z' - z_0}{\sigma_0 (1+z)} \right)^2 \right]. \end{aligned} \quad (3.29)$$

The second Gaussian is there to describe the effect of strong outliers acting a bit like an overall reduction of the observable. The parameters that go into this are all fixed to experimental specifications. In the next step, we can calculate the binned galaxy distribution

$$\hat{n}_i(z) = \mathcal{N} \int_{z_i^{\min}}^{z_i^{\max}} \hat{n}(z') p(z, z') dz' \approx \int_{z_i^{\min}}^{z_i^{\max}} \hat{n}(z) p(z, z') dz', \quad (3.30)$$

where we have used, that the function $p(z, z')$ is strongly centered around $z = z'$. The integration limits are the edges of the redshift bins and the factor \mathcal{N} in front is a normalization that is calculated to be

$$\mathcal{N}^{-1} = \int_{z^{\min}}^{z^{\max}} \int_{z_i^{\min}}^{z_i^{\max}} \hat{n}(z) p(z, z') dz' dz \quad (3.31)$$

Finally, since this is a counting experiment we need to add shot noise N_{ij}^{XY} to the angular power spectrum. Since the noise of different bins and probes should be uncorrelated, we have

$$N_{ij}^{\text{GG}} = \delta_{ij} \frac{1}{\bar{n}_i}, \quad N_{ij}^{\text{LL}} = \delta_{ij} \frac{\sigma_\epsilon^2}{\bar{n}_i} \text{ and } N_{ij}^{\text{GL}} = N_{ij}^{\text{LG}} = 0, \quad (3.32)$$

where σ_ϵ^2 is the variance of measured ellipticities. The covariance is thus given by $C_{ij}^{\text{XY}} \rightarrow C_{ij}^{\text{XY}} + N_{ij}^{\text{XY}}$. To calculate the likelihood we can now construct a combined observable and covariance

$$\mathbf{a}(\ell, m) = \begin{pmatrix} a_1^L(\ell, m) \\ \vdots \\ a_{N_{\text{bin}}}^L(\ell, m) \\ a_1^G(\ell, m) \\ \vdots \\ a_{N_{\text{bin}}}^G(\ell, m) \end{pmatrix} \quad \text{and} \quad C_\ell = \begin{pmatrix} C_\ell^{LL} & C_\ell^{LG} \\ C_\ell^{GL} & C_\ell^{GG} \end{pmatrix} \quad (3.33)$$

In the likelihood formula this combined probe can be understood as one observable with twice the bins, so for multipole moments ℓ where we have both observables, we can replace N_{bin} with $2 \times N_{\text{bin}}$. When we start to cut scales due to resolution or the lack of an adequate non-linear model, we can find that both observables have different ℓ_{max} . For every summand of the likelihood with only one probe, we stick to the equation given above with the covariance of the single probe. To be able to probe higher wave numbers k we need to be able to predict the nonlinear power spectrum. To obtain our nonlinear power spectrum we use the `HMCODE` halo model that is described in chapter 2. Unlike the nonlinear prescription in the case of the spectroscopic probe, we do not need to add additional nuisance parameters to our modelling. All open parameters have already been fixed by fits to N-body simulations covering a wide range of $w_0 w_a$ CDM cosmologies with massive neutrinos.

3.3 The Effect of Massive Neutrinos

In our definition of the galaxy window function W^G due to massive neutrinos the galaxy bias becomes scale dependent. If we follow our prescription from the spectroscopic probe, we can use a scale-dependent bias by replacing the matter power spectrum with the CDM+baryon spectrum. To calculate the angular power spectrum of the galaxy clustering we then find

$$\begin{aligned} (C_\ell^{GG})_{ij} &= \int_{z_{\text{min}}}^{z_{\text{max}}} \frac{W_i^G(k, z) W_j^G(k, z)}{\eta^2(z) H(z)} P_{mm} \left[k = \frac{\ell + \frac{1}{2}}{\eta(z)}, z \right] dz. \\ &= \int_{z_{\text{min}}}^{z_{\text{max}}} \frac{H(z) \hat{n}_i(z) \hat{n}_j(z)}{\eta^2(z)} b^2(k, z) P_{mm} \left[k = \frac{\ell + \frac{1}{2}}{\eta(z)}, z \right] dz. \\ &= \int_{z_{\text{min}}}^{z_{\text{max}}} \frac{H(z) \hat{n}_i(z) \hat{n}_j(z)}{\eta^2(z)} \hat{b}^2(z) P_{cb} \left[k = \frac{\ell + \frac{1}{2}}{\eta(z)}, z \right] dz. \end{aligned} \quad (3.34)$$

After the replacement of power spectra the new scale independent bias \hat{b} is approximated as a step-like function that is constant in every bin. We can then treat the value of the bias in each bin as a free nuisance parameter and marginalize them. We can use the new bias to define a modified scale-independent window function for galaxy clustering

$$\hat{W}_i^G(z) = \hat{b}(z) \hat{n}_i(z) H(z)$$

For the sheering part of the weak lensing window function, we note that we do not need to do any modifications. The neutrinos still contribute to the lensing power spectrum $\Psi + \Phi$ even on scales where they do not cluster, thus the lensing power spectrum is not a probe of the CDM+baryon

power spectrum but of the total matter power spectrum.

For the initial alignment, the question becomes not so straightforward. Firstly the window function of IA has a growth factor in the denominator. It is scale-independent in Λ CDM but now due to massive neutrinos, it becomes scale-dependent, making the whole window function scale-dependent. The scale dependence propagates until equation 3.27, where the limber approximation replaces k by the fraction $(\ell + 1/2)/r(z)$.

The next difficulty arises when we remind ourselves of the reason, why we could write the contribution of IA as an additional term in a window function. We assumed that IA could be modelled as a biased tracer of the underlying density contrast. It is not so clear if the underlying density contrast is the total matter field or the CDM+baryon field. An argument for the latter would be that IA arises when close galaxies interact with each other. The galaxies themselves are biased tracers of the CDM+baryon field such that over-densities of that field form clusters that get populated with galaxies later on.

We still believe that the IA should be a probe of the total matter field as it is not the interaction of the halos with each other that aligns them but rather their interaction with their surrounding tidal fields. As neutrinos do contribute to the gravitational field, as seen in the Poisson equation, we stick to the total matter field.

There is still some debate on the crosscorrelation of lensing and galaxy clustering. To write the expression for this we need to start earlier in equation 3.25. When we did our derivation, in the next step we used the expectation value of the product of the density contrasts in the power spectrum. But now the subtlety that was alluded to earlier in the chapter of the spectroscopic probe comes into play. For the cross-correlation we find

$$\begin{aligned} (C_\ell^{\text{GL}})_{ij} &= \int W_i^G(\eta) W_j^L(\eta') Y_{\ell m}(\Omega) Y_{\ell m}^*(\Omega') \langle \delta(\eta \Omega) \delta(\eta' \Omega') \rangle d^2\Omega d^2\Omega' d\eta d\eta' \\ &= \int \hat{W}_i^G(\eta) W_j^L(\eta') Y_{\ell m}(\Omega) Y_{\ell m}^*(\Omega') \langle \delta_{cb}(\eta \Omega) \delta(\eta' \Omega') \rangle d^2\Omega d^2\Omega' d\eta d\eta'. \end{aligned} \quad (3.35)$$

This means that the power spectrum that enters the cross-correlation is not the matter power spectrum nor the power spectrum of CDM+baryons. To resolve this problem we use the approximation

$$\langle \delta_{cb}(\mathbf{k}) \delta(\mathbf{k}') \rangle \approx \sqrt{P_{cb}(\mathbf{k}) P_{mm}(\mathbf{k})} \delta(\mathbf{k} - \mathbf{k}'). \quad (3.36)$$

This approximation would be correct if the power spectra were linear and had scale-independent growth. The latter is approximately true as the scale-dependent growth induced from neutrinos is very small at the level of 0.4% [Euclid Collaboration: Blanchard et al., 2020]. For the first requirement, we argue that the neutrinos never become nonlinear as they are still too hot to cluster. On the scales where the matter power spectra become nonlinear the neutrino perturbations have already decayed so much that the difference between the CDM+baryon power spectrum and the total matter power spectrum is just a constant factor. This means that this approximation only starts to break down at intermediate scales around the BAO. We can use the approximation to find

$$(C_\ell^{\text{GL}})_{ij} = \int_{z^{\min}}^{z^{\max}} \frac{\hat{W}_i^G(z) W_j^L\left(k = \frac{\ell + \frac{1}{2}}{\eta(z)}, z\right)}{\eta^2(z) H(z)} \sqrt{P_{cb} P_{mm}}\left(k = \frac{\ell + \frac{1}{2}}{\eta(z)}, z\right) dz \quad (3.37)$$

The next difficulty arises when we need to predict the nonlinear CDM+baryon power spectrum. The HMCODE fit was done to predict the total matter power spectrum of cosmologies with massive neutrinos. To resolve this we remind ourselves that the power spectra are related to each other, i.e.

Survey Spec		Value
Redshift bins	N_{bin}	10
Minimum redshift	z_{\min}	0.001
Maximum redshift	z_{\max}	2.5
Redshift bin edges	$z_1^{\max}, \dots, z_5^{\max}$	0.418, 0.560, 0.678, 0.789, 0.9
Redshift bin edges	$z_6^{\max}, \dots, z_9^{\max}$	1.019, 1.155, 1.324, 1.576
Galaxy distribution redshift	z_0	0.6363
Redshift scaling	c_b	1
Redshift offset	z_b	0
photometric error	σ_0	0.05
Outlier fraction	f_{out}	0.1
Outlier redshift scaling	c_0	1
Outlier redshift offset	z_0	0.1
Outlier photometric error	σ_0	0.05
Intrinsic alignment normalization	C_{IA}	0.0134
IA nonlinear slope	β_{IA}	2.17
Elliptisity error	σ_{ϵ}	0.3
Integrated mean galaxy distribution	\bar{n}_i	3 arcmin^{-2}
Minimum multipole	ℓ_{\min}	10
Maximum multipole Lensing	ℓ_{\max}^{WL}	3000/5000
Maximum multipole Clustering	$\ell_{\max}^{\text{GCph}}$	750/1500
Sky coverage	f_{sky}	0.3636

Table 3.1: Survey specifications needed to calculate the Photometric likelihood. For the Maximum multipole ℓ_{\max} we noted two values that represent pessimistic and optimistic settings respectively.

$$P_{mm} = f_{cb}^2 P_{cb} + 2 f_{cb} f_{\nu} P_{cb \times \nu} + f_{\nu}^2 P_{\nu}, \quad (3.38)$$

where we encounter the total matter fractions f_{cb} and f_{ν} , which are not to be confused with the growth rates of these perturbations. The power spectrum $P_{cb \times \nu}$ is the cross-correlation power spectrum of neutrinos and CDM+baryons while the other two are the auto-correlation spectra that we know. Next, we note that the power spectrum of neutrinos is always linear thus we can replace it in the equation with the linear version. For the cross-correlation power spectrum, we again use our approximation, that the neutrino perturbations have already decayed so much on the nonlinear scales that we can approximate the cross-correlation power spectrum with its linear counterpart. Since we can predict the nonlinear total matter power spectrum with our halo model we can solve the equation for the nonlinear CDM+baryon power spectrum and find

$$P_{cb}(k, z) \approx \frac{1}{f_{cb}^2} [P_{mm}(k, z) - 2 f_{cb} f_{\nu} P_{cb \times \nu}^{\text{lin}} - f_{\nu}^2 P_{\nu}^{\text{lin}}]. \quad (3.39)$$

In tables 3.1 are the specifications and fiducial values needed to compute the likelihood.

Nuisance Param	Fiducial Value	Nuisance Param	Fiducial Value
b_1	1.10	b_7	1.44
b_2	1.22	b_8	1.50
b_3	1.27	b_9	1.57
b_4	1.32	b_{10}	1.74
b_5	1.36	\mathcal{A}_{IA}	1.72
b_6	1.40	η_{IA}	-0.41

Table 3.2: Fiducal values of nuisance parameters needed to calculate the Spectroscopic likelihood.

Chapter 4

The Spectroscopic Probe

One of the main two instruments of the *Euclid* mission. It is supposed to measure the redshift of galaxies to high precision and obtain from that a three-dimensional map of galaxies. One could use this map of galaxies to define a density field

$$\rho_g(\mathbf{r}) := \sum_i \delta^{(3)}(\mathbf{r} - \mathbf{r}_i), \quad (4.1)$$

where we use a Dirac-delta centred around the measured position of the galaxies \mathbf{r}_i . This is achieved by doing a long-time exposure of the galaxies and using some characteristic emission lines to measure the redshift of the galaxy. By assuming some arbitrary reference cosmology one would then translate the redshift and the angles into a position. The measurement of the redshift is much more precise than with the method of the photometric probe, but it is limited by a smaller sample size and a smaller survey volume. For the *Euclid* mission, it is planned to further bin the galaxies into four separate redshift bins with redshifts between 0.9 and 1.8. Each bin will have its separate survey volume V_i that can be approximated by multiplying the comoving volume by the planned sky fraction $f_{\text{sky}} = 0.35$.

The final likelihood is modelled as a Gaussian likelihood where the observed power spectrum P^{obs} is compared with a theoretically predicted one P^{th} :

$$\mathcal{L} \propto \exp \left[-\frac{1}{2} \sum_i \frac{1}{2V_{\mathbf{k},i}} \int_{\Delta V_{\mathbf{k},i}} \frac{(P^{\text{th}} - P^{\text{obs}})^2}{(\sigma_{P^{\text{obs}}})^2} d^3\mathbf{k} \right], \quad (4.2)$$

where the summation is done over each redshift bin. The factor $1/2$ in front of the integral stems from the fact, that we want to integrate over the entire three-dimensional \mathbf{k} -space, but we should only integrate over independent modes. Since the power spectrum is a real quantity it must have $P(\mathbf{k}) = P(-\mathbf{k})$, thus the factor is needed to account for this. $V_{\mathbf{k},i}$ is the volume of \mathbf{k} -space that each mode has and is given through

$$V_{\mathbf{k},i} := \frac{(2\pi)^3}{V_i}.$$

This chapter will be structured like this: First we will briefly explain how the observed power spectrum is extracted from the galaxy catalogue. Then we will talk about the modeling of the

predicted power spectrum. We will have a separate section to explain the effects that massive neutrinos will have on the predicted power spectrum, and explain our changes to the IST method of calculating the predicted power spectrum to more accurately describe these effects. The survey specifications needed for the calculation of the likelihood are found at the end of the chapter.

4.1 Extracting the Power Spectrum from Observation

The derivation of how to extract the matter power spectrum from observation is very close to the derivation of the halo model discussed in the section 2.1. We will thus only give the main steps and refer the reader to that section if one wants step-by-step instruction on the results. In the derivation, one needs to assume that all galaxies have the same mass and have a delta-peak density profile. The simplification is later dropped when discussing the finite resolution of the instrument. One could then extract from this density field the underlying probability density field $p_g(\mathbf{r})$. This would define a local deviation $\delta_g(\mathbf{r})$ from a homogenous distribution by factorizing out the mean number density \tilde{n} and some local detection probability $p_{\text{det}}(\mathbf{r})$:

$$p_g = \tilde{n} p_{\text{det}}(\mathbf{r}) (1 + \delta_g(\mathbf{r})). \quad (4.3)$$

This quantity is the equivalent of the distribution density contrast from section 2.1. For the *Euclid* mission we assume, that the detection probability is just a constant. For simplicity, we will assume in the following derivation a constant probability $p_{\text{det}}(\mathbf{r}) = 1$, but it should be noted, that as long as it is sufficiently constant every step could be done with a non-constant probability.

The two-point correlation function $\xi_g(\Delta\mathbf{r})$ of this quantity of the deviation is the Fourier transform of the power spectrum $P^{\text{obs}}(\mathbf{k})$:

$$\xi_g(\Delta\mathbf{r}) = \langle \delta_g(\mathbf{x}) \delta_g(\mathbf{x} + \Delta\mathbf{r}) \rangle_{\mathbf{x}} \quad (4.4)$$

$$P^{\text{obs}}(\mathbf{k}) = \int_V \xi_g(\Delta\mathbf{r}) e^{-i\mathbf{k} \cdot \Delta\mathbf{r}} d^3\Delta\mathbf{r}. \quad (4.5)$$

The quantity that will be called the one-halo term of the section 2.1 will be added later. In this case, it will be just a constant Poisson noise. The measurement of the galaxies does not give us their real comoving coordinates \mathbf{r} but the observational coordinates $\mathbf{x} = (z, \phi, \theta)$, where z is their redshift and ϕ and θ there sky angles. In observation space, we can define the power spectrum as

$$P(\mathbf{u}) := \int \xi(\Delta\mathbf{x}) e^{i\mathbf{u} \cdot \Delta\mathbf{x}} d^3\Delta\mathbf{x}, \quad (4.6)$$

where the quantity $\xi(\Delta\mathbf{x})$ is extracted similarly to $\xi_g(\Delta\mathbf{r})$. Using this observed power spectrum we can then derive the likelihood

$$\mathcal{L} \propto \exp \left[-\frac{1}{2} \sum_i \frac{1}{2V_{u,i}} \int \frac{(P^{\text{th}}(\mathbf{u}) - P(\mathbf{u}))^2}{(\sigma_P)^2} d^3\mathbf{u} \right]. \quad (4.7)$$

$V_{x,i}$ is the unitless volume of a redshift bin in observation space. Since the calculation of the observed power spectrum is not done in observation space but in real space, we need to translate the quantities in the likelihood, for this, we need to assume a reference cosmology, the effects of

choosing this are discussed later below. To translate from observation space to comoving space we can use the transformation of measures

$$\begin{aligned} dr_{\parallel} &= \frac{c}{H(z)} dz \\ dr_{\perp} &= (1+z) D_A(z) d\theta, \end{aligned} \quad (4.8)$$

where the subscripts \parallel and \perp stand for the component parallel and orthogonal to the line of sight respectively. This directly tells us how to translate V_x into V by doing the variable transformation

$$V_x \approx \frac{H(\bar{z})V}{c(1+\bar{z})^2 D_A(\bar{z})^2},$$

where \bar{z} denotes the center of a redshifts bin.

Since we work with binned redshifts z and in a flat sky approximation, the typical separations Δx are small, such that we can approximate the transformation also for the coordinate separations to find

$$\Delta r_{\parallel} = \frac{c}{H(\bar{z})} \Delta x_{\parallel} \quad (4.9)$$

$$\Delta r_{\perp} = (1+\bar{z}) D_A(\bar{z}) \Delta x_{\perp} \quad (4.10)$$

The conjugated variables for Δr and Δx \mathbf{k} and \mathbf{u} respectively should scale inversely. This leads to the transformation of the measure

$$d^3\mathbf{k} = \frac{1}{c(1+\bar{z})^2} \frac{H(\bar{z})}{(D_A(\bar{z}))^2} d^3\mathbf{u}. \quad (4.11)$$

we can use the transformation from observation space to real space we find how the power spectra are related:

$$P^{\text{obs}}(\mathbf{k}) = c(1+\bar{z})^2 \frac{(D_A(\bar{z}))^2}{H(\bar{z})} P(\mathbf{u}). \quad (4.12)$$

When doing the standard FKP method of extracting an estimator of the two-point correlation and power spectrum one finds that the error σ_P is given by

$$\sigma_P^2(\mathbf{u}) = \frac{(2\pi)^3}{V_x V_u} P(u)^2. \quad (4.13)$$

Finally, the resolution of the instrument is finite the angles and redshifts have some error associated with them σ_z and σ_{θ} respectively. This makes it, that the galaxy density in real space is no longer a summation over Dirac-deltas but over Gaussians. In Fourier space, the power spectrum is then suppressed by a Gaussian such that

$$\begin{aligned} P(k, z) &\rightarrow P(k, z) \exp \left[-\sigma_{\parallel}^2 k_{\parallel}^2 - \sigma_{\perp}^2 k_{\perp}^2 \right] := q_{\sigma}(k, \mu, z) P(k, z) \quad \text{where} \\ \sigma_{\parallel} &= \frac{c}{H} \sigma_z \quad \text{and} \quad \sigma_{\perp} = (1+z) D_A \sigma_{\theta}. \end{aligned} \quad (4.14)$$

The final formula is this simple as the Fourier transform of a Gaussian is again a Gaussian. This leaves us with the equivalent quantity to the two-halo term from chapter 2. The relation of this to the bias is discussed in the next section. Finally, we can add the one-halo term to this. But its interpretation is quite different, since the galaxy count is a counting experiment, we can identify it as shot noise. The contribution is exactly like for Poisson noise such that for each bin we add

$$P(k, z) \rightarrow P(k, z) + 1/n_i^{\text{ref}}, \quad (4.15)$$

where n_i^{ref} is the mean number density of galaxies in the redshift bin i calculated at the reference cosmology.

If we insert everything now into the likelihood we find that

$$\mathcal{L} \propto \exp \left[-\frac{1}{2} \sum_i \frac{V_i}{2(2\pi)^3} \int_{\Delta V_{k,i}} \frac{(P^{\text{th}}(\mathbf{k}) - P^{\text{obs}}(\mathbf{k}))^2}{(P^{\text{th}}(\mathbf{k}))^2} d^3k \right]. \quad (4.16)$$

In the next step, we can use, that the power spectrum can only be a function of the modulus of the wave vector $k := \|\mathbf{k}\|$ as well as the angle between the line of sight $\hat{\mathbf{n}}$ and the wave vector $k\mu := \mathbf{k} \cdot \hat{\mathbf{n}}$. We can use this to integrate over the azimuth angle of the wave vector and find that the likelihood is given by

$$\mathcal{L} \propto \exp \left[-\frac{1}{2} \sum_i \frac{V_i}{8\pi^2} \int_{k_{\min}}^{k_{\max}} \int_{-1}^1 k^2 \frac{(P^{\text{th}}(k, \mu) - P^{\text{obs}}(k, \mu))^2}{(P^{\text{th}}(k, \mu))^2} d\mu dk \right]. \quad (4.17)$$

It should be noted, that the quantities k and μ are very much still dependent on the reference cosmology. When we do an MCMC what would happen, is that we calculate the theoretical power spectrum $P^{\text{th}}(k, \mu)$ that is predicted by some other cosmology that we will call sample cosmology. We then use the likelihood to test how likely it is to measure the observed data given the sample cosmology. But since all the integration is done in the reference cosmology we need to account for that during the transformation from observation space to real space, described by equations 4.8 as well as when we translate the power spectrum from \mathbf{u} -space to \mathbf{k} -space 4.12. This leads to the equations describing the *Alcock-Paczynski* effect. The components of the wave vector parallel and orthogonal to the line of sight are transformed into

$$\begin{aligned} k_{\parallel}^{\text{smp}} &:= k^{\text{smp}} \mu^{\text{smp}} = \frac{H^{\text{smp}}(z)}{H^{\text{ref}}(z)} k^{\text{ref}} \mu^{\text{ref}}, \\ k_{\perp}^{\text{smp}} &:= k^{\text{smp}} \sqrt{1 - (\mu^{\text{smp}})^2} = \frac{D_A^{\text{ref}}(z)}{D_A^{\text{smp}}(z)} k^{\text{ref}} \sqrt{1 - (\mu^{\text{ref}})^2}, \\ P^{\text{smp}}(k^{\text{ref}}, \mu^{\text{ref}}) &= \left(\frac{D_A^{\text{ref}}(z)}{D_A^{\text{smp}}(z)} \right)^2 \frac{H^{\text{smp}}(z)}{H^{\text{ref}}(z)} P^{\text{smp}}(k^{\text{smp}}, \mu^{\text{smp}}), \end{aligned} \quad (4.18)$$

where we have used the index 'smp' to note quantities calculated in the sample cosmology and ref for quantities calculated in the reference cosmology. This can be used to find equations describing the transformation of k and μ to find the final equations

$$k^{\text{smp}} = k^{\text{ref}} \sqrt{\left[\frac{H^{\text{smp}}(z)}{H^{\text{ref}}(z)} \mu^{\text{ref}} \right]^2 + \left[\frac{D_A^{\text{ref}}(z)}{D_A^{\text{smp}}(z)} \sqrt{1 - (\mu^{\text{ref}})^2} \right]^2} \quad \text{and}$$

$$\mu^{\text{smp}} = \mu^{\text{ref}} \frac{H^{\text{smp}}(z)}{H^{\text{ref}}(z)} \sqrt{\left[\frac{H^{\text{smp}}(z)}{H^{\text{ref}}(z)} \mu^{\text{ref}} \right]^2 + \left[\frac{D_A^{\text{ref}}(z)}{D_A^{\text{smp}}(z)} \sqrt{1 - (\mu^{\text{ref}})^2} \right]^2}^{-1}. \quad (4.19)$$

Using these transformations we can write now the effective χ^2 only using functions of the reference cosmology

$$\chi^2 = \sum_i \int_{k_{\min}}^{k_{\max}} \int_{-1}^1 \frac{V_i k_{\text{ref}}^2}{8\pi^2} \frac{(q_{\parallel} q_{\perp}^2 P_{\text{smp}}^{\text{th}}(k^{\text{smp}}(k^{\text{ref}}, \mu^{\text{ref}}, \bar{z}_i), \mu^{\text{smp}}(\mu^{\text{ref}}, \bar{z}_i), \bar{z}_i) - P_{\text{ref}}^{\text{obs}}(k^{\text{ref}}, \mu^{\text{ref}}, \bar{z}_i))^2}{(q_{\parallel} q_{\perp}^2 P_{\text{smp}}^{\text{th}}(k^{\text{smp}}(k^{\text{ref}}, \mu^{\text{ref}}, \bar{z}_i), \mu^{\text{smp}}(\mu^{\text{ref}}, \bar{z}_i), \bar{z}_i))^2} d\mu^{\text{ref}} dk^{\text{ref}},$$

where we have defined the redshift dependent parameters $q_{\parallel} := H^{\text{smp}}/H^{\text{ref}}$ and $q_{\perp} := D_A^{\text{ref}}/D_A^{\text{smp}}$.

A Footnote about Units

When working in cosmology there are two different units we use for the wave number k , you could either pass it with units Mpc^{-1} or $h \text{ Mpc}^{-1}$. There are arguments to use that specific unit in both cases but one consequence of the second way of doing it, is that now the value of the wave number is dependent on the value of the observable h . This has the following effect: If we use the units with h then the integration in the likelihood is done over k^{ref} in $h^{\text{ref}} \text{ Mpc}^{-1}$. The wave number of the sample cosmology k^{smp} would still be in units $h^{\text{smp}} \text{ Mpc}^{-1}$. To fix this we need to do a substitution of $k^{\text{smp}} \rightarrow k' = \frac{h^{\text{ref}}}{h^{\text{smp}}} k^{\text{smp}}$, fixing the unit of the integration variable to the unit in the reference cosmology and multiplying a factor $h_{\text{smp}} h_{\text{ref}}^{-1}$ in front of $P_{\text{smp}}^{\text{th}}$. By absorbing the substitution in equations 4.18 we find the modified equation

$$k'_{\text{smp}} = k_{\text{ref}} \frac{h_{\text{smp}}}{h_{\text{ref}}} \sqrt{q_{\perp}^2 + (q_{\parallel}^2 - q_{\perp}^2) \mu_{\text{ref}}^2}$$

$$\mu'_{\text{smp}} = k_{\text{ref}} q_{\parallel} \sqrt{q_{\perp}^2 + (q_{\parallel}^2 - q_{\perp}^2) \mu_{\text{ref}}^2}^{-1}.$$

Also, the unit of the power spectrum could be either Mpc^3 or $\text{Mpc}^3 h^{-3}$. Again the second choice has the effect that when we compare the power spectra the units do not match. One would need to absorb this unit change again by multiplying $P_{\text{smp}}^{\text{th}}$ with a factor $h_{\text{ref}}^3 h_{\text{smp}}^{-3}$. In the final likelihood choose the units of k^{ref} to be $h \text{ Mpc}^{-1}$ while the unit of the power spectrum is Mpc^3 such that the formula for the effective χ^2 is given as

$$\chi^2 = \sum_i \int_{k_{\min}}^{k_{\max}} \int_{-1}^1 \frac{V_i k_{\text{ref}}^2}{8\pi^2} \frac{(q_{\parallel} q_{\perp}^2 \frac{h^{\text{smp}}}{h^{\text{fid}}} P_{\text{smp}}^{\text{th}}(k'_{\text{smp}}, \mu'_{\text{smp}}, \bar{z}_i) - P_{\text{ref}}^{\text{obs}}(k^{\text{ref}}, \mu^{\text{ref}}, \bar{z}_i))^2}{(q_{\parallel} q_{\perp}^2 \frac{h^{\text{smp}}}{h^{\text{fid}}} P_{\text{smp}}^{\text{th}}(k'_{\text{smp}}, \mu'_{\text{smp}}, \bar{z}_i))^2} d\mu^{\text{ref}} dk^{\text{ref}}. \quad (4.20)$$

4.2 Extracting the Power Spectrum from Theory

For the calculation of the likelihood, we will compare the observed power spectrum and a power spectrum that we calculate from theoretical modelling. Since we have no real data yet, for the forecast we will use the same recipe that we use to calculate the theoretical power spectrum for the observed power spectrum. For this, we will choose some fiducial cosmology and let it coincide with the reference cosmology for simplicity.

The power spectrum of galaxies is assumed to be a tracer of the matter power spectrum. In the most naive way, we say that the density contrast of galaxies is related to the density contrast of matter via a linear bias b , just like we did in the halo model. We can thus write

$$\delta_g(k, z) = b(z, k) \delta(k, z).$$

Calculating the variance of this on both sides extracts the power spectrum, and finds that the bias just factors out to find

$$P_g(k, z) = b^2(z, k) P_{mm}(k, z). \quad (4.21)$$

If we assume the bias to be scale independent (which is known to be good in cosmologies without massive neutrinos and on small intermediate scales) we could treat the bias as one free parameter for each redshift bin and in the end marginalize over it. The matter power spectrum at the scales where the instrument is sensitive begins to deviate from the linear power spectrum predicted by the linear perturbation theory. This is also discussed in chapter 2, but the effect of this is that the baryonic acoustic oscillations are damped by the individual k -modes interacting with each other. To model this we use the prescription of [Euclid Collaboration: Blanchard et al., 2020], which "de-wiggles" the power spectrum by taking a weighted sum of the linear power spectrum P_{mm}^{lin} and a "no-wiggle" power spectrum P_{nw}

$$P_{mm}(k, \mu, z) = P_{mm}^{\text{lin}}(k, z) e^{-g} + P_{nw}(k, z) (1 - e^{-g}) \quad (4.22)$$

$$g(k, \mu, z) = \sigma_v(z)^2 \left(k_{\perp}^2 + k_{\parallel}^2 (1 + f^{\text{fid}}(z))^2 \right). \quad (4.23)$$

The parameter $\sigma_v(z)$ is again a nuisance parameter that describes the velocities of the galaxies on large scales. It can be thus modelled as the variance of the velocity divergence field, which on linear scales is given as an integral over the matter power spectrum. As this is very much open for debate, in the final forecast we will vary σ_v and use the value inferred from the integral as our fiducial value

$$[\sigma_v^{\text{fid}}]^2 = \frac{1}{6 \pi^2} \int_{k_{\min}}^{k_{\max}} P_{mm}^{\text{lin}}(k, z) dk. \quad (4.24)$$

In the formula of the de-wiggling weight g , we have also fixed the linear growth rate $f(z)$ to its fiducial value. This is done such that the modelling of the de-wiggling weight is not cosmology-dependent and thus does not lead to further constraining power. To obtain the "no-wiggle" spectrum we apply a *Savitzky-Golay* filter to the linear spectrum. Notice the similarity between the calculation of the de-wiggled power spectrum in `HMCODE` to the calculation presented in this section. At the fiducial, the only difference is the addition of the factor f in the exponential and the numeric calculation of the "no-wiggle" spectrum.

This is further modified by other observational effects that we have discussed like the *Alcock-Paczynski*-effect and the finite resolution of the instrument. One effect we have not discussed yet is

redshift space distortions (RSD). These stem from the fact, that the redshift inferred from galaxies is not only of cosmological origin but also part of it is from their particular velocities. The effect can be described by the following example: Imagine two mass points in space moving towards each other due to their attractive force. The point that is further away from the observer will have its projected velocity towards the observer and thus appear to have a smaller redshift. Since the opposite is true for the point closer to the observer the points will move towards each other in redshift space. If the collapse is slow enough, this would lead to an overall amplification of the power spectrum, as the points look like they are closer to each other. The effect is strongest when the two points align with the line of sight and vanishes when they are perpendicular to the line of sight, thus the function describing this effect has to be a function of μ^2 . The effect would also be proportional to the clustering parameter ¹ $\sigma_8 f$ to have these spherically collapsing matter distributions. As the observation is done in redshift space we multiply the redshift space power spectrum with the Kaiser correction factor

$$q_{\text{RSD}} = (b(z) + f(z) \mu^2)^2. \quad (4.25)$$

To find the clustering parameter, which is better constrained by clustering experiments, we expand with σ_8 and find

$$q_{\text{RSD}} = (b(z)\sigma_8(z) + f(z)\sigma_8(z) \mu^2)^2 \frac{1}{\sigma_8^2(z)}.$$

The combination $b\sigma_8$, or to be more precise the log of this parameter, is varied as a nuisance parameter in the forecast for each bin.

If the matter points happen to approach each other very quickly, then at some point in observation space the point further away in real space will have a smaller redshift than the closer one. This effect is called the "fingers of god" (FOG) effect, as spherically collapsing matter distribution can end up looking like very elongated ellipses. As the two points look like they would be further away, the overall power spectrum will be reduced. The effect should have the same angle dependence, should be stronger on smaller, more non-linear, scales and again be stronger in stronger clustering cosmologies. One possible parametrization of this effect is given as

$$q_{\text{FOG}} = \frac{1}{1 + [f^{\text{fid}}(z) \sigma_p(z) k \mu]^2}. \quad (4.26)$$

The parameter σ_p describes the variance of the peculiar velocities of the galaxies and is again modelled as an integral over the linear velocity divergence power spectrum. As this is again a source of theoretical modelling uncertainty we will fix f to its fiducial value and vary σ_p . The fiducial value of σ_p is chosen to coincide with σ_v

$$\sigma_p^{\text{fid}} = \sigma_v^{\text{fid}}. \quad (4.27)$$

Finally, we add some additional shot noise P_i^{shot} for each bin as an additional nuisance parameter. Our final model for the power spectrum of some cosmology evaluated at the fiducial cosmology is thus

¹More often the term clustering parameter refers to the parameter $S_8 = \sqrt{\Omega_m/0.3} \sigma_8$ and not the combination $f \sigma_8$. These two quantities are very similar to each other as in Λ CDM the growth rate can be approximated as $f \approx \Omega_m^\gamma$ with $\gamma = 0.55$. When looking at the 2-D couture of similar galaxy clustering experiments we see that the definition with $\gamma = 0.55$ describes the degeneracy in the $\sigma_8-\Omega_m$ plane better than $\gamma = 0.5$, so we will continue calling it the clustering parameter $f \sigma_8$.

$$\begin{aligned}
P^{\text{th}}(k^{\text{fid}}, \mu^{\text{fid}}, z_i) &= q_{\parallel} q_{\perp}^2 q_{\text{RSD}} q_{\text{FOG}} q_{\sigma} P_{mm} + \frac{1}{n_i^{\text{fid}}} + P_i^{\text{shot}} \\
&= \left[\frac{H(z_i)}{H^{\text{fid}}(z_i)} \left[\frac{D_A^{\text{fid}}(z_i)}{D_A(z_i)} \right]^2 \frac{(b_i \sigma_8(z_i) + f(z_i) \sigma_8(z_i) \mu^2)^2}{1 + [f^{\text{fid}}(z_i) \sigma_p(z_i) k \mu]^2} \right. \\
&\quad \times \exp \left[-\sigma_{\parallel}^2 k^2 \mu^2 - \sigma_{\perp}^2 k^2 (1 - \mu^2) \right] \frac{P_{mm}(k, z)}{\sigma_8^2(z)} \\
&\quad \left. + \frac{1}{n_i^{\text{fid}}} + P_i^{\text{shot}} \right] \frac{H^{\text{ref}}}{c [(1 + z_i) D_A^{\text{ref}}]^2} ,
\end{aligned} \tag{4.28}$$

where we have left away the arguments $k(k^{\text{fid}}, \mu^{\text{fid}}, z_i)$ and $\mu = \mu(\mu^{\text{fid}}, z_i)$. We also note that the factor $H^{\text{ref}}/c [(1 + z_i) D_A^{\text{ref}}]^2$, that converts the power spectrum from real space to redshift space, cancels out in the final likelihood but is here for completeness's sake.

4.3 The Effect of Massive Neutrinos

The main sources of this section are the papers [Raccanelli et al., 2018] and [Vagnozzi et al., 2018] which I will cite throughout. One assumption we made in the last section was that the galaxy bias b would be scale-independent. The reason this can not be true is that since the neutrinos become free streaming at some scale they contribute to the power spectrum like CDM at large scales and do not contribute to the matter power spectrum on small scales. This adds an overall scale dependence to the bias as now there is a scale at which the content of the clustered matter changes.

One method of getting rid of the scale dependence in the bias is to understand what this bias is describing. It is a light-to-mass bias meaning that it associates some matter distortion for each galaxy or halo observed. Since these structures are much smaller than the free streaming scale, they are tracers not of the total matter spectrum P_{mm} , but the power spectrum of CDM+baryons P_{cb} . It has been shown in [Villaescusa-Navarro et al., 2014] and the follow-up papers thereof, that by using the CDM+baryon power spectrum the bias is again scale-independent large scales. In real space, we can write

$$\begin{aligned}
P_g(k) &= b^2(k, z) P_{mm}(k, z) = \hat{b}^2(z) P_{cb}(k, z), \\
\hat{b}(z) &:= b(k, z) \frac{T_{mm}(k, z)}{T_{cb}(k, z)},
\end{aligned} \tag{4.29}$$

where we used the transfer function T_{mm} and T_{cb} . We define the bias with the transfer functions and not with the power spectra as the bias originally connects the density contrasts and not the power spectra. The difference is a bit subtle but will become apparent in section 3.3 when we discuss the neutrino effect in the photometric probe.

In the presence of RSD, we have to modify the Kaiser correction factor to account for the change from the matter power spectrum to the CDM+baryon power spectrum. The factor becomes

$$q_{\text{RSD}} = \left(\hat{b}(z) + f_{cb}(z, k) \mu^2 \right)^2. \tag{4.30}$$

We can notice two changes here, first the aforementioned change from b to \hat{b} and the change from the growth rate f to the related quantity f_{cb} . It is calculated exactly like f but using the growth of the CDM+baryon perturbations. To again find the clustering parameter of the CDM+baryon distribution we also have to multiply with the quantity σ_8^{cb} that is calculated again using the CDM+baryon power spectrum. The reason is simple, if we remind ourselves of the definition of σ_R to be the variance of perturbations that are smoothed in real space over balls of radius R . We argued that the Kaiser correction should be a function of $f\sigma_8$ as this combination describes the clustering of the matter distribution. Now we want to see how much the CDM+baryon clusters, so we want to smooth the CDM+baryon field and find that this has to be proportional to σ_8^{cb} . This finally leads to

$$q_{\text{RSD}} = \left(\hat{b}(z) \sigma_8^{cb}(z) + f_{cb}(z, k) \sigma_8^{cb}(z) \mu^2 \right)^2 \frac{1}{(\sigma_8^{cb}(z))^2}.$$

The FOG effect remains unchanged. It could be argued that in order to describe again the effect of the redshift space distortions we should change the fiducial value of $f\sigma_p$ to quantities computed using the CDM+baryon power spectrum. We decided to keep them though, since the effect of the FOG is coming from random peculiar velocities of the individual halos towards each other. As the velocities are related to the gravitational potential inside these structures by the Virial theorem the effect of the neutrinos should still apply. Thus, we stick to the prescription with the quantities calculated using the total matter distribution.

Again an open question would be how to correctly calculate the non-linear power spectrum. We decide to stick to the method of de-wiggling and the question becomes if we want to change the fiducial values to use quantities calculated with the CDM+baryon power spectrum in the weight g . We decided against this. The physical effect of de-wiggling comes from large-scale flows of the matter structures and is thus related to the underlying gravitational potential. As the neutrinos still contribute to the potential we stick to the quantities calculated with the total matter power spectrum.

The other factors do not depend on the power spectrum and are kept like before. The final power spectrum we use to more robustly describe the effect of massive neutrinos is given as

$$\begin{aligned} P^{\text{th}}(k^{\text{fid}}, \mu^{\text{fid}}, z_i) = & \left[\frac{H(z_i)}{H^{\text{fid}}(z_i)} \left[\frac{D_A^{\text{fid}}(z_i)}{D_A(z_i)} \right]^2 \frac{\left(\hat{b}_i \sigma_8^{cb}(z_i) + f^{cb}(z_i) \sigma_8^{cb}(z_i) \mu^2 \right)^2}{1 + [f^{\text{fid}}(z_i) \sigma_p(z_i) k \mu]^2} \right. \\ & \times \exp \left[-\sigma_{\parallel}^2 k^2 \mu^2 - \sigma_{\perp}^2 k^2 (1 - \mu^2) \right] \frac{P_{mm}(k, z)}{(\sigma_8^{cb}(z))^2} \\ & \left. + \frac{1}{n_i^{\text{fid}}} + P_i^{\text{shot}} \right] \frac{H^{\text{ref}}}{c \left[(1 + z_i) D_A^{\text{ref}} \right]^2} . \end{aligned} \quad (4.31)$$

In tables 4.1 and 4.2 are the specifications and fiducial values needed to compute the likelihood.

Nuisance Param	Fiducial Value	Nuisance Param	Fiducial Value
$\log(\hat{b}\sigma_8^{cb})_1$	-0.3270	$\sigma_p(z_1)$	5.2554
$\log(\hat{b}\sigma_8^{cb})_2$	-0.3128	$\sigma_p(z_2)$	4.8287
$\log(\hat{b}\sigma_8^{cb})_3$	-0.3087	$\sigma_p(z_3)$	4.4606
$\log(\hat{b}\sigma_8^{cb})_4$	-0.3186	$\sigma_p(z_4)$	4.0677
P_1^{shot}	0	$\sigma_v(z_1)$	5.2554
P_2^{shot}	0	$\sigma_v(z_2)$	4.8287
P_3^{shot}	0	$\sigma_v(z_3)$	4.4606
P_4^{shot}	0	$\sigma_v(z_4)$	4.0677

Table 4.1: Fiducial values of nuisance parameters needed to calculate the Spectroscopic likelihood.

Survey Spec	Value	Survey Spec	Value
\bar{n}_1	$6.68 \cdot 10^{-4} h^3 \text{ Mpc}^{-3}$	$[z_{\min}, z_{\max}]_1$	[0.9, 1.1]
\bar{n}_2	$5.58 \cdot 10^{-4} h^3 \text{ Mpc}^{-3}$	$[z_{\min}, z_{\max}]_2$	[1.1, 1.3]
\bar{n}_3	$4.21 \cdot 10^{-4} h^3 \text{ Mpc}^{-3}$	$[z_{\min}, z_{\max}]_3$	[1.3, 1.5]
\bar{n}_4	$2.61 \cdot 10^{-4} h^3 \text{ Mpc}^{-3}$	$[z_{\min}, z_{\max}]_4$	[1.5, 1.8]
σ_θ	0	z_1	1.0
σ_z	0.001	z_2	1.2
k_{\min}	$0.001 h\text{Mpc}^{-1}$	z_3	1.4
k_{\max}	$(25/30) h\text{Mpc}^{-1}$	z_4	1.65

Table 4.2: Survey specifications needed to calculate the Spectroscopic likelihood. For k_{\max} we noted two values that represent pessimistic and optimistic settings respectively.

Chapter 5

Methodology

The main goal of a forecast is to figure out how well some experiment will be able to measure some set of parameters. In our case, the experiment will be the different probes of the *Euclid* mission while the parameters that we want to measure are cosmological parameters. For this, we generate some fake data that the experiment could have measured given an underlying fiducial model of the universe, free parameters that show up in our modelling of the data, and the different survey specifications.

The two main methods of forecasting we will deploy in this work are the Markov chain Monte Carlo (MCMC) method and the Fisher Information (FI) method. They are both based in the framework of Bayesian statistics as they are methods of obtaining the posterior distributions, i.e. the probability, $p(\boldsymbol{\theta}|\mathbf{D})$, of observing the model parameters, $\boldsymbol{\theta}$, given the data, \mathbf{D} . The posterior is really what we are after, from it we can extract the mean and the measurement uncertainties of the model parameters. We can group all of our model parameters into 3 groups, cosmological parameters, nuisance parameters, and fixed parameters. While cosmological parameters are really what we are after the nuisance parameters show up during modelling and represent uncertainties in the modelling of the observed data or the observation process itself. In the end, they are not of interest to us, so we often only look at the marginal posterior. That is the posterior when the different values of nuisance parameters have been integrated over, i.e.

$$p(\boldsymbol{\theta}_c|\mathbf{D}) = \int p(\boldsymbol{\theta}|\mathbf{D}) d\boldsymbol{\theta}_n \quad (5.1)$$

In this work, we will employ Bayesian statistics, where the posterior is related to the likelihood, \mathcal{L} , i.e. the probability of measuring the data given the parameters. For this we employ the central theorem of Bayesian statistics called the Bayes' theorem. It reads

$$p(\boldsymbol{\theta}|\mathbf{D}) = \frac{p_{\text{prior}}(\boldsymbol{\theta})}{E_{\text{evidence}}(\mathbf{D})} \mathcal{L}(\mathbf{D}|\boldsymbol{\theta}). \quad (5.2)$$

The prior encompasses all of our previous knowledge. It could be either an experimental prior when there was already a measurement of the model parameter done in the past, or it is a theoretical prior. A theoretical prior tells us that the theory requires parameters to be within some bounds, this could be for example the requirement that the neutrino mass is higher than zero or that there are more than zero neutrino species.

The Evidence can be understood as the normalization of the likelihood function. It is not accessible with MCMC methods or FI methods, so we will not go into further details of its interpretation. We just want to note that it is used when comparing different models to explain the same data. If we obtain the Evidence its value represents the goodness of the fit while also punishing adding additional parameters.

In the next sections, we will very briefly go over the two different forecasting methods.

5.1 The Markov Chain Monte Carlo Method

If we wanted to get the posterior from the likelihood we could just use the equation 5.1. In reality, this is not feasible as most cosmological problems do not have analytical solutions. Even the most simple problems like comoving distances have no analytical expression once you add dark energy into the mix. This is why we resort to numerical methods like the MCMC method. In this method the goal is to obtain a sequence of random variables, we call them $\{\boldsymbol{\theta}_i | i = 1, \dots, N\}$. In our case, these variables will be a vector of our model parameters, but the idea is much more general. When this sequence or chain is marcovian it can be shown that the distributions of the random variables converge to the distributions of the parameters, i.e. the posterior. The requirement Marcovian means that each element of the chain has a probability that is only a function of the last element of the chain.

There are different algorithms to generate such a chain but the simplest one and the one that we use in this work is the Metropolis-Hastings algorithm. The Metropolis-Hastings algorithm starts with a random point in parameter space that is our first chain element $\boldsymbol{\theta}_1$. It then proposes a new point $\boldsymbol{\theta}'$. For the proposal of the new point, we typically use some multivariate Gaussian that was our initial guess of the distributions of the parameters $\boldsymbol{\theta}$. We denote the distribution that we sample the point from as $q(\boldsymbol{\theta}'|\boldsymbol{\theta}_1)$.

This new point is then accepted with an acceptance probability

$$A(\boldsymbol{\theta}_1 \rightarrow \boldsymbol{\theta}') = \min \left(1, \frac{\mathcal{L}(\mathbf{D}|\boldsymbol{\theta}')}{\mathcal{L}(\mathbf{D}|\boldsymbol{\theta}_1)} \frac{q(\boldsymbol{\theta}_1|\boldsymbol{\theta}')}{q(\boldsymbol{\theta}'|\boldsymbol{\theta}_1)} \right). \quad (5.3)$$

The next element of the chain becomes then either $\boldsymbol{\theta}'$ or stays $\boldsymbol{\theta}_1$ with a probability given by the acceptance probability. This procedure is then iterated until the element of the chain have converged to follow a static distribution.

When the distribution of points, $\pi(\boldsymbol{\theta})$, has become static, the probabilities of going from one point to another need to fulfil the condition of reversibility. This means that the points fulfil

$$\pi(\boldsymbol{\theta}') P(\boldsymbol{\theta}' \rightarrow \boldsymbol{\theta}) = \pi(\boldsymbol{\theta}) P(\boldsymbol{\theta} \rightarrow \boldsymbol{\theta}'), \quad (5.4)$$

where P denotes the transition probability of going from one point to the other. This condition is called detailed balance and is an expression of the condition that equilibrium states should not change under time reversal.

If we use our acceptance probability and the suggestion probability to calculate the transition probability we find

$$\pi(\boldsymbol{\theta}') q(\boldsymbol{\theta}|\boldsymbol{\theta}') A(\boldsymbol{\theta}' \rightarrow \boldsymbol{\theta}) = \pi(\boldsymbol{\theta}) q(\boldsymbol{\theta}'|\boldsymbol{\theta}) A(\boldsymbol{\theta} \rightarrow \boldsymbol{\theta}'). \quad (5.5)$$

Next we realize that either $A(\boldsymbol{\theta}' \rightarrow \boldsymbol{\theta}) = 1$ or $A(\boldsymbol{\theta} \rightarrow \boldsymbol{\theta}') = 1$ as the fraction on the right side of equation 5.3 is reciprocal under the exchange of the states. Without loss of generality we chose that

$A(\boldsymbol{\theta}' \rightarrow \boldsymbol{\theta}) = 1$ this leads to

$$\begin{aligned} \pi(\boldsymbol{\theta}') q(\boldsymbol{\theta}|\boldsymbol{\theta}') &= \pi(\boldsymbol{\theta}) q(\boldsymbol{\theta}'|\boldsymbol{\theta}) \frac{\mathcal{L}(\mathbf{D}|\boldsymbol{\theta}')}{\mathcal{L}(\mathbf{D}|\boldsymbol{\theta})} \frac{q(\boldsymbol{\theta}|\boldsymbol{\theta}')}{q(\boldsymbol{\theta}'|\boldsymbol{\theta})} \\ \frac{\pi(\boldsymbol{\theta}')}{\mathcal{L}(\mathbf{D}|\boldsymbol{\theta}')} &= \frac{\pi(\boldsymbol{\theta})}{\mathcal{L}(\mathbf{D}|\boldsymbol{\theta})}. \end{aligned} \quad (5.6)$$

This means that the static distribution that the points tend to converge to is the likelihood up to some constant factor. Inserting this into equation 5.1 gives us our posterior up to some factor. This is precisely why when doing the Metropolis-Hastings algorithm there is no way of obtaining the evidence.

Some detail needs to be said about the good convergence of Markovian chains. Firstly to define what we mean by a converged chain. Different metrics are being used but in our case, we use the Gelman-Rubin test. In this test, we launch multiple chains from different starting points, and they all converge to the final distribution of the likelihood. Then we calculate two quantiles. The first quantity is the variance of the mean of the chains, i.e. how far apart the different chains centres from one another. The second quantity is the mean of the variance of each chain, i.e. how much are the chains themselves vary from their centre. For a converged chain, we would expect that the ratio of these two quantities is close to one, so we use this ratio to measure chain convergence.

Often denoted as the R-1 test we often require a chain to fulfill

$$R - 1 := \sqrt{\frac{\text{Var}(\text{chain means})}{\text{mean}(\text{chain variances})}} - 1 \stackrel{!}{<} 0.1 \quad (5.7)$$

to be considered converged. This requires our distribution q from which we propose points should be already quite close to target distribution \mathcal{L} . The reasoning is the follows, if the suggested points would be way off of the bulk of the likelihood then they would never be accepted and the chain could not move very much. In the end, the individual chains would have very low variances. The opposite effect happens when the proposal distribution would only propose points in the very centre of the likelihood, then the chains would accept every suggestion. This would make it that firstly the variance of the chain means would be quite high as the random walk would not converge to the center of the likelihood. Secondly, this would also have the effect that there could be regions of the likelihood that would never be explored by the chains.

To help with the convergence during each run when the chains had enough time to burn in and reached some milestones of convergence we update the proposal distribution. For this, we calculate the covariance of the chains and use a multivariate Gaussian with the sample covariance to propose points out of. This has the effect that the main requirement of a Markovian chain gets broken, this is because now the probability of going from one point to the next depends not only on the last point but also on previous points. This means that if we want to analyze the chains we need to always throw away the points of the chains before the last update of the proposal distribution.

The code that we use to run our MCMC is called MontePython (**MP**) and has two modes that are of interest to us. The first mode is the Metropolis-Hastings mode, it uses the same strategy that was discussed earlier to generate the chains where we also update the proposal distribution to have fast convergence. The second mode is the Fisher mode which is discussed in the next section. The reason why we use both modes of **MP** will become clearer in the Chapter about Validation.

5.2 The Fisher Information Method

We observe that for well-constrained parameters the posterior looks often like a multivariate Gaussian. The FI method employs this in that it is an approximation where the Gaussian is tailored to the likelihood and then the error is extracted from the Gaussian. The Idea of the formalism is the following: To parametrize a multivariate Gaussian you only need the covariance matrix, C , and the mean of the variables, μ . In our case, the variables would be cosmological parameters and the covariance then would contain the measurement uncertainties.

Assuming that the posterior can be approximated as a Gaussian we can write it as

$$p(\boldsymbol{\theta}|\mathcal{D}) \propto p_{\text{prior}}(\boldsymbol{\theta}) \mathcal{L}(\mathcal{D}|\boldsymbol{\theta}') \approx \mathcal{N} \exp \left[-\frac{1}{2} (\boldsymbol{\theta} - \boldsymbol{\mu}) \cdot C^{-1} (\boldsymbol{\theta} - \boldsymbol{\mu}) \right]. \quad (5.8)$$

For a Gaussian posterior, the mean is also at the best fit, this is why when we do a forecast we directly know the value of μ . It is the value of the model parameters at the fiducial point where we generated our fake data. We can now use that the covariance can be extracted from the log of the posterior by calculating the second derivative. It is

$$-\frac{\partial^2}{\partial \theta_i \partial \theta_j} \log(p(\boldsymbol{\theta}|\mathcal{D})) \Big|_{\boldsymbol{\theta}=\boldsymbol{\mu}} \approx (C^{-1})_{ij}. \quad (5.9)$$

If we assume flat priors in the region of interest we can directly calculate the derivative of the likelihood. This leads to the definition of the Fisher Information matrix as

$$F_{ij} := -\frac{\partial^2}{\partial \theta_i \partial \theta_j} \log \mathcal{L}(\mathcal{D}|\boldsymbol{\theta}) \quad (5.10)$$

For Gaussian priors, we can just add the term later. We will discuss later on how to do that when we discuss adding different experiments. Non-Gaussian or flat priors are harder to approximate. The easiest method of dealing with exponential priors is to make it flat prior by transforming the relevant parameters into log space. This might make the contours less Gaussian depending on how well-constrained the parameters are.

The difficulty of the FI method is that often times it is not so clear how to obtain the second-order derivatives of the likelihood. Some codes were purposefully built to be differentiable i.e. that you can obtain the derivatives for free. The typical Einstein-Boltzmann solvers (EBS) `CLASS`[Blas et al., 2011] and `CAMB`[Lewis et al., 2000] do not have that functionality, so we need to obtain the derivatives numerically. This is what `MP` does in Fisher mode. We calculate the second-order derivatives using a double-sided finite differences scheme. We note numerical derivatives with the symbol D, thus we can write

$$\begin{aligned} \frac{D^2 \log \mathcal{L}}{D \theta_i D \theta_j} &= \frac{1}{4 h_i h_j} [\log \mathcal{L}(\theta_i + h_i, \theta_j + h_j) - \log \mathcal{L}(\theta_i + h_i, \theta_j - h_j) \\ &\quad - \log \mathcal{L}(\theta_i - h_i, \theta_j + h_j) + \log \mathcal{L}(\theta_i - h_i, \theta_j - h_j)] \quad \text{for } i \neq j \end{aligned} \quad (5.11)$$

$$\frac{D^2 \log \mathcal{L}}{D^2 \theta_i} = \frac{1}{h_i^2} [\log \mathcal{L}(\theta_i + h_i) + \log \mathcal{L}(\theta_i - h_i) - 2 \log \mathcal{L}(\theta_i)], \quad (5.12)$$

where we have left out the arguments of the log-likelihood that do not vary in each line. Here the advantage of using the FI method becomes clear, while the MCMC often needs multiple thousand

calls of the EBS the FI method needs much less. In the Implementation we use for N parameters we have to call the likelihood $2N$ times for the diagonal elements and $2N(N - 1)$ times for the off-diagonal elements, making our total calls $2N^2$. Even then we can shave off some more time if we use that when varying nuisance parameters there is no need for calling the EBS anymore.

The calculation of the second derivative is numerically quite sensitive to the choice of stepsize. It was shown before in [Euclid Collaboration: Blanchard et al., 2023] that the optimal stepsize to calculate the derivatives is of the order of a few per cent of the marginalized error. And even then one needs to use very high precision settings of the EBS to be able to have stable results. This does defeat the purpose of the FI method as to obtain the marginalized error we would need to run an MCMC.

To make the computation of the FI matrix numerically stable we can use the explicit form of the photometric and spectroscopic likelihoods to write it using only the first derivates of the observables. For the photometric likelihood we find

$$F_{ij} = \frac{1}{2} \sum_{\ell=\ell_{\min}}^{\ell_{\max}} (2\ell + 1) f_{\text{sky}} \text{Tr} \left[(C_{\ell}^{\text{fid}})^{-1} (\partial_i C_{\ell}^{\text{th}}|_{\text{fid}}) (C_{\ell}^{\text{fid}})^{-1} (\partial_j C_{\ell}^{\text{th}}|_{\text{fid}}) \right]. \quad (5.13)$$

We have replaced the observed angular power spectrum with the theoretical angular power spectrum calculated at the fiducial like in the spectroscopic probe. There are two advantages of calculating the FI matrix like this, firstly the derivatives that show up are first order and thus much easier to calculate. To calculate them we use either of two finite differences stencils

$$\frac{DC_{\ell}^{\text{th}}}{D\theta_i} = \frac{1}{2h_i} [C_{\ell}^{\text{th}}(\theta_i + h_i) - C_{\ell}^{\text{th}}(\theta_i - h_i)] \quad (5.14)$$

$$\text{or } = \frac{1}{6h_i} [-11C_{\ell}^{\text{th}}(\theta_i) + 18C_{\ell}^{\text{th}}(\theta_i + h_i) - 9C_{\ell}^{\text{th}}(\theta_i + 2h_i) + 2C_{\ell}^{\text{th}}(\theta_i + 3h_i)]. \quad (5.15)$$

By default, we will stick to the double-sided finite difference and not to the one-sided one but to check the numerical stability of our derivatives we have tested both methods. First-order derivatives have the property to be more numerically stable. That is why we do not need to tune our stepsize as much as in the case of the second-order derivatives. We always use a relative stepsize of 1% for the cosmological parameters except for the neutrino mass, where we vary it by a relative 10%. The choice for the neutrinos stems from the fact, that the neutrino mass only has a small effect on our observables. For a 1% change of the neutrino mass, the change of the observables would be dominated by numerical noise, so we had to choose a higher stepsize. We will also test that the choice of a 10% stepsize for massive neutrinos produces stable results.

The second advantage of this method is that to compute all derivatives one only needs to call the code $2N$ since the first-order derivates of the observables can then be multiplied to find the second-order derivates of the likelihood.

For the spectroscopic likelihood, we find a similar expression for the likelihood

$$F_{ij} = \frac{1}{8\pi^2} \sum_i \int k_{\text{fid}}^2 \partial_i [\log P_{\text{th}}(k_{\text{fid}}, \mu_{\text{fid}}, z_i)|_{\text{fid}}] \partial_i [\log P_{\text{th}}(k_{\text{fid}}, \mu_{\text{fid}}, z_i)|_{\text{fid}}] V_i^{\text{fid}} dk_{\text{fid}} d\mu_{\text{fid}}. \quad (5.16)$$

Again we find that the FI matrix can be written with products of first-order derivatives. To calculate the FI matrix for our forecast we will use the code Cosmicfish (CF) that we have modified such that our changes to the recipes of the observables are consistent with our MP Implementation. Since CF

never calculates the actual likelihood this gives us a great test for our likelihood Implementation if the FI matrix obtained by MP in Fisher mode agrees with the FI matrix from CF. This is further discussed in the chapter 6 about the Validation.

Finally, the FI formalism gives us a guiding principle to make educated guesses for the proposal distributions. Firstly when we have already a covariance matrix of a previous MCMC, and we want to launch another MCMC but with fewer parameters, then just deleting the file's corresponding rows is not optimal but was the Implementation in MP. We have added a new method of fixing that leads to a better initial guess.

We calculate a matrix from the covariance of the MCMC that approximates the FI matrix by just inverting it. The matrix now has all the parameters that the actual Fisher would have. Now if we remind ourselves of the definition of the FI matrix as the second derivate of the log-likelihood then fixing a parameter is the same as never adding the corresponding lines to the matrix. Inversion then leads us to the desired covariance matrix. We illustrate this procedure below.

$$\begin{array}{cc} \boldsymbol{\theta}_o & \boldsymbol{\theta}_f \\ \boldsymbol{\theta}_o \begin{pmatrix} C_{oo} & C_{of} \\ C_{fo} & C_{ff} \end{pmatrix} & \xrightarrow{\text{invert}} \begin{pmatrix} F_{oo} & F_{of} \\ F_{fo} & F_{ff} \end{pmatrix} \xrightarrow{\text{extract } F_{oo}} F_{oo} \xrightarrow{\text{invert}} \tilde{C}_{oo} \\ \boldsymbol{\theta}_f & \end{array}$$

We have denoted the parameters we want to keep open with $\boldsymbol{\theta}_o$ and the parameters we want to fix with $\boldsymbol{\theta}_f$. In the Fisher approximation the new covariance \tilde{C}_{oo} is the covariance of the MCMC if the parameters had been fixed from the beginning. This also gives us an interpretation of what the diagonal elements of the Fisher mean. If we were to fix all parameters except one then the matrix F_{oo} is just a number. The inversion is then just its reciprocal value but the interpretation of this number would be the variance when every other parameter was fixed. This is precisely what the unmarginalized error is thus the diagonal of a Fisher contains the reciprocal unmarginalized errors. Next, we can ask ourselves the question of how to add multiple experiments together. On the level of the likelihood when neglecting cross-correlation the likelihood of a combined probe, \mathcal{L} , factorizes into the likelihoods of the individual probes, \mathcal{L}^1 and \mathcal{L}^2 . For the Fisher, we thus can write

$$F_{ij} = \frac{\partial^2}{\partial \theta_i \partial \theta_j} \log \mathcal{L} = \frac{\partial^2}{\partial \theta_i \partial \theta_j} [\log \mathcal{L}^1 + \log \mathcal{L}^2] = F_{ij}^1 + F_{ij}^2. \quad (5.17)$$

This means that combining two uncorrelated probes is the same as adding their fisher matrix. We can again use this to make an educated guess on the proposal distribution of an MCMC with combined probes, like the spectroscopic and the photometric probes when there are previous runs. Firstly we have to separate all of our parameters into parameters that are common to both likelihoods $\boldsymbol{\theta}_c$, i.e. the cosmological parameters, and then the nuisance parameters of both likelihoods $\boldsymbol{\theta}_1$ and $\boldsymbol{\theta}_2$. Calculating the derivates of one likelihood with respect to the nuisance parameters of the other likelihood makes little sense but could be done mathematically. The derivatives would just vanish so the Fisher Matrix would have empty rows of zeros in these and would be not invertible. But this helps us in the formulation of our recipe.

We start by inverting our MCMC covariance matrices to have the approximate FI matrices. We then add columns and rows of zeros that correspond to the nuisance parameters of the other likelihood. Finally, we can add the matrices and invert the result to get our new guess for the proposal covariance. Typically, this works very well for complimentary probes since breaking degeneracies makes the final posterior Gaussian enough for the approximation. We illustrate the final combination

recipe below

$$\begin{array}{c}
 \theta_c \begin{pmatrix} \theta_c & \theta_1 \\ C_{cc}^1 & C_{c1}^1 \\ \theta_1 & C_{1d}^1 \\ C_{1d}^1 & C_{11}^1 \end{pmatrix}, \quad \theta_c \begin{pmatrix} \theta_c & \theta_2 \\ C_{cc}^2 & C_{c2}^2 \\ \theta_2 & C_{2c}^2 \\ C_{2c}^2 & C_{22}^2 \end{pmatrix} \xrightarrow{\text{invert}} \theta_c \begin{pmatrix} \theta_c & \theta_1 \\ F_{cc}^1 & F_{c1}^1 \\ \theta_1 & F_{1d}^1 \\ F_{1d}^1 & F_{11}^1 \end{pmatrix}, \quad \theta_c \begin{pmatrix} \theta_c & \theta_2 \\ F_{cc}^2 & F_{c2}^2 \\ \theta_2 & F_{2c}^2 \\ F_{2c}^2 & F_{22}^2 \end{pmatrix} \\
 \\
 \xrightarrow{\substack{\text{add zeros} \\ \hookrightarrow}} \theta_1 \begin{pmatrix} \theta_c & \theta_1 & \theta_2 \\ F_{cc}^1 & F_{c1}^1 & 0 \\ F_{1d}^1 & F_{11}^1 & 0 \\ 0 & 0 & 0 \end{pmatrix}, \quad \theta_1 \begin{pmatrix} \theta_c & \theta_1 & \theta_2 \\ F_{cc}^2 & 0 & F_{c2}^2 \\ 0 & 0 & 0 \\ F_{2d}^2 & 0 & F_{22}^2 \end{pmatrix} \xrightarrow{\text{add}} \theta_1 \begin{pmatrix} \theta_c & \theta_1 & \theta_2 \\ F_{cc}^1 + F_{cc}^2 & F_{c1}^1 & F_{c2}^2 \\ F_{1c}^1 & F_{11}^1 & 0 \\ F_{2d}^2 & 0 & F_{22}^2 \end{pmatrix} \\
 \\
 \xrightarrow{\text{invert}} \tilde{C}
 \end{array}$$

This also explains how to add a Gaussian prior to a Fisher afterwards when looking at the Bayes theorem 5.1 again. The prior can be pulled into the likelihood and act like an effective second experiment. The covariance matrix of the multivariate Gaussian prior directly defines an FI matrix that can be just added like an experiment afterwards. This of course needs the prior to be centred on the fiducial cosmology of the forecast.

A script to merge covariance matrices for MP was added by us. To show how well this works we have combined two test MCMCs of the two main *Euclid* probes and present the results in figure ?? . We generated this plot with the use of GetDist ¹ [Lewis, 2019].

¹<https://getdist.readthedocs.io>

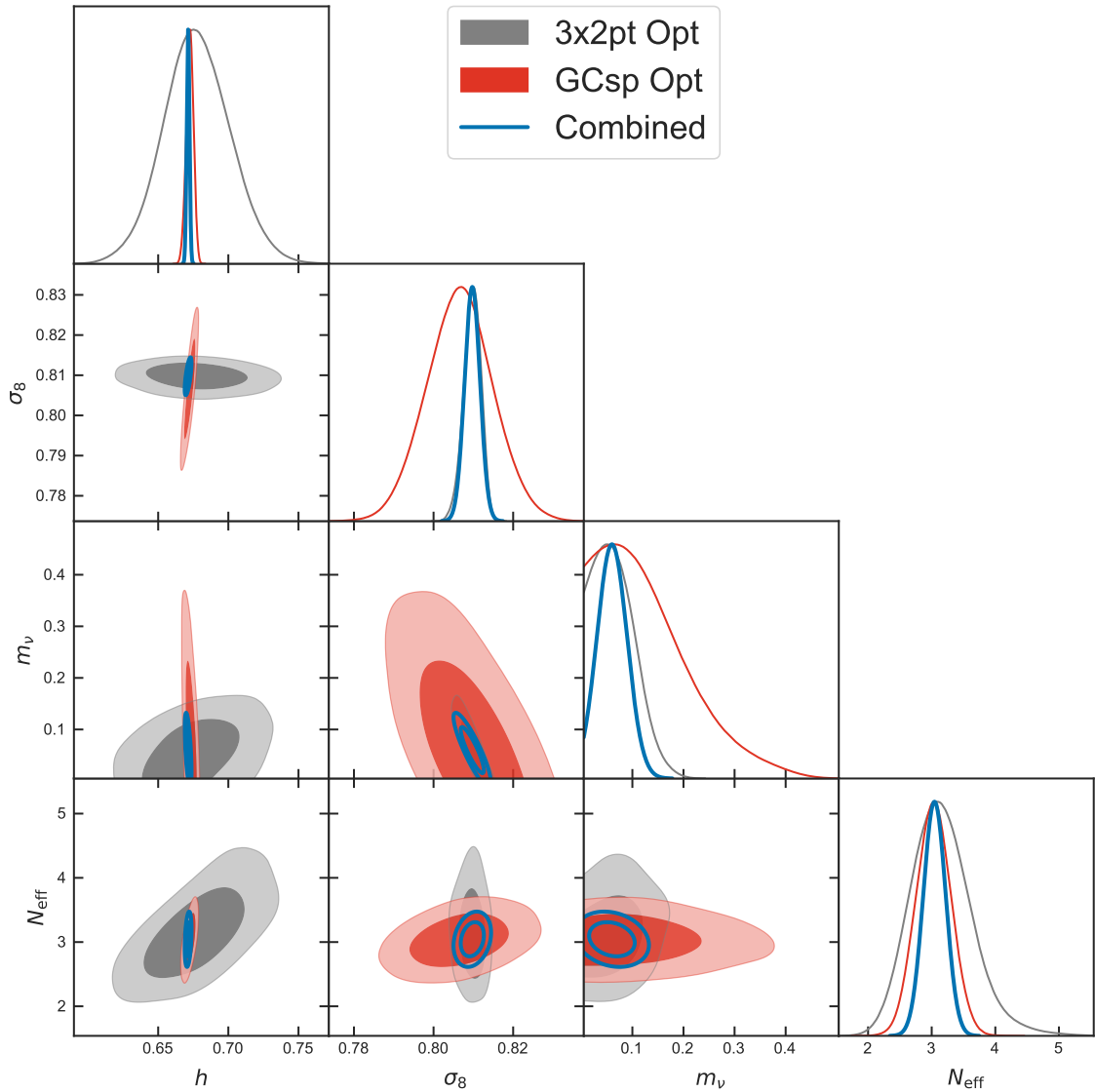


Figure 5.1: Demonstration of the covariance combination recipe. The MCMCs are done with the settings of the Validation section. The combined probe is not an MCMC, but the ellipses from the Gaussian approximation obtained with the recipe. This also demonstrates very well the complementarity of the *Euclid* probes.

Chapter 6

Validation of the Forecasting Pipeline

In this work, the main goal is a validated and robust sensitivity forecast for the neutrino parameters. For this, we have adopted a validation pipeline from [Euclid Collaboration: Blanchard et al., 2023]. It starts with the code CF that was validated in the *Euclid* project [Euclid Collaboration: Blanchard et al., 2020]. In this work, we have modified the recopies of the nonlinear modelling and modelling of the neutrino-induced scale-dependent growth to better describe the effect of massive neutrinos. Thus, we decided to do a re-validation of the MP pipeline. We will also check how well the Fisher formalism works for the neutrino mass that is close to a theoretical prior at zero mass.

In this section, we choose a different model that we will use in the final Forecasting results to have posteriors that are Gaussian enough to be able to be approximated using the FI methods. The parameters are given in table 6.1.

The Extensions to the Λ CDM models in this section are varied in pairs of two, we first look at a model where we vary $w_0 + w_a$. These parameters are an approximation to a dark energy equation of state that is slowly varying. It is parametrized as having $w(a) = w_0 + w_a(1 - a)$. We note that when fixing the parameters to their fiducial we recover Λ CDM. This w_0w_a CDM model was the original model that was validated in the work of We kept it in our validation pipeline to be sure that we did not break the previous validation with our changes to the pipeline.

The second model that we look at is a model where we vary the constant pressure-to-density ratio of dark energy w_0 (fixing w_a) and the approximated neutrino mass m_ν . We will use the symbol m_ν in this section rather than $\sum m_\nu$ to denote this quantity as in our parametrization we approximate that all the neutrino mass is concentrated into one massive neutrino with a temperature of

$$\frac{T_\nu}{T_\gamma} = \left(\frac{4}{11}\right)^{1/3} \left(\frac{3.044}{3}\right)^{1/4} = 0.716369. \quad (6.1)$$

This is different from the parametrization of [Euclid Collaboration: Blanchard et al., 2023]. In their parametrisation, the neutrino temperature had a factor of N_{eff} in their second factor instead of its fiducial value. In that sense their parameter N_{eff} is different from ours as it was partly accounting for additional N_{eff} to a higher neutrino temperature. For us, N_{eff} is accounting for additional massless degrees of freedom and thus a higher value of N_{eff} does not also mean a higher energy density of massive neutrinos.

We also note that this approximated mass of massive neutrinos is also not exactly the mass of a massive neutrino because it is the mass of a neutrino in an instantaneous decoupling approximation.

Table 6.1: Fiducial values of the parameters varied in the validation section. The Λ CDM parameters were always varied during the Validation runs while the extended Models were only varied two at a time. The meaning parameters are described in the text.

Fiducial								
Λ CDM					Extensions			
$\Omega_{m,0}$	$100 \times \Omega_{b,0}$	h	n_s	σ_8	m_ν (meV)	N_{eff}	w_0	w_a
0.314571	4.92	0.6737	0.9661	0.81	60	3.044	0	-1

It corresponds to a neutrino density fraction, Ω_ν , of

$$\Omega_\nu h^2 = \frac{m_\nu}{94.07 \text{ eV}} \left(\frac{3.044}{3} \right)^{3/4} = \frac{m_\nu}{0.06 \text{ eV}} 6.44826 \cdot 10^{-4} \quad (6.2)$$

In reality the factor of 94.07 eV in the denominator of the first factor would be given through an integral over the neutrino phase space distribution. To better match the parametrization between our two EBS `CLASS` and `CAMB`, we stick to the instantaneous decoupling approximation done in `CAMB`. The change to the neutrino temperature propagates to this equation, as the second factor is proportional to the neutrino temperature.

In the third model, we fix the dark energy equation of state to its Λ CDM value and vary the approximated neutrino mass and the effective relativistic degrees of freedom. As we stated before our changes to the neutrino parametrization make the value of N_{eff} correspond to the actual numbers of massless species N_{ur} . We can translate these quantities in this case to another by

$$N_{\text{ur}} = N_{\text{eff}} - \frac{3.044}{3}, \quad (6.3)$$

where the second term stands for the one massive neutrino. In the actual forecasting results, we will change our neutrino parametrization to have three massive neutrinos with degenerate masses. In this case, we will subtract three times that from the N_{eff} , such that the parameter will correspond to any additional species of relativistic light relics. We will denote this quantity as ΔN_{eff} with a theoretical prior bound at zero.

In all the validation models we have fixed the modelling parameters of nonlinear effects in the spectroscopic probe, namely σ_p and σ_v , to their fiducial values. This is done because especially σ_p is very degenerate with the cosmological parameter, making the Gaussian approximation needed for the FI method break.

We will validate our pipeline separately for both main probes of the *Euclid* mission, for both the optimistic and pessimistic settings and all three models totalling twelve total tests. The tests itself are done in three steps

- We will first validate our EBS implementation by validating the FI results of `CF` for the two codes `CAMB` and `CLASS`.
- We will then validate our likelihood implementation by validating those two results with the FI obtained by `MP` in Fisher mode.
- We will test for the validity of the Gaussian approximation by comparing the obtained FI matrices with the posteriors obtained by an MCMC run in `MP` with the Metropolis-Hastings algorithm.

In the last step, there is by construction no possibility of a theoretical error showing up as the same likelihood is used to generate the MCMC to calculate the FI matrix. We decide that our implementation is validated when the marginalized and unmarginalized one-dimensional errors are within 10% of the median. This validation criterion is taken from the previous *Euclid* validation standard from [Euclid Collaboration: Blanchard et al., 2023].

This chapter will be structured like the following. Firstly, we discuss the precision settings for the two EBSs `CAMB` and `CLASS` that we needed to set to get their fiducial power spectra to match to sub-percent level. We will then show the agreement of the three different FI matrices and discuss their stability under change of stepsizes and derivation methods. In the next step, we will then compare the FI matrices with the MCMC results and try to explain the derivations. In the last section, we will discuss the effect of nonlinear modelling and analyze possible biasing.

6.1 The Einstein-Bolzmann Solvers

To match the results from the two EBS we needed to first understand the differences between codes. The first difference was already alluded to in the introduction to this section. `CAMB` uses the phase space integral for the neutrinos in the limit of instantaneous decoupling while `CLASS` does not. To circumvent this problem we added a new parameter `m_nu_camb` that is converted to the neutrino density fraction Ω_ν via equation 6.2, before each call of `CLASS`.

The total matter density parameter Ω_m is also defined slightly differently in `CAMB` and `CLASS`. While `CAMB` defines the total matter density as CDM+baryons+massive neutrinos, `CLASS` does not include the massive neutrinos. To match the codes we defined a new parameter `Omega_m_camb` that is converted to the density parameter of cold dark matter, Ω_c , before the run by just subtracting the other two ingredients.

Another detail in our implementation was that `CAMB` is not able to use σ_8 as an input parameter. This is because it is computed from the linear matter power spectrum. In `CLASS`, we have a shooting functionality where we use a reference value of A_s to calculate σ_8 from. As σ_8 is directly proportional to A_s , by rescaling A_s we can match the desired value of σ_8 . Since this functionality does not exist in `CAMB`, we mimic the shooting by doing a first reference run of `CAMB` to obtain the matter power spectrum and then rescale to match σ_8 inside `CF`. With these three modifications, we were able to match the input parameters between `CLASS` and `CAMB`.

The next step in the validation of the EBS is a careful choice of the accuracy settings. This is done such that

- A: The power spectra are numerically stable enough such that their derivatives are not dominated by noise,
- B: Small differences in the approximation schemes of the EBS do not propagate to the final forecasting results.

The choice of the accuracy settings inside `CAMB` is simple. There are generic parameters that boost the accuracy of the `CAMB` code in multiple different places. We decided to use the following accuracy settings in `CAMB`.

Listing 6.1: `CAMB:HP` precision settings

```
do_late_rad_truncation = T
high_accuracy_default = T
```

```

transfer_interp_matterpower = T
accurate_reionization = F
accuracy_boost = 3
l_accuracy_boost = 3
accurate_massive_neutrino_transfers = T

```

In the rest of the discussion, these settings will be called **CAMB:HP**. The intrinsic accuracy settings in the code, like integration cutoffs, truncation of the Boltzmann hierarchy, and stepsizes, are all multiplied by the corresponding accuracy boost. The parameter `do_late_rad_truncation` truncates the Boltzmann hierarchy for radiation at high ℓ after matter domination. The option for `accurate_massive_neutrino_transfers` allows us to obtain the neutrino transfer functions that are needed in the modelling of our photometric probe.

The high-precision settings that we chose in **CLASS** are summarized in the following.

Listing 6.2: **CLASS:HP** precision settings

```

k_per_decade_for_bao = 50
k_per_decade_for_pk = 50
l_max_g = 20
l_max_pol_g = 15
radiation_streaming_approximation = 2
radiation_streaming_trigger_tau_over_tau_k = 240.
radiation_streaming_trigger_tau_c_over_tau = 100.
tol_ncdm_synchronous = 1.e-5
background_Nloga = 6000
thermo_Nz_log = 20000
thermo_Nz_lin = 40000
tol_perturbations_integration = 1.e-6
halofit_tol_sigma = 1.e-8
l_max_ncdm = 25
ncdm_fluid_trigger_tau_over_tau_k = 100.

```

The approximation schemes of **CLASS** are described in [Blas et al., 2011]. In **CLASS**, we truncate the Boltzmann hierarchy for our ultra-relativistic species, i.e. photons and neutrinos, like in **CAMB**. This cutoff is governed by the precision parameters `l_max_xxx`, where `xxx` stands for the species.

Once deep inside the horizon we further simplify the equations of radiation and light relics by doing a fluid approximation. This means that we approximate the species with an imperfect fluid with anisotropic stress. This essentially truncates the hierarchy at 2. For our massive neutrino, the time of this approximation is governed by the parameter `ncdm_fluid_trigger_tau_over_tau_k`. The fluid approximation is not present in **CAMB**.

To match the output of the two codes we have to deactivate the fluid approximation. This is done by passing the parameter `ncdm_fluid_approximation=3`. We further found that the effect of the fluid approximation is negligible in the highly nonlinear regime. This is why we decided to use a different set of precision parameters in the validation of the different probes. For the photometric probe, we stick to the **CLASS:HP** settings while for the spectroscopic probe, we have adjusted our setting to the ultra-high precision settings **CLASS:UHP**.

Listing 6.3: **CLASS:UHP** precision settings

```
k_per_decade_for_bao = 50
```

```

k_per_decade_for_pk = 50
l_max_g = 20
l_max_pol_g = 15
radiation_streaming_approximation = 2
radiation_streaming_trigger_tau_over_tau_k = 240.
radiation_streaming_trigger_tau_c_over_tau = 100.
tol_ncdm_synchronous = 1.e-5
background_Nloga = 6000
thermo_Nz_log = 20000
thermo_Nz_lin = 40000
tol_perturbations_integration = 1.e-6
halofit_tol_sigma = 1.e-8
l_max_ncdm = 40
ncdm_fluid_appoxmation = 3.
evolver = 0

```

The two precision settings in listings 6.2 and 6.3 differ by three parameters. Firstly, the truncation of the Boltzmann hierarchy for massive neutrinos happens at a higher $\ell = 40$. This is done to better match the cutoff of **CAMB**. With our precision settings, the truncation happens at a high ℓ of 75. The second change is the deactivation of the neutrino fluid approximation and the last one is the change of the evolver. The changes to the ultra-high precision settings of **CLASS** with the standard evolver have made a typical call of the code to be of the order of tens of minutes. By switching the evolver from the stiff ndf15 evolver to a standard Runge-Kutta integrator we could cut down the computation time to approximately 20%.

Finally, when running the MCMCs we can set the precision parameters back to the **CLASS** defaults. The changes that the precision parameters make only affect the final power spectrum per mille level. As this only propagates to small changes in the final likelihood, the MCMC is unaffected by our precision parameters. The default precision parameters are denoted by us with **CLASS:DP**.

We present our Comparison between the different power spectra obtained by our EBS in figure 6.1. For the linear power spectrum, we can see that the fluid approximation leads to an underprediction of 0.05% on the matter power spectrum at intermediate k . At the smallest scales, it has a much smaller effect such that the **CLASS:HP** and **CLASS:UHP** settings agree very well with each other. What can also be seen, is that in the sensitivity region the power spectra of **CLASS:HP** and **CLASS:DP** only differ by a small bump at large scales, but then start diverging at small scales.

For the nonlinear spectrum we can see a similar discrepancy between the different power spectra on large and intermediate scales, but then start converging again on the smallest scales, where the power spectra are dominated by the one halo term. We believe that the reason they start converging comes from the fact that the effective scalar index enters the smoothing region between one and two halo terms is slightly different. This can be explained by the fact that we observe a stronger neutrino-induced suppression on intermediate scales when doing the fluid approximation.

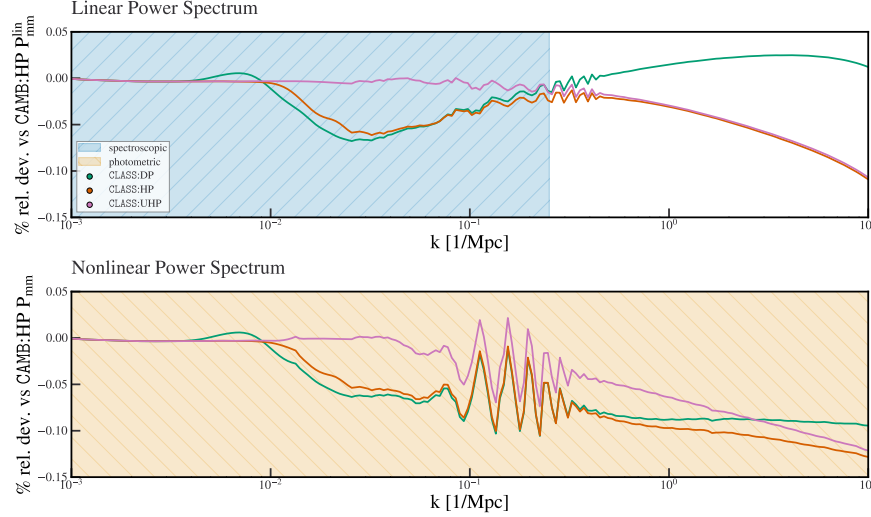


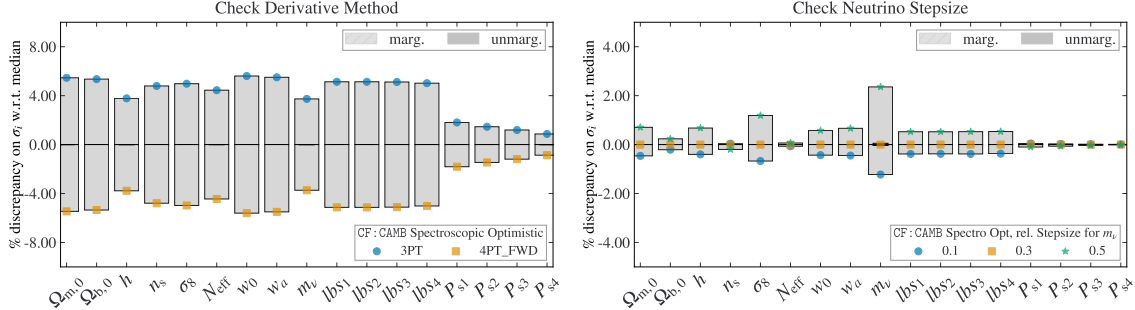
Figure 6.1: Comparison of the different Class precision settings to our ‘default’ high precision setting for **CAMB**. On the y axis we plot the difference to the power spectra obtained from **CAMB**, normalized to the mean value. We have marked the regions where the individual probes are sensitive to their corresponding colours.

6.2 Comparison of the different Fisher Information Methods

After careful setting of the input parameters and precision settings of our two EBS, the next step is to validate our forecasting results. For this, we will first discuss the choices we made in our forecasting pipeline. The first choice we have is for the derivate method. As we have discussed, in **CF** the first-order derivate of the observable can either be calculated using an equal-sided three-point derivative (3PT), or a four-point forward derivative (4PT_FWD). For this test, we have compared the one-dimensional marginalized and unmarginalized errors obtained via **CF**. We use **CAMB** as the underlying EBS. We denote the **CF** pipelines as either **CF:CAMB** or **CF:CLASS** depending on the underlying EBS. The comparison is found in figure 6.2a. The derivative methods validate each other as the total deviation is within 5% of each other for all parameters. We can see a systematic underprediction of the error when using the 4PT_FWD derivatives instead of the 3PT derivatives. The agreement of the errors for the forecast is within 10% of the mean for the case of varying all 9 cosmological parameters, thus the derivative is stable for all cosmological parameters. We can use two derivative methods for the rest of our forecast. We will use the 3PT derivatives in this work.

The next free choice we had in our forecasting was the stepsize for the approximate neutrino mass. As we have said before the relative stepsizes for the cosmological parameters were chosen to be 1% of its fiducial value (or simply 1% for w_a). We chose a higher stepsize of 10% for the massive neutrino since small changes of the neutrino mass only change the power spectrum to little. To check if the derivative with a relative stepsize of 10% is numerically stable we did the forecast with higher stepsizes of 30% and 50%. The result of the comparison can be found in figure 6.2b. We

Figure 6.2: Comparisons of the one-dimensional marginalized (in light grey) and unmarginalized errors (in dark grey). The *Euclid* probe is the spectroscopic probe with the optimistic settings. We use the abbreviation lbs_i stands for the nuisance parameter $\ln(\hat{b}\sigma_8)_i$, where i denotes the redshift bin. We plot the percentage deviation from the median error obtained by CF:CAMB.



(a) Comparison of the errors when switching the derivative method (b) Comparison of the errors when changing the relative stepsize for the neutrino mass.

Figure 6.3: In this figure we compare the results from CF using either of the two different Einstein Boltzmann solvers and MontePython in fisher mode, denoted with MP:Fisher.

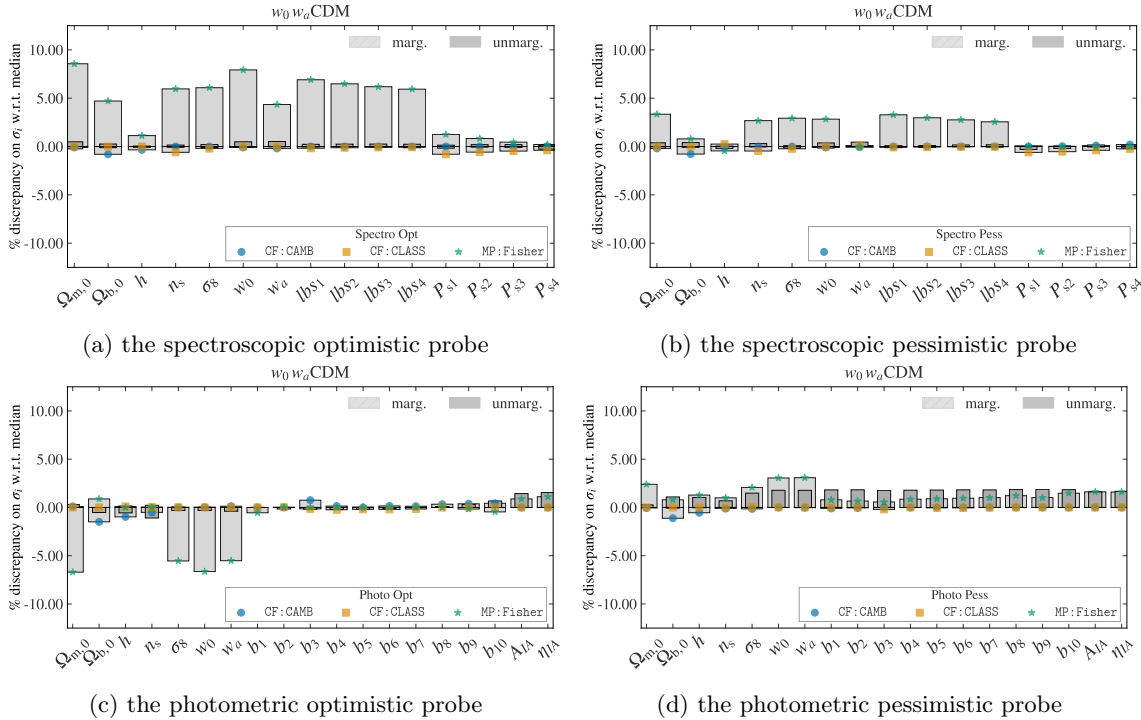
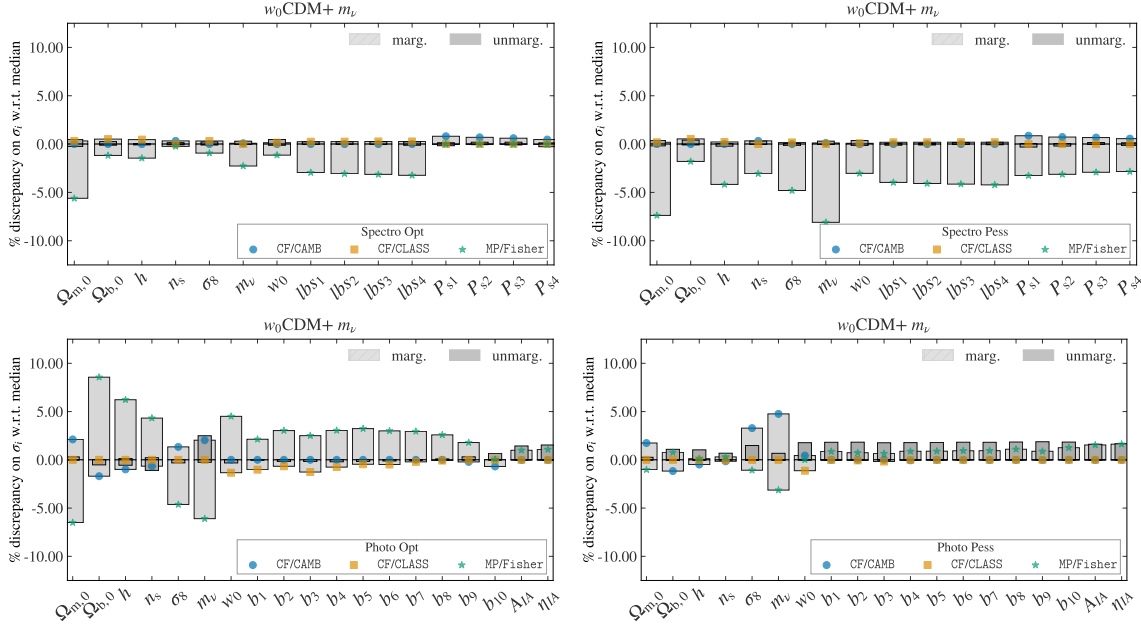
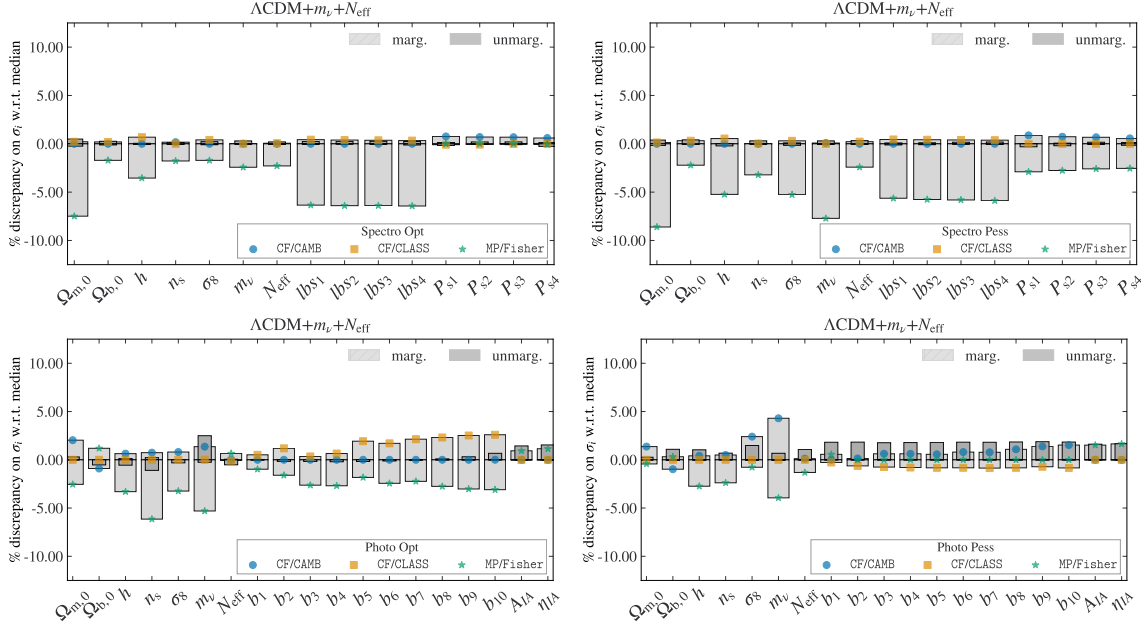


Figure 6.4: Same as figure 6.3 but for the $w_0\text{CDM}+m_\nu$ modelFigure 6.5: Same as figure 6.3 but for the $\Lambda\text{CDM}+m_\nu + N_{\text{eff}}$ model

can see that the derivative with a stepsize of 10% is very stable as the errors of the higher stepsize choices are within 5% of each other. Since we have shown that the validation holds for the case with all 9 cosmological parameters, it is also valid for our smaller validation cases. As the error of a three-point numerical derivative is proportional to the stepsize squared, we will use a relative stepsize of 10% for the approximate neutrino mass.

For each of the validation cases, we present the comparison for both survey settings and both probes. The comparisons are found in figures 6.3-6.5. We show the errors of all cosmological parameters and nuisance parameters. We can see that all forecast errors are within 10% of the median value and thus the validating is successful. With our careful setting of the precision parameters, we obtain very good agreement between the two Boltzmann codes. The biggest discrepancy between the different Cosmicfish FI methods is a 5% difference in the neutrino mass. We believe this is due to residual small differences in the truncation of the Boltzmann hierarchy.

The comparison between MP and CF is a bit worse with typical discrepancies of 5-10%. The main contribution to this is that second-order derivatives are very sensitive to the choice of stepsize and there is no reasonable way to find the optimal one. The prescription for the stepsize was taken from [Euclid Collaboration: Blanchard et al., 2023] where they optimized the FI element for $w_0 - w_a$. This was chosen as that particular element was very sensitive to stepsizes due to the strong correlations. With this, we show that the prescription still works well enough for the validation but might be suboptimal now. Another reason for the worse agreement we will show in the next section is the deviation from Gaussianity. This might be a subleading effect, as the deviation of the unmarginalized errors tends to be much smaller than marginalized ones. Typically, when there is non-Gaussianity the double-sided second-order derivatives get an additional contribution which becomes visible in the unmarginalized errors.

6.3 The validity of the Fisher approximation

As we have stated before, the Validation of the FI results from MP:Fisher validates the same likelihood that we use for the MCMC. The next step is to check the validity of the FI method by comparison with the MCMC. We do the comparison only for the optimistic cases as the pessimistic cases have the same general tendencies. To compare the results we compare the one-dimensional marginalized posteriors and the two-dimensional contours. We obtain the MCMC results from MP running in Metropolis-Hastings mode and analyze them using GetDist. The comparison can be seen in figures 6.6-6.8.

Firstly, we can see in the contours of the $w_0 w_a$ CDM model that the MCMCs and the FI match very well. With this, we recover the validation from [Euclid Collaboration: Blanchard et al., 2023] with our changes to the modelling and nonlinear corrections. This was expected as our modelling should only affect the contours of dark energy only slightly due to the modelling of the nonlinear corrections. For the other parameters, the switch from HALOFIT to HMCODE came with the widening of the contours which is discussed further in the next section.

In the other two cases, we can see strong deviations in the MCMC from FI approximation. Most striking in this is the posteriors of m_ν . The one-dimensional posteriors of m_ν show that the Fisher approximation holds well at the fiducial value, but starts to deviate. For lower values m_ν hits the theoretical prior, while for higher values it falls off quicker. We believe that the deviations of the other parameters can be explained solely by this.

Firstly, in the spectroscopic probe of figure 6.7 we can very clearly see that the parameters that are uncorrelated with m_ν have next to no deviations from the Gaussian approximation while the

Figure 6.6: Comparison of the one and two-dimensional marginalized contours obtained by MontePython in MCMC mode (MP:MCMC) with the contours of CF:CAMB and MP:Fisher. The contours depict the 68% and 95% confidence intervals for the $w_0 w_a$ CDM model respectively. We plot only the cosmological parameters for the different probes. On the left, we show the spectroscopic probe and on the right, we show the photometric probe.

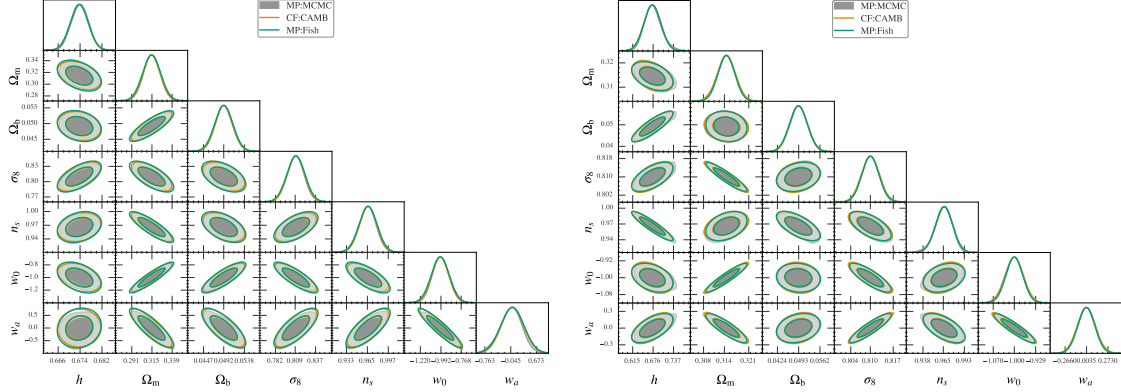


Figure 6.7: Same as figure 6.6 but for the w_0 CDM+ m_ν model.

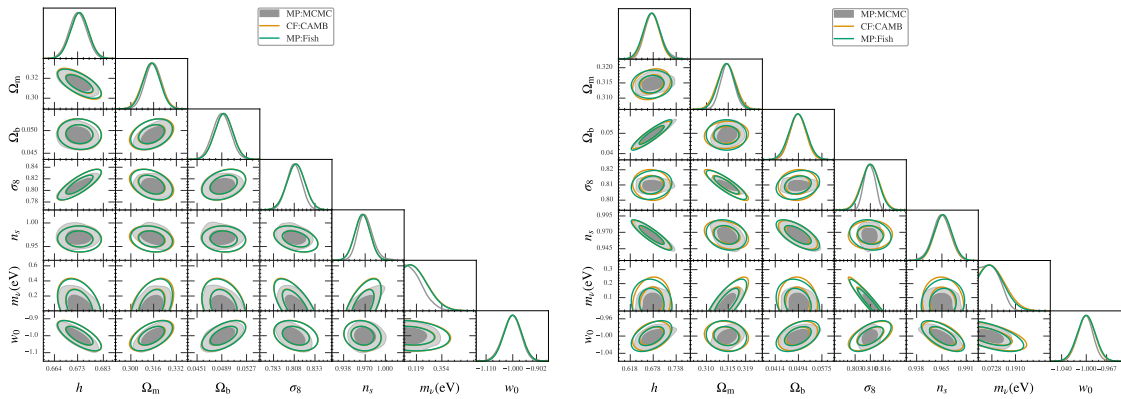
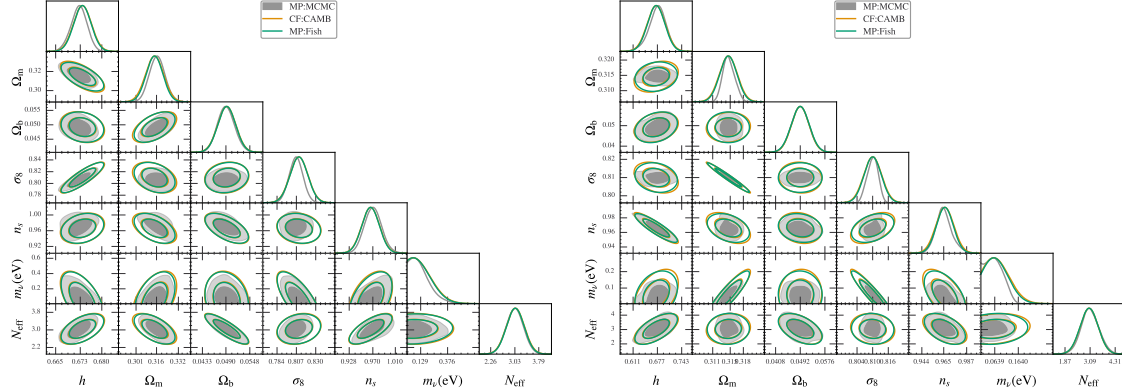


Figure 6.8: Same as figure 6.6 but for the Λ CDM + m_ν + N_{eff} model.

stronger correlated parameter is affected more strongly. We see that due to the theoretical prior at zero mass important degeneracy directions get cut off and thus the posteriors deviate from the Gaussian approximation.

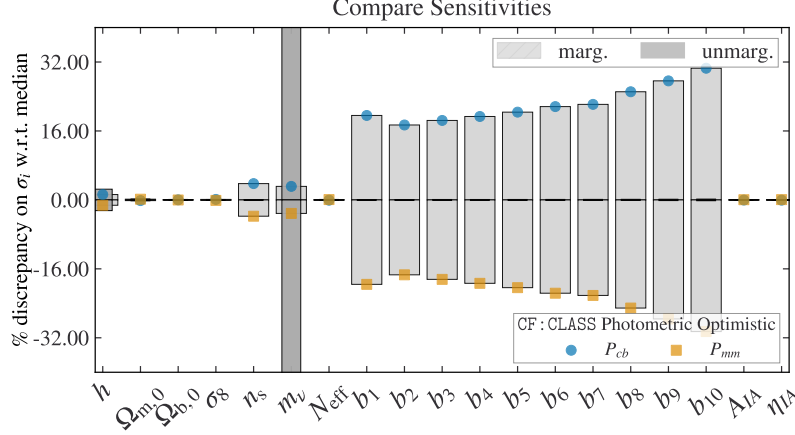
For higher values of the neutrino mass, we can also see a faster decay of the likelihood of the neutrino mass. This is further amplified for the photometric probe. For that probe, the likelihood falls off so dramatically that the inside the 68% confidence bound of the fisher coincides with the 95% confidence bound of the MCMC. This has the effect that the strongly correlated parameters namely σ_8 and Ω_m not only get cut off at higher or lower values respectively, but also fall off quicker on the other side. We can also see a slight rotation of the FI contours for these parameters as the Gaussian approximation starts to fail even at the maximum likelihood.

We can see the same tendencies in the comparisons of figure 6.8. This further confirms our hypothesis that all deviations from Gaussianity are due to the prior and the deviation from Gaussian for the parameter m_ν . With these results, we think that our implementations are fully validated, and also prove that to have a good forecast for neutrino parameters we have to move on from the standard FI formalism.

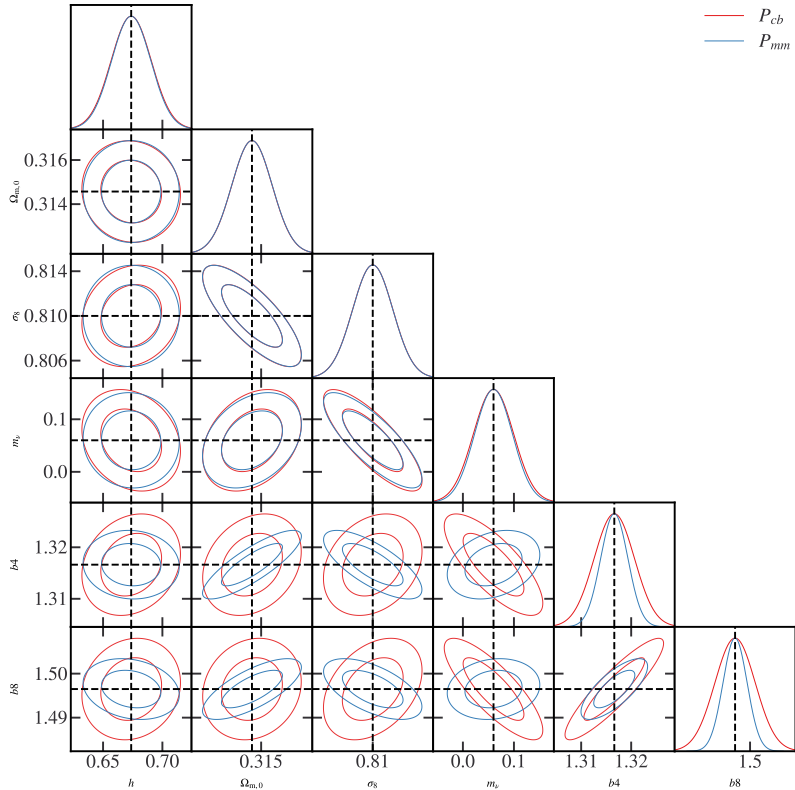
6.4 Bias from Modeling

Before we come to the forecasting results, we wanted to have a brief discussion about the effects of our modelling. We first discuss our switch from the total matter power spectrum to the CDM+baryon power spectrum. As we have discussed before due to massive neutrinos the CDM+baryon matter power spectrum is suppressed by a factor $\sim (1 - 6f_\nu)$ on scales smaller than the minimum clustering scale k_{\min} . We have also discussed how this translates into a shift of the order $\sim (1 - 8f_\nu)$ for the total matter power spectrum. This means that overall the formulation of the likelihood is less sensitive to the neutrino mass when changing from P_{mm} to P_{cb} . When doing a parameter inference it would have two effects. Firstly, due to power spectra reacting less strongly to the neutrino mass, its constraints get wider. Secondly, if we assume that our description of the galaxy power spectrum would be the truth of the underlying data then trying to fit the data with the 'wrong' description would bias our parameters.

Figure 6.9: We show the effect of switching the formulation of our observables to use P_{mm} instead of P_{cb} . We compare the results of the fisher forecast for the photometric optimistic using CF:CLASS as our code.



(a) Comparision of the one-dimensional marginalized and unmarginalized errors obtained by either using P_{mm} to formulate our observables or P_{cb} . For the parameter m_ν the difference in the unmarginalized error goes outside of the frame and is of the order of 43% away from the mean.



(b) Comparision of the one and two-dimensional marginalized FI contours for the two formulations. We marginalized over other cosmological and nuisance parameters as their trends are the same.

To exemplify this claim we can make the following gedankenexperiment. Let's say we have a galaxy clustering probe that is only sensitive to the smallest scales. Then the data power spectrum with an underlying neutrino mass m_ν would be suppressed by a factor $(1 - 6f_\nu)$. When we would fit the data our model power spectrum would try to different values of m'_ν until the power spectrum matches the data. The problem is that the suppression of the model power spectrum is given by $(1 - 8f'_\nu)$. Since the probe only measures the suppressed power spectrum the inference code will be able to find a matching f'_ν to perfectly fit the data. We will find

$$6 f_\nu \stackrel{!}{=} 8 f'_\nu \implies m'_\nu = \frac{3}{4} m_\nu, \quad (6.4)$$

as the neutrino fraction is directly proportional to the mass. This effect is lessened by the fact that the minimum clustering scale is also proportional to the root of the neutrino mass. This can be used to break the biasing but since the dependence is less strong this biasing effect is still there.

To test both of these effects we did two separate analyses. We first wanted to check how much the inferred errors change when changing the prescription to use P_{mm} instead of P_{cb} . As a simplification, we presume that the fiducial value of the galaxy bias does not change between the two runs, i.e. $\hat{b} = b$. This can be done as the forecast error should not depend on the actual value of the biases. To do our comparison, we compare the results for the photometric probe in optimistic settings, and we chose the $\Lambda\text{CDM} + m_\nu + N_{\text{eff}}$ model.

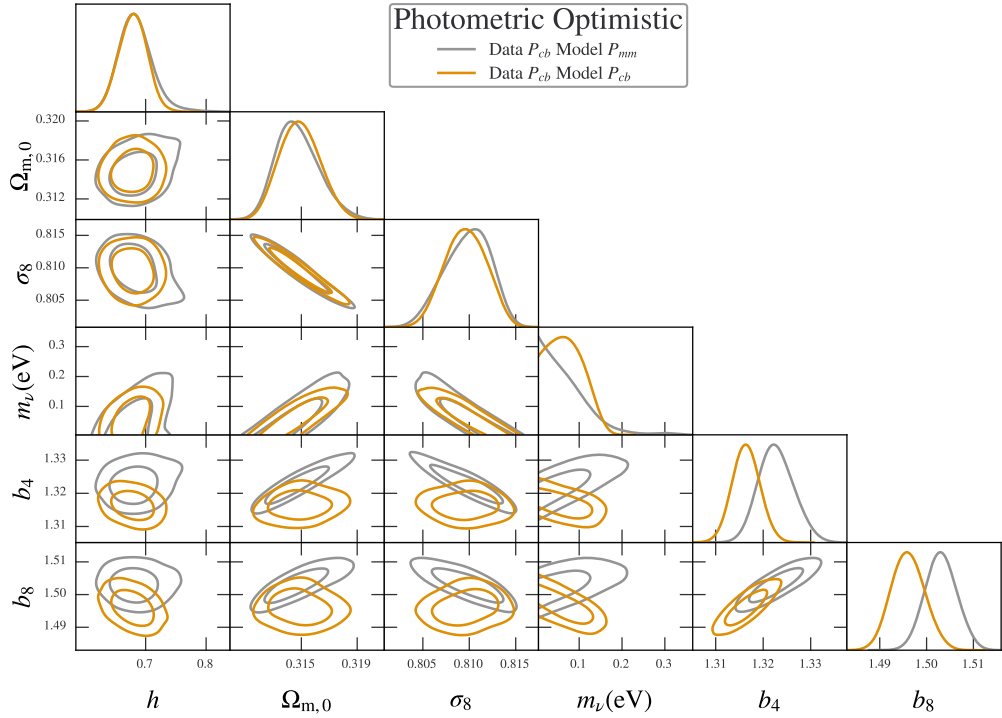
The results of this comparison are found in figure 6.9. In the upper figure 6.9a, we can see that the change in the inferred error for the cosmological parameters apart from the neutrino mass is negligible. This was expected as the effect of those parameters on the matter power spectrum and the CDM+baryon power spectrum is very similar. For the neutrino mass, we find a strong discrepancy of 80% in the unmarginalized error while the marginalized error is more comparable. We also see a strong 40%-80% shift in the errors of the galaxy biases. We believe that these two effects are related to one another. Viz., the difference between the matter power spectrum and the CDM+baryon power spectrum can be absorbed by the biases. This is due to the definition of the galaxy bias. If we remember how it was defined we can see that on scales much smaller than k_{\min}

$$\begin{aligned} P_{gg}(k, z) &= b^2(k, z) P_{mm}(k, z) = \hat{b}^2(z) P_{cb}(k, z) \\ \iff & b^2(k, z) (1 - f_\nu)^2 P_{cb}(k, z) = \hat{b}^2(z) P_{cb}(k, z). \end{aligned}$$

This means that the strength of the suppression of the matter power spectrum can be absorbed by accordingly shifting all galaxy biases enough to mimic the missing suppression. Furthermore, this leads to a change in the degeneracy directions of the biases concerning the other cosmological parameters. This effect of compensation can be seen in figure 6.9b

For our next check, we wanted to make a naive biasing test, where we generate our data vector using our more correct description using P_{cb} and then try fitting it using the P_{mm} description. The results of this test are found in figure 6.10 where we have picked out some indicative parameters. We can see how the posteriors of m_ν shift to lower values and hit the theoretical prior. This is due to the discrepancy between the suppression of the two power spectra. This effect is partially broken by adding the sheering probe. The angular power spectrum of WL is calculated by the total matter power spectrum alone and thus independent of our modelling of the galaxy bias. The remaining shift of the neutrino mass induces a slight shift in Ω_m and σ_8 in their respective correlation directions. As we had discussed before, we can now see how the bias parameters try to compensate for the reduction of P_{mm} on the smallest scales by shifting to higher values. Their

Figure 6.10: The biasing in the parameter inference when switching the prescription of the observables but fixing the data to P_{cb} . This is using the photometric probe in optimistic settings in a $\Lambda\text{CDM} + m_\nu + N_{\text{eff}}$ model. In yellow, we show the posteriors if we try to fit the data using our P_{cb} formulation. In grey, we show how we fit the data using our P_{mm} formulation.



correlation with the cosmological parameters Ω_m , σ_8 and m_ν again shift since they will need to compensate for additional shifts of the power spectra. This degeneracy is broken by the fact that the probes are also sensitive to intermediate ranges where the neutrino-induced suppression has not flattened out yet. To take care of this effect, we would have needed to switch to a scale-dependent galaxy bias in the P_{mm} case.

Our next discussion will be about the switch from `HALOFIT` to `HMCODE`. As we had stated earlier, the difference between them is that `HMCODE` is a semi-analytical model and `HALOFIT` is a direct fit. This means they react slightly differently to a change in cosmological parameters. We will try to analyze this change in our first test like we did before.

All codes trying to predict the nonlinear power spectrum give slightly different results. It is unclear which of them describes the reality better. We know that `HMCODE` matches better simulations with massive neutrinos like the *Euclid* flagship simulations so we went with it for our forecast. To check how much this can bias our results for our second test we will try fitting data generated with different underlying models with the same model. This essentially answers the question of how inferred parameters would shift if our nonlinear prescription did not match reality.

The results of the first test are found in the figure. We can see large discrepancies between the

forecast errors for all parameters. The largest discrepancy is in the unmarginalized errors for the neutrino mass. There we have a 15% discrepancy between the two codes. We believe this is due to the many different places where the `HMCODE` algorithm treats massive neutrinos, that do not get caught in the `HALOFIT` fitting formula. The effect of massive neutrinos only in the total matter power spectrum while many effects of nonlinear collapse really should be dictated by the dynamics of the CDM+baryon power spectrum. Other than that `HMCODE` also uses correction factors that are directly proportional to the neutrino mass.

The largest discrepancy in the marginalized errors is in the parameters Ω_m, σ_8 and n_s where the discrepancy is of the order of 60-70%. In the two-dimensional marginalized contours, we can also see a rotation of the degeneracy directions of these parameters with respect to h . The forecast errors of `HALOFIT` are systematically below the errors from `HMCODE` for the cosmological parameters implying that the fitting formula description of `HALOFIT` depends more strongly on the values of cosmological parameters than the collapse physics behind it.

Our next test regarding the bias of `HMCODE`. For this, we generate the data using `HALOFIT` and then try fitting it with `HMCODE`. The result of this test can be seen in figure 6.11. Compared to the first biasing test the difference is that we fixed the model and changed the data and not the other way around. We believe that the bias shift for both methods should be of the same order of magnitude. Testing it this way around just keeps the posteriors of similar size such that they can be better compared.

We can see in figure 6.11 that this time the shifts in bias are much more prominent than in the first biasing test. To explain these shifts we have to look into [Mead et al., 2021]. There we can see that `HALOFIT` overpredicts the matter power spectrum by up to 15% on the smallest scales. To compensate for this we go to smaller values of h (essentially reducing ω_b) and higher values of n_s and m_ν to fix the intermediate ranges. Fixing the amplitude then needs Ω_m and σ_8 . The degeneracy of the amplitude is broken by the sheering and cross-correlation probe essentially fixing Ω_m and σ_8 to the cosmic banana. Due to the higher neutrino mass, the galaxy biases need to shift up matching the different suppressions of matter and CDM+baryon spectrum.

Both tests indicate that our nonlinear modelling strongly influences our parameter inference. This is why it is important to have a good handle on N-body simulations to fit our halo models. Through extensive comparisons of different nonlinear models, it was found that `HMCODE` matches the *Euclid* flagship simulations better than `HALOFIT`. On scales $k < 1 \text{ hMpc}^{-1}$ `HMCODE` matches the simulations on a 2% level while `HALOFIT` for late times starts diverging at a 5-6% level. Our second test shows how this discrepancy is already leading to multiple standard deviation shifts in the inferred parameters.

We also believe that our modelling of the neutrino-induced scale-dependent bias is important to not underestimate our errors. With these conclusions, we can consider our pipeline to forecast as thoroughly validated and checked against biasing.

Figure 6.11: The biasing in the parameter inference when switching the data from being generated using HMCODE to being generated using HMCOde. We then try to fit the data using HMCOde. This depicts the photometric probe with optimistic settings in a Λ CDM + m_ν + N_{eff} model. In yellow, we show the posteriors if our model HMCOde would describe the underlying universe. In grey, we show how our model performs when the truth would be HALOFIT.

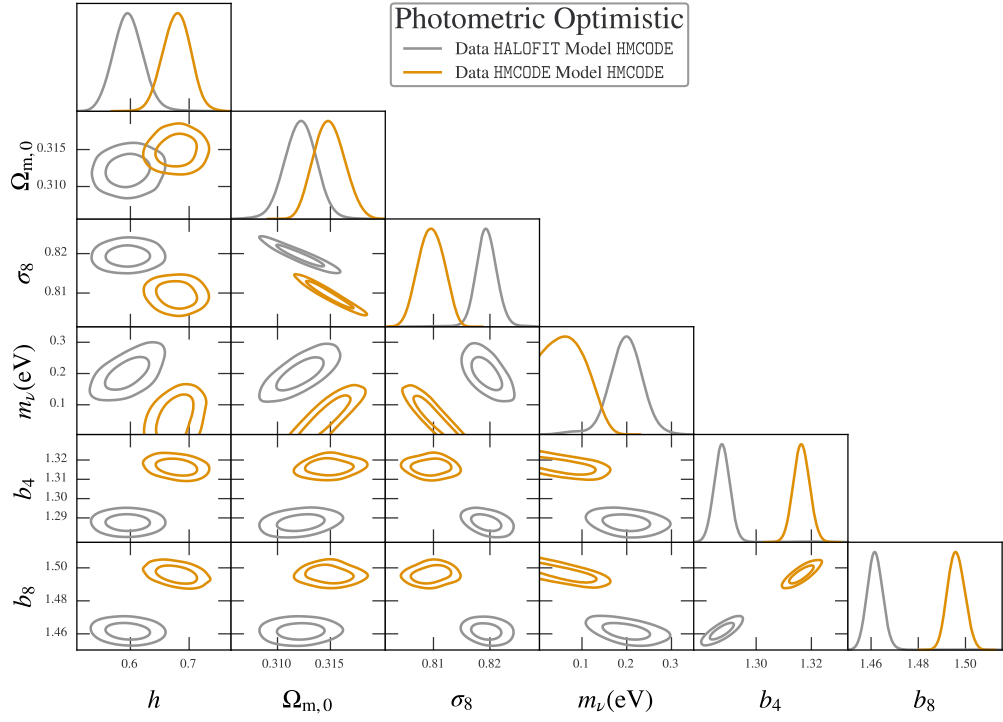
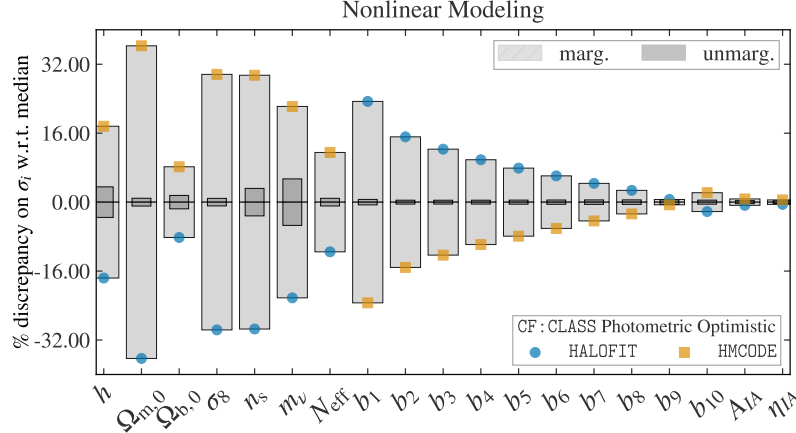
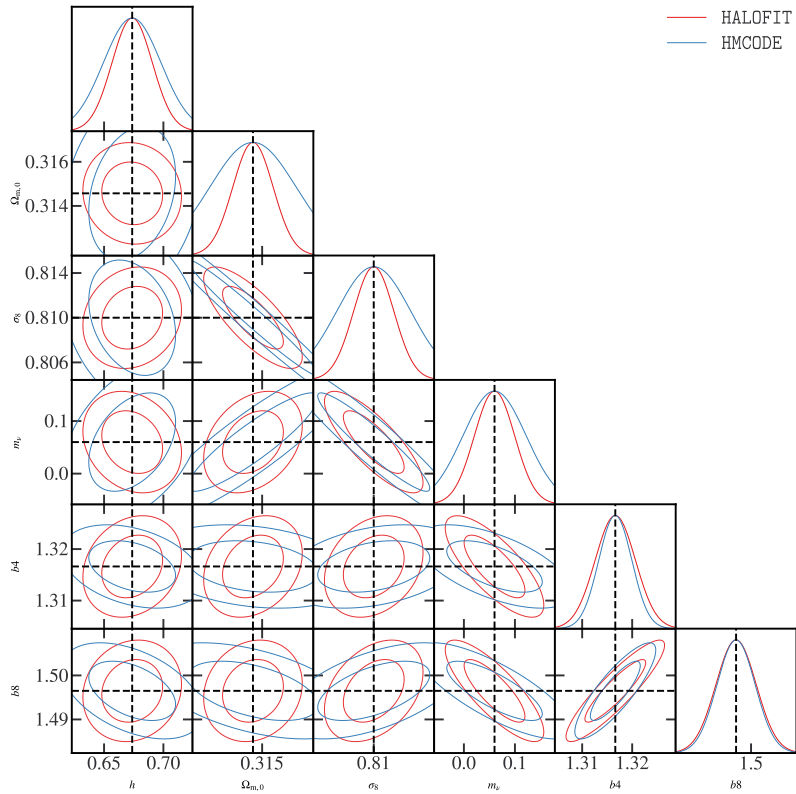


Figure 6.12: Same as figure 6.9 but switching the nonlinear model from HMCODE to HALOFIT.



(a) Comparision of the one-dimensional marginalized and unmarginalized errors obtained by using either of the two nonlinear correction codes.



(b) Comparision of the one and two-dimensional marginalized contours for the two different nonlinear correction codes. We marginalized other cosmological and nuisance parameters as their trends are the same.

Chapter 7

Results

In this chapter, we present our forecast results for neutrino parameters and dark energy. Compared to our validation runs there are multiple differences in our parameters. Firstly the neutrino mass m_ν is no longer condensed into one massive neutrino but evenly split between three neutrino species. To differentiate this quantity from the neutrino mass from the last chapter we will call it $\sum m_\nu$. This is done by setting the number of degenerate non-cold dark matter particles ' $\text{deg}_n \text{cdm} = 3$ '. Because of this we also change our definition of N_{eff} . Before it could have been understood as a change in the temperature of the massless neutrinos and could vary freely to higher and lower values. Now all neutrinos have the same temperature of

$$T_\nu = T_{\text{CMB}} \left(\frac{3.044}{3} \right)^{1/4} \left(\frac{11}{4} \right)^{1/3}. \quad (7.1)$$

This parameter now just parametrises any additional massless relic particle. Typical models predict only additional species that contribute positively to N_{eff} . From this, we define a new parameter ΔN_{eff} . This parameter is essentially equivalent to the parameter N_{ur} inside of **CLASS**.

Our next change is, that we vary the parameter σ_v and σ_p now that govern the nonlinear corrections of the spectroscopic probe. In order to be more conservative we also stick to the pessimistic settings of the probes. We will also vary all 9 cosmological parameters for our MCMC.

For $\sum m_\nu$ and ΔN_{eff} we chose prior edges with a theoretical prior at 0 as a lower bound and a higher bound far enough away to not change our results. The dark energy parameters chose a bit tighter prior edges to not probe unphysical regions of the parameter space. These parameters are in reality only some approximation to a wider set of theories where dark energy has an equation of state that is slowly varying. When the posterior hits the prior edges for the dark energy parameters we will consider them as unconstrained. For the other cosmological and nuisance parameters we have chosen arbitrary priors that will not get hit but speed up convergence.

A summary of our cosmological parameters, their fiducial and their prior edges can be seen in the table 7.1. The results can be seen in figure 7.1. We see that the photometric and spectroscopic probes are sensitive to different cosmological parameters. The spectroscopic probe dominates the sensitivity for ΔN_{eff} and h . These are the parameters whose main effect is on the BAO. Since the spectroscopic probe is sensitive to that region, it measures these well. The spectroscopic probe is nearly insensitive to the amplitude of the power spectrum as it is multiplied by the galaxy biases. To break this it needs the redshift space distortions where the clustering parameter $f \sigma_8$ enters.

Figure 7.1: One and two-dimensional marginalized posteriors for the different *Euclid* probes. We depict the 68% and 95% confidence intervals for the cosmological parameters of the full nine-parameter model. We depict the photometric probe in purple, the spectroscopic probe in cream and the combined probe in red.

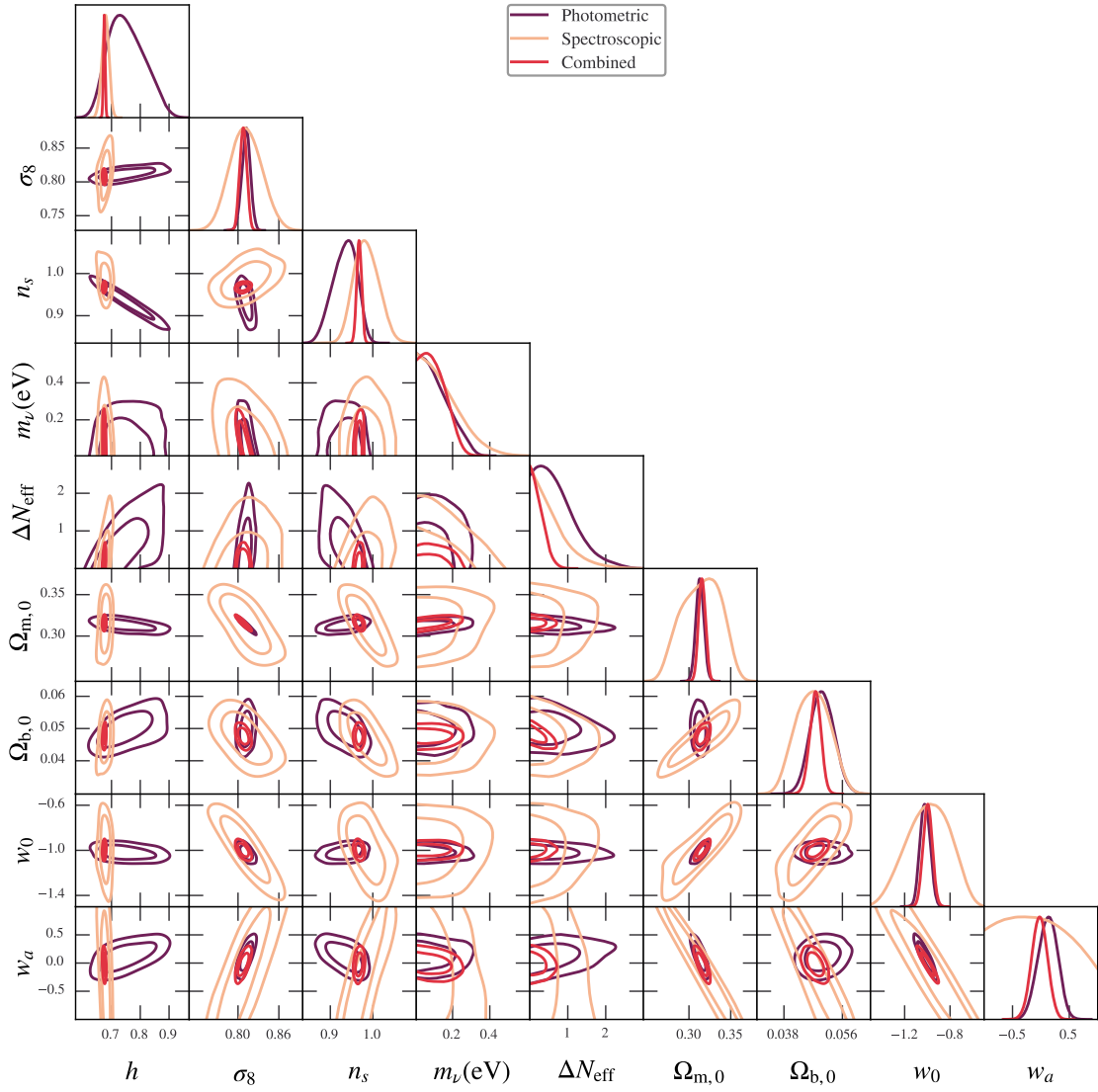


Table 7.1: Settings for the final forecast MCMCs. The fiducial values of the Nuisance parameters have been listed in the section for the respective probes.

Varied parameters								
Ω_m	$100 \times \Omega_b$	h	n_s	σ_8	$\sum m_\nu$ (meV)	ΔN_{eff}	w_0	w_a
Fiducial Value								
0.314571	4.92	0.6737	0.9661	0.81	60	0	0	-1
Prior Edges								
[0.005, 1]	[0.5, 100]	[0.1, 1.5]	[0.8, 1.2]	[0.7, 0.9]	[0, 1000]	[0, 5]	[-1.5, -0.5]	[-1, 1]

We also see that it alone is not able to constrain the time-dependent dark energy equation of state w_a . This parameter controls only slightly the time evolution of the amplitude of the matter power spectrum. Its sensitivity to the baryon density parameter Ω_b is greatly reduced by varying σ_v . The photometric probe is very sensitive to the amplitude of the power spectrum and dominates thusly the dark energy parameters, the neutrino mass, Ω_m , and σ_8 . Its sensitivity to Ω_b comes also from the BAO that leaves a small impact on the actual C_l . Since the scale of the BAO is fixed at around $5 \cdot 10^{-2} \text{Mpc}^{-1}$ the imprint shows up at different multipoles ℓ for different redshift bins. This leaves a very clear signature of Ω_b . It loses its sensitivity to h and ΔN_{eff} for the same reason, as the actual scale of the BAO is washed out by the integration over z . Essentially the photometric probe loses its sensitivity to scales.

In that sense, both probes are very complimentary to each other. In the figure, one can see how the correlation directions of the different probes are often perpendicular to one another breaking correlation directions and drastically improving the constraints on h , n_s , and ΔN_{eff} .

Nevertheless judging from this forecast *Euclid* alone will not be able to detect the neutrino mass alone. This is why in our final forecasting results in tabel we can only give a 95% confidence interval. It should be noted that by adding CMB data to our forecast we can achieve a measurement of the neutrino mass on the 68% confidence level for this nine-parameter model. If we go to a smaller model with only $\Lambda\text{CDM}+m_\nu$ we can even achieve a 99% confidence detection. We will not discuss these results further in this work as we have not discussed the CMB as an additional probe.

The marginalized errors are found in the table 7.2. The constraints of *Euclid* for the cosmological parameters are tighter than for *Planck*. They never gave constraints on our nine-parameter model. We can compare the constraints on submodels though as the four parameters in our case are not too strongly correlated. This means that we expect similar errors for the parameters if we have run the smaller models. In an analysis of the $w_0 w_a$ CDM *Planck* + BAO + Supernovae gives constraints on the dark energy parameters

$$w_0 = -0.957 \pm 0.08 \quad \text{and} \quad w_a = -0.29 \pm 0.3$$

This means that we can better constrain these parameters already with a bigger model. The main part of the constraints of *Planck* to these parameters are from contributions in additional late ISW effects, while *Euclid* we can see a redshift dependant reduction of the amplitude on all scales.

The parameters $\sum m_\nu$ and ΔN_{eff} are constrained by *Planck* +BAO+lensing to

$$\sum m_\nu < 0.12 \quad \text{and} \quad \Delta N_{\text{eff}} < 0.34. \quad (7.2)$$

These are both tighter than in our *Euclid* forecast. The main sensitivity to these parameters comes

from their background effects shifting the angular scale of recombination and the redshift of equality. Both of these parameters are very tightly constrained by the CMB measurements.

As both experiments measure probes that are very complimentary to one another as well as having additional Information in their cross-correlation, we believe that a combined analysis will bring us a new milestone in precision cosmology.

Table 7.2: Forecast 68% confidence levels for the different *Euclid* probes and the combined probe. For the parameters $\sum m_\nu$ and ΔN_{eff} we only state the 95% upper limit as they are bound from below by their theoretical prior. The spectroscopic probe alone was not able to constrain w_a within our prior edges.

Forecast Results									
Probe	Ω_m	$100 \times \Omega_b$	h	n_s	σ_8	w_0	w_a	$\sum m_\nu (\text{meV})$	ΔN_{eff}
Photometric	0.0049	0.38	0.065	0.029	0.0065	0.05	0.18	68% Sensitivity	
Spectroscopic	0.0258	0.56	0.013	0.031	0.024	0.20	—	< 260.	< 1.70
Combined	0.0043	0.18	0.0030	0.0060	0.0054	0.04	0.14	< 350.	< 1.50
								< 220.	< 0.57

Bibliography

- [Blas et al., 2011] Blas, D., Lesgourgues, J., and Tram, T. (2011). The Cosmic Linear Anisotropy Solving System (CLASS) II: Approximation schemes. *JCAP*, 07:034.
- [Collaboration et al., 2023] Collaboration, E., Tanidis, K., et al. (2023). Euclid preparation. tbd. the effect of linear redshift-space distortions in photometric galaxy clustering and its cross-correlation with cosmic shear.
- [Dolag et al., 2004] Dolag, K., Bartelmann, M., Perrotta, F., Baccigalupi, C., Moscardini, L., Meneghetti, M., and Tormen, G. (2004). Numerical study of halo concentrations in dark-energy cosmologies. 416:853–864.
- [Euclid Collaboration: Blanchard et al., 2020] Euclid Collaboration: Blanchard, A. et al. (2020). Euclid preparation: VII. Forecast validation for Euclid cosmological probes. *Astron. Astrophys.*, 642:A191.
- [Euclid Collaboration: Blanchard et al., 2023] Euclid Collaboration: Blanchard, A. et al. (2023). Euclid: Validation of the montepython forecasting tools.
- [Lesgourgues et al., 2013] Lesgourgues, J., Mangano, G., Miele, G., and Pastor, S. (2013). *Neutrino Cosmology*. Cambridge University Press.
- [Lewis, 2019] Lewis, A. (2019). GetDist: a Python package for analysing Monte Carlo samples.
- [Lewis et al., 2000] Lewis, A., Challinor, A., and Lasenby, A. (2000). Efficient computation of CMB anisotropies in closed FRW models. *Astrophys. J.*, 538:473–476.
- [Mead, 2016] Mead, A. J. (2016). Spherical collapse, formation hysteresis and the deeply non-linear cosmological power spectrum. *Monthly Notices of the Royal Astronomical Society*, 464(2):1282–1293.
- [Mead et al., 2021] Mead, A. J., Brieden, S., Tröster, T., and Heymans, C. (2021). hmcode-2020: improved modelling of non-linear cosmological power spectra with baryonic feedback. *MNRAS*, 502(1):1401–1422.
- [Nakamura and Suto, 1997] Nakamura, T. T. and Suto, Y. (1997). Strong gravitational lensing and velocity function as tools to probe cosmological parameters: Current constraints and future predictions. *Progress of Theoretical Physics*, 97(1):49–81.
- [Navarro et al., 1997] Navarro, J. F., Frenk, C. S., and White, S. D. M. (1997). A universal density profile from hierarchical clustering. *The Astrophysical Journal*, 490(2):493.

- [Press and Schechter, 1974] Press, W. H. and Schechter, P. (1974). Formation of Galaxies and Clusters of Galaxies by Self-Similar Gravitational Condensation. *187*:425–438.
- [Raccanelli et al., 2018] Raccanelli, A., Verde, L., and Villaescusa-Navarro, F. (2018). Biases from neutrino bias: to worry or not to worry? *Monthly Notices of the Royal Astronomical Society*, 483(1):734–743.
- [Takahashi et al., 2020] Takahashi, R., Nishimichi, T., Namikawa, T., Taruya, A., Kayo, I., Osato, K., Kobayashi, Y., and Shirasaki, M. (2020). Fitting the nonlinear matter bispectrum by the Halofit approach. *ApJ*, 895(2):113.
- [Vagnozzi et al., 2018] Vagnozzi, S., Brinckmann, T., Archidiacono, M., Freese, K., Gerbino, M., Lesgourgues, J., and Sprenger, T. (2018). Bias due to neutrinos must not uncorrect'd go. *JCAP*, 09:001.
- [Villaescusa-Navarro et al., 2014] Villaescusa-Navarro, F., Marulli, F., Viel, M., Branchini, E., Castorina, E., Sefusatti, E., and Saito, S. (2014). Cosmology with massive neutrinos i: towards a realistic modeling of the relation between matter, haloes and galaxies. *Journal of Cosmology and Astroparticle Physics*, 2014(03):011–011.